

Reproduced by

DOCUMENT SERVICE CENTER

ARMED SERVICES TECHNICAL INFORMATION AGENCY

U. S. BUILDING, DAYTON, 2, OHIO

DEL-C

5763

T.I.

128961

NOTICE: When Government or other drawings, specifications or other data are used for any purpose other than in connection with definitely related Government procurement operation, the U.S. Government thereby incurs no responsibility, nor any obligation whatsoever; and the fact that the Government may have formulated, furnished, or in any way supplied the said drawings, specifications or other data is not to be regarded by implication or otherwise as in any manner licensing the holder or any other person or corporation or conveying any rights or permission to manufacture, use or in any way imitate invention that may in any way be related thereto."

UNCLASSIFIED

CLASSIFIED

UNCLASSIFIED

ATI 128 961

(COPIES OBTAINABLE FROM ASTIA-DSC)

OHIO STATE UNIVERSITY RESEARCH FOUNDATION, COLUMBUS
(REPORT NO. 41)

HEAT TRANSFER AND PRESSURE DROP DATA FOR CIRCULAR CYLINDERS
IN DUCTS AND VARIOUS ARRANGEMENTS - AND APPENDIXES I THRU V

ROBINSON, W.; HAN, L.S.; ESSIG, R.H. AND OTHERS
SEPT 1951 CAMP PHOTO, TABLES, DIAGRS, GRAPHS

USAF CONTR. NO. W-33-038-AC-14987

ELECTRONIC EQUIPMENT - COOLING ELECTRONICS (3)
DUCTS, INTAKE GENERAL (0)
HEAT TRANSFER

UNCLASSIFIED

CADD
FILE COPY

ATTN. NO. 128961

Report No. 41

September 1951

HEAT TRANSFER AND PRESSURE DROP DATA FOR CIRCULAR CYLINDERS IN DUCTS AND VARIOUS ARRANGEMENTS

W. Robinson
L. S. Han
R. H. Essig
C. F. Heddleson

THE OHIO STATE UNIVERSITY RESEARCH FOUNDATION
Columbus 10, Ohio

Contract W33-032oc-14987
EO. 111-72 SR-6-J

United States Air Force
Wright Air Development Center
Wright-Patterson Air Force Base, Dayton, Ohio

HEAT TRANSFER AND PRESSURE DROP DATA
FOR CIRCULAR CYLINDERS IN
DUCTS AND VARIOUS ARRANGEMENTS

W. Robinson
L. S. Hart
R. H. Essig
C. F. Heddleson

THE OHIO STATE UNIVERSITY RESEARCH FOUNDATION
Columbus 10, Ohio

Contract W33-038ac-14987
E.O. 111-72 SR-6d1

United States Air Force
Wright Air Development Center
Wright-Patterson Air Force Base, Dayton, Ohio

ABSTRACT

Heat transfer and pressure drop relationships of cylinders in ducts with air flow normal to the axis, are presented for air velocities from 3 to 120 feet per second. Overall heat transfer coefficients and distributions of point heat transfer coefficients around cylinders are given for single, in-line, symmetrically staggered, and unsymmetrically staggered arrangements. The overall heat transfer and pressure drop data are correlated for all arrangements. They are reduced to single equations by the determination of factors describing configuration characteristics.

TABLE OF CONTENTS

	<u>Page</u>
FOREWARD - - - - -	ii
ABSTRACT - - - - -	iii
I. INTRODUCTION - - - - -	1
II. SUMMARY - - - - -	4
III. EXPERIMENTAL INVESTIGATION - - - - -	7
IV. RESULTS AND DISCUSSION - - - - -	14
Data Reduction - - - - -	15
Test Data Summary - - - - -	17
Peripheral Distribution - - - - -	41
Pressure Gradients in Ducts - - - - -	56
Overall Heat Transfer - - - - -	58
V. CORRELATION OF RESULTS - - - - -	67
VI. BIBLIOGRAPHY - - - - -	77
<u>APPENDICES</u>	
I. TEST APPARATUS AND INSTRUMENTATION - - - - -	78
II. TEST CYLINDER CONSTRUCTION - - - - -	80
III. TEST PROCEDURE - - - - -	84
IV. CALIBRATION OF TEST CYLINDERS - - - - -	86
V. METHODS OF CALCULATION - - - - -	89

ILLUSTRATIONS

<u>FIGURE</u>	<u>Page</u>
1. Sketch of Test Apparatus for the Study of Forced Convection Heat Dissipation - - - - -	8
2. Exploded View of Test Section with Staggered Cylinder Arrangement - - - - -	9
3. Construction Details of Heated Test Cylinder and Typical Test Duct - - - - -	11
4. Sketch of Test Configurations - - - - -	12
5. - 31. Peripheral Distributions of Modified Point Nusselt Number (Test Cylinder B) - - - - -	23 - 37
5. - 7. Single Cylinder - - - - -	23 - 24
8. - 19. In-Line Configuration - - - - -	24 - 29
20. - 26. Staggered Configuration - - - - -	29 - 32
27. - 31. Staggered Double-Row Configuration - - - - -	33 - 37
32. - 34. Peripheral Distributions of Modified Point Nusselt Number for Single Cylinder (Test Cylinder A) - - - - -	38
35. - 38. Variations of Static Pressure at Duct Wall - - - - -	39 - 40
35. Single Cylinder in Ducts of Various Widths - - - - -	39
36. Three Cylinders in Line at Various Mass Velocities and Constant Spacing in 3-Inch Duct - - - - -	39
37. Single Cylinder and Three Cylinders in Line with Various Spacings in 3-Inch Duct - - - - -	40
38. Single Cylinders of Various Diameters in 3.5-Inch Duct - - - - -	40
39. - 51. Circumferential Variations of Ratio of Point to Average Modified Nusselt Number - - - - -	42 - 48
39. - 41. Single Cylinder - - - - -	42
42. - 45. In-Line Configuration - - - - -	43 - 44

FIGUREPage

46. - 49.	Staggered Configuration - - - - -	45 - 46
50. - 51.	Staggered Double-Row Configuration - - - - -	47 - 48
52. - 54.	Peripheral Distributions of Modified Point Nusselt Number for In-Line Arrangement and Unequal Spacings - - - - -	52
55. - 57.	Average Modified Nusselt Numbers vs. Bulk Reynolds Numbers - - - - -	59 - 61
55.	Single, In-Line and Staggered Cylinders in 2-Inch Duct - - - - -	59
56.	Single, In-Line and Staggered Cylinders in 3.5-Inch Duct - - - - -	60
57.	Staggered Double-Row Configuration in 3- and 3.5-Inch Duct - - - - -	61
58. - 60.	Variations of Ratio of Modified Nusselt Number to Static Pressure Drop - - - - -	64
61.	Effect of Duct Width on Nusselt Number Distribution for Single Cylinder - - - - -	68
62.	Correlation with Free Stream Data of Point Nusselt Number at Forward Stagnation Point for Single Cylinder in Various Ducts - - - - -	68
63. - 68.	Correlation with Free Stream Data of Average Nusselt Number for Single and Multiple Cylinders in Various Configurations - - - - -	70 - 73
69. - 71.	Pressure Drop Correlation Curves for Various Configurations - - - - -	75
72.	Method of Installation of Dummy Cylinders for In-Line Configurations - - - - -	83
73.	Method of Installation of Dummy Cylinders for Staggered Configurations - - - - -	83
74. - 75.	Typical Test Data and Calculated Nusselt Number Distribution - - - - -	91

TABLEPage

I.	Test Configurations - - - - -	13
II.	Data Summary for Single and In-Line Cylinders in 2-Inch Duct - - - - -	19
III.	Data Summary for Single and In-Line Cylinders in 3-Inch Duct - - - - -	19
IV.	Data Summary for Single and In-Line Cylinders in 3.5-Inch Duct - - - - -	20
V.	Data Summary for Staggered Cylinders in 2-Inch Duct - -	20
VI.	Data Summary for Staggered Cylinders in 3-Inch and 3.5-Inch Ducts - - - - -	21
VII.	Data Summary for Double-Row Staggered Cylinders in 3-Inch and 3.5-Inch Ducts - - - - -	21
VIII.	Data Summary for Single Cylinder in 3-Inch, 4-Inch and 6-Inch Duct (Test Cylinder A) - - - - -	22

I. INTRODUCTION

Because of ever-widening demand for reliable operation under all probable flight conditions, adequate cooling is being recognized as an important and integral part of the design of airborne electronic equipment. Past practices of cooling electronic equipment by means of natural convection and by the use of blowers as auxiliary devices does not fulfill most present and future requirements. They stem from (1) aircraft operation at increased flight speeds and altitudes, (2) equipment designs of greater capacity and higher heat concentration, and (3) severer restriction in available installation space.

Among methods of heat rejection from electronic components and equipments, details of cooling by means of forced convective air flow offer a vast field for exploration. This mode of cooling embraces the use of air flow which may either be induced from the environment of the aircraft in flight, or from the installation compartment of the electronic equipment, or may circulate at high velocity within the equipment case. The effective application of this mode of heat dissipation from components requires knowledge of overall heat transfer coefficients as well as of the variations of local heat transfer coefficients on component surfaces. For the evaluation of these coefficients, the effects of air temperature and pressure, rate of air flow, and arrangement of components must be known. Together with the knowledge of heat transfer coefficients, knowledge of pressure drops and their relation with the above factors is of importance. The power requirement for cooling is determined by pressure drop and air flow rate. Expressing the power requirement in the same units of energy as the heat dissipated from the components provides a means for the evaluation of the efficiency of a given cooling application.

The problem of cooling of electronic equipment is made complex by the presence of hot spots on surfaces of components or assemblies having non-uniform distribution of surface heat dissipation, resulting from an uneven distribution of internal heat sources. To provide for removal of these hot spots, peripheral distributions of local surface heat transfer coefficients, obtained by forced convective air cooling, must be explored as function of component arrangement and air flow characteristic. The knowledge of peripheral distribution aids effectively in the elimination of hot spots and in the reduction of power requirements, if arrangements are chosen in which maximum heat transfer coefficients coincide with usual hot spot locations.

The purpose of the present investigation has been to produce fundamental heat transfer information which would add to the required knowledge for the internal design of electronic equipment cooled by forced convective air flow. Literature survey has disclosed that some previous work has been concerned with the determination of heat transfer coefficients on bodies of shapes and in arrangements similar to those of components in electronic equipment. However, the data are only applicable in part and then mainly in a qualitative sense. Little information is available on overall and local heat transfer coefficients on bodies in ducts similar to components installed in baffled passages. Pressure drop data on cross-flow over banks of circular tubes in different

arrangements, although found in the literature, have not been correlated on a general basis of tubular arrangement, thus rendering the data inapplicable to the present need.

Most previous investigations were performed under actual or simulated free-stream conditions. Reiher (7) and Hilpert (4, 5)⁺ were the only ones who investigated overall heat transfer coefficients on surfaces of actual streamlined and square tubes arranged in banks and singly. The data obtained by Reiher on tube banks were qualitative and exploratory. In general, non-circular tubes give greater heat transfer than circular tubes under the same temperature and air flow conditions. Pierson (10) and Hoge (6) obtained overall heat transfer coefficients and static pressure drops with circular tubes of various sizes arranged in tube banks for both heating and cooling of air. Grimson (3) attempted to correlate these heat transfer coefficients but used an arbitrarily chosen tube arrangement as the reference basis for presenting the data. The static pressure drop was expressed by a friction factor based on the velocity head in the minimum flow area and the number of major restrictions and no attempt was made to correlate the data in terms of configuration geometry.

The variation of the point unit heat transfer coefficient around a single cylinder, its axis normal to a free airstream, was studied by a number of investigators, notably Schmidt and Wenner (11), Giedt (2) and Winding and Cheny (13). The data of Schmidt and Wenner were obtained for isothermal cylinders of three different diameters. Giedt's data were for a non-isothermal surface. However, the circumferential variation in surface temperature was less than 5°F. His 4-inch diameter test cylinder gave relatively large Reynolds numbers with fairly low air velocities. By means of naphthalene models, Winding and Cheny, employing the analogy between mass and heat transfer, also determined the circumferential variation of point unit heat transfer coefficient around cylindrical, streamlined, and flat tubes, located in ducts in both single and multiple configurations. Their data could be considered analogous to those obtained from isothermal surfaces. Some discrepancies resulted in the comparison of these data with those obtained in conventional heat transfer measurements because of the differences in diffusion processes of a vapor to air and of heated air to cooler air. Similar experimental work with staggered tube banks was also performed by Thoma (12) and Lohrisch (8) who reported results of qualitative interest.

For various reasons, the results of previous investigations are not directly applicable to the evaluation of forced convective cooling of electronic components. They do not describe circumferential variation of point unit heat transfer coefficients around individual components in banks. They do not contain correlation of the overall heat transfer coefficient of individual components in banks with respect to configuration geometry. They do not relate the overall heat transfer coefficients

⁺See Bibliography for reference.

of components in banks to the inherent static pressure drops. They indicate only the circumferential variation of the point unit heat transfer coefficient around isothermal bodies, or nearly isothermal bodies, in free air flow which should be appreciably different from those obtained on bodies located in confined passages and having large surface temperature variations.

In view of the deficiencies of existing information, as applied to the problem of cooling of electronic components, the present investigation was conducted for the following purposes: (1) to determine the circumferential variations of point unit heat transfer coefficient for a simulated electronic component located in various ducted arrangements, (2) to find the relationship between overall heat transfer coefficients and flow characteristics in terms of configuration parameters, and (3) to determine the air pressure drop across one or several bodies in ducts, correlated in terms of arrangement geometry, and therefore qualitatively and exactly applicable to cooling design for electronic components.

The shapes of electronic components vary. They consist of cylinders, prisms and combinations thereof. The range in absolute dimensions is appreciable. This great variety in shape and size of electronic components makes their use for fundamental experimental studies impractical. Therefore, it is necessary to idealize the problem for experimental investigation. The right circular cylinder here chosen for representative studies because of its convenient shape, simulates many electronic components such as tubes, resistors, sealed units and potted miniaturized assemblies. Also, the basic data obtained from cylinders could be of general usefulness for other purposes, in addition to the design of electronic component arrangements and the orientation of individual components on the basis of coincidence of their hot spot locations with maxima of point unit heat transfer.

II. SUMMARY

Scope of Investigation

The heat transfer and pressure drop relationships of cylinders in air ducts were studied. The direction of air flow was normal to the cylinder axis. Single cylinders, multiple cylinders in line, multiple cylinders staggered symmetrically about the center plane of the duct, and multiple cylinders staggered asymmetrically in double rows were studied.

Heat transfer occurred from non-isothermal surfaces produced by heat flow from an isothermal element through an insulating layer. The temperature differentials so determined were used for the calculation of point heat transfer rates.

The range of surface temperature differences, referred to the cooling air, was from 50 to 390°F. Air velocities from 3 to 120 feet per second were used. The test cylinder diameter was 1.5 inches. Duct widths varied from 2 to 6 inches. The spacings of multiple cylinders varied from 1.625 to 3 inches.

The peripheral variations of the point Nusselt number were determined from the test results and were correlated to correct for surface temperature of the test model. The average Nusselt numbers were correlated with the film Reynolds number of the air flow and were reduced to a single relationship of the same form as found in the literature for cylinders in free air flow. Modification factors describing the configuration geometry were devised by numerical analysis of the experimental data. In similar manner, overall pressure drop data were correlated by the use of configuration factors for each type of cylinder arrangement.

Results

The most noteworthy results may be summarized as follows:

1. Point heat transfer coefficients on cylindrical surfaces in ducts may vary from 160 to 100 per cent from the average value. The variation is a function of the configuration and the flow rate. Expressed in terms of ratio of point-to-average heat transfer coefficient, this variation is increased by reduced air velocity. The greatest ratio variations are obtained for in-line arrangements of cylinders, the least for single cylinders. Also with multiple cylinder arrangements, greater variation of the ratio of point-to-average coefficient is obtained for closer spacings than for wider spacings. The opposite applies for single cylinders which exhibit increasing ratio variations with decreasing duct width.

2. Locations of maximum and minimum heat transfer coefficients are dependent on configuration and flow rate. Maximum coefficients on single cylinders occur 180 degrees apart, at the forward and rear stagnation points. On cylinders in line they occur 120 degrees apart, approximately 60 degrees on either side of the forward stagnation

point. On staggered cylinders one or two maximum coefficients may occur, depending on the spacing. Two maxima occur for close spacings.

3. The distribution and magnitudes of heat transfer coefficients on the upstream and downstream half of a cylinder are only affected by the spacing of the upstream and downstream cylinder, respectively. It is feasible to construct the distribution on a cylinder with unequally spaced upstream and downstream cylinders from data obtained with the corresponding two equal spacings.

4. Cylinders arranged in a double-row asymmetrically staggered configuration in reference to the center plane of the duct have distributions of heat transfer coefficients which resemble a composite of distributions obtained with in-line and symmetrically staggered arrangements. The half adjacent to the duct wall exhibits the distribution of an in-line cylinder, the other half that of a staggered cylinder.

5. Higher rates of overall heat transfer than for a single cylinder are obtainable from multiple cylinders for the same air flow energy requirement. Also, on the same basis, higher rates are obtainable from staggered cylinders than from in-line cylinders.

6. The form of the correlation factors for rates of overall heat transfer of in-line and staggered cylinders indicates that for each configuration an optimum spacing exists at which the greatest quantity of heat may be transferred from a surface of given temperature, using the least amount of energy to convey the cooling air.

7. Using symbols defined in the section on nomenclature on page 14 the following equations are valid:

- a. for point heat transfer at the forward stagnation point of a single cylinder in a duct,

$$Nu_f = 1.01 [Re_f(1 + \sqrt{d/w})]^{0.5};$$

- b. for average overall heat transfer in general,

$$Nu_f(ave) = CF [Re_f(ave)]^n,$$

where the values of C and n vary with Reynolds number as follows:

$Re_f(ave)$	C	n
1,000 - 6,000	0.409	0.531
6,000 - 50,000	0.212	0.606
50,000 - 100,000	0.139	0.806

for a single cylinder in a free air stream

$$F = 1;$$

for a single cylinder in a duct,

$$F = F_1 = 1 + \sqrt{d/w};$$

for in-line cylinders,

$$F = F_2 = (1 + \sqrt{1/S_T}) \left\{ 1 + \left[(1/S_T) - (0.872/S_T^2) \right] \times \right. \\ \left. \times \left[1.81/S_T^2 - 1.46/S_T + 0.318 \right] \left[Re_f (0.526 - 0.354/S_T) \right] \right\};$$

for staggered cylinders,

$$F = F_3 = (1 + \sqrt{1/S_T}) \left\{ 1 + \left[(f_1/\sqrt{S_L}) - f_2/S_L \right] Re_f^{0.13} \right\}$$

$$\text{where } f_1 = \left[15.50/S_T^2 - 16.80/S_T + 4.15 \right]$$

$$\text{and } f_2 = \left[14.15/S_T^2 - 15.53/S_T + 3.69 \right]$$

c. for the pressure drop per cylinder, in general

$$(\Delta p)/n = 0.0111 C^2/\psi;$$

for a single cylinder,

$$\psi = \psi_1 = (1 - 1/S_T)^{2.7};$$

for in-line cylinders,

$$\psi = \psi_2 = \psi_1 (1 + 1/S_L)^{1.65};$$

for staggered cylinders,

$$\psi = \psi_3 = \psi_1 (1 + 1/S_L)^{(4.36 - 3.52/S_L)}.$$

III. EXPERIMENTAL INVESTIGATION

Objectives and Scope

The ultimate objective of this study has been to produce design information which could be applied to the cooling of electronic equipment. To meet this demand, overall and local heat transfer coefficients of heated cylindrical bodies with non-uniform radial heat flow, arranged singly or multiply in ducted passages, and the pressure drop across such configurations were determined. The heat transfer and pressure drop data were intended to provide a rational basis for evaluation of the economy of cooling systems from the standpoint of heat removal versus the power necessary to convey the required air quantity through the system.

The major requirements of a cooling design for airborne electronic equipment were recognized to be: (1) compact component arrangement, (2) minimum use of power for cooling, and (3) reliable operation of components at allowable temperatures. All variables affecting these requirements were examined. These variables were: (1) surface temperature, (2) heat flux, (3) flow rate, (4) duct dimension, and (5) spacing between components. The range of average surface temperature in the test runs was approximately 160 to 496°F corresponding to a difference in temperature from surface to cooling air of 50 to 390°F. The range of cooling air temperature was 80 to 110°F approximately. The range of heat flux was 7 to 85 Btu per hour - square inch (2 to 25 watts per square inch). The range of air flow rate was 0.14 to 8.5 pounds per second per square foot of gross duct area. This corresponded to air velocities of 3 to 120 feet per second approximately, and Reynolds numbers of 1200 to 85,000, based on the diameter of all test cylinders of 1.5 inches. Ducts 2 to 6 inches wide were used. Center spacings between multiple cylinders arranged in line, symmetrically staggered and asymmetrically staggered in reference to the duct center line were from 1.625 to 3 inches.

Test Apparatus and Models

The test set-up consisted principally of a centrifugal fan, a metering section with a thin-plate orifice and a steel or aluminum test duct of rectangular cross section in which various cylinder arrangements were installed. A detailed sketch of the entire test set-up and instrumentation is shown in Figure 1.

An exploded view of a typical test section is shown in Figure 2. The cylinders are arranged in a staggered configuration in which the heated test cylinder, shown removed from its mounting ring, is surrounded by unheated dummy cylinders, thus simulating a multiple component configuration. Two 1.5-inch diameter internally heated cylinders were used as test models. The construction of the two cylinders was basically the same. They each contained four heating coils surrounded by a 3/32-inch thick shell of Transite, an asbestos-cement material, consisting of 85 per cent Portland cement and 15 per cent asbestos by weight. The first

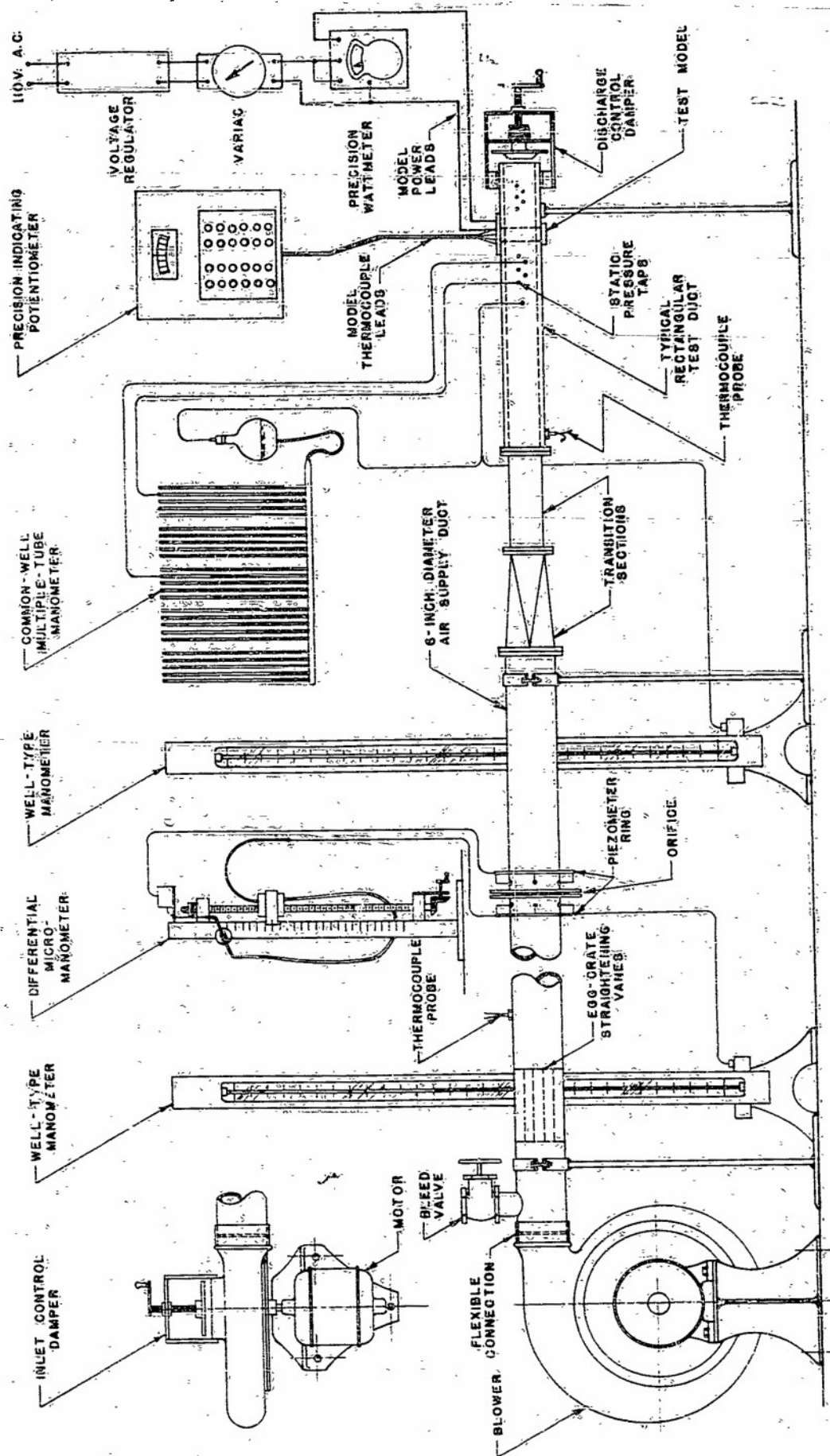


FIGURE 1. SKETCH OF TEST APPARATUS FOR THE STUDY OF FORCED CONVECTION HEAT DISSIPATION OF CYLINDERS IN DUCTS

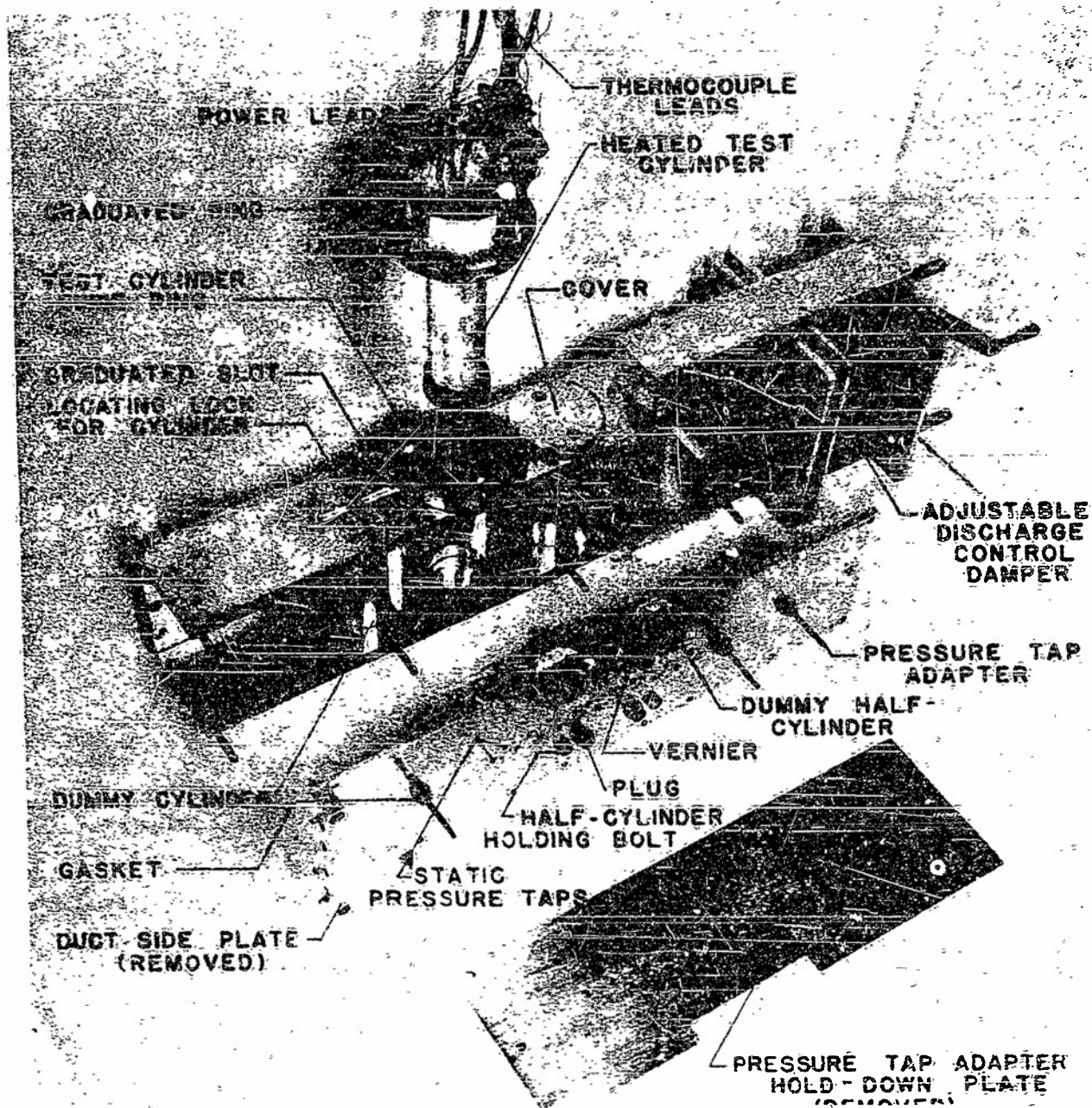


FIGURE 2. EXPLODED VIEW OF TEST SECTION WITH STAGGERED CYLINDER ARRANGEMENT

cylinder, hereafter designated as cylinder A, was used in the steel ducts for preliminary exploratory tests. A second cylinder, hereafter designated as cylinder B, was much more carefully constructed and more completely instrumented than cylinder A and was used in the aluminum ducts to obtain most of the data presented herein. A cross section of test cylinder B showing details of construction and instrumentation is shown in Figure 3. Temperature drops across the Transite shell were measured by means of imbedded thermocouples and were used to calculate radial heat flow.

For multiple cylinder arrangements, the heated cylinder B was used with other unheated cylinders. The latter cylinders were made of polished 1.5-inch diameter aluminum bar stock. They were mounted so that their spacings could be adjusted. Two unheated cylinders of 1- and 1.938-inch diameter, respectively, were used singly in place of the heated test cylinder to provide additional data for the correlation of pressure drops.

A detailed description of the test apparatus and its instrumentation are contained in Appendix I. The design of the heated and of the unheated test models is discussed in Appendix II. The test procedure is described in Appendix III.

Test Data

Thirty different cylinder arrangements were tested in five ducts of different width, each 4 inches high. Measurements of circumferential temperature distribution around the heated cylinder A, installed singly in 3-inch, 4-inch, and 6-inch wide steel ducts were obtained over a range of Reynolds numbers and surface temperatures. As explained in pages 55 to 56, these data were considered not reliable. However, they are presented in this report for qualitative comparison with the other test data. Measurements of circumferential temperature distributions around test cylinder B over a range of Reynolds numbers and surface temperatures were obtained for the cylinder located in 27 different single and multiple arrangements in 2-inch, 3-inch, and 3.5-inch wide aluminum ducts. The basic cylinder arrangements and their designations are shown in Figure 4. Transverse, longitudinal, diagonal, and row pitches are designated as S_T , S_L , S_D , and S_R , respectively, being multiples of cylinder diameter d . The specific test configurations are itemized in Table I. The individual pitches are given in terms of cylinder diameter.

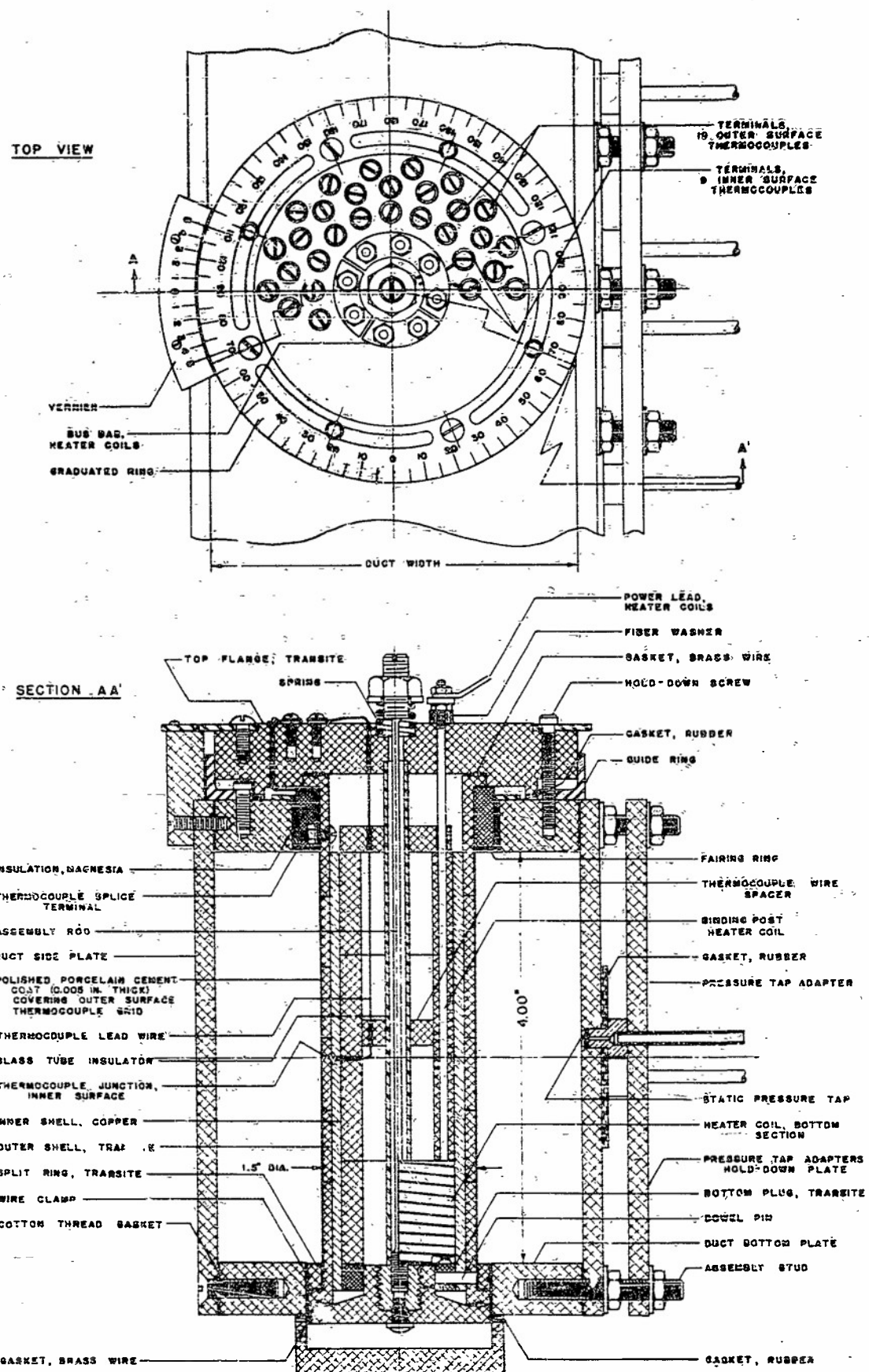


FIGURE 3. CONSTRUCTION DETAILS OF HEATED TEST CYLINDER AND TYPICAL TEST DUCT

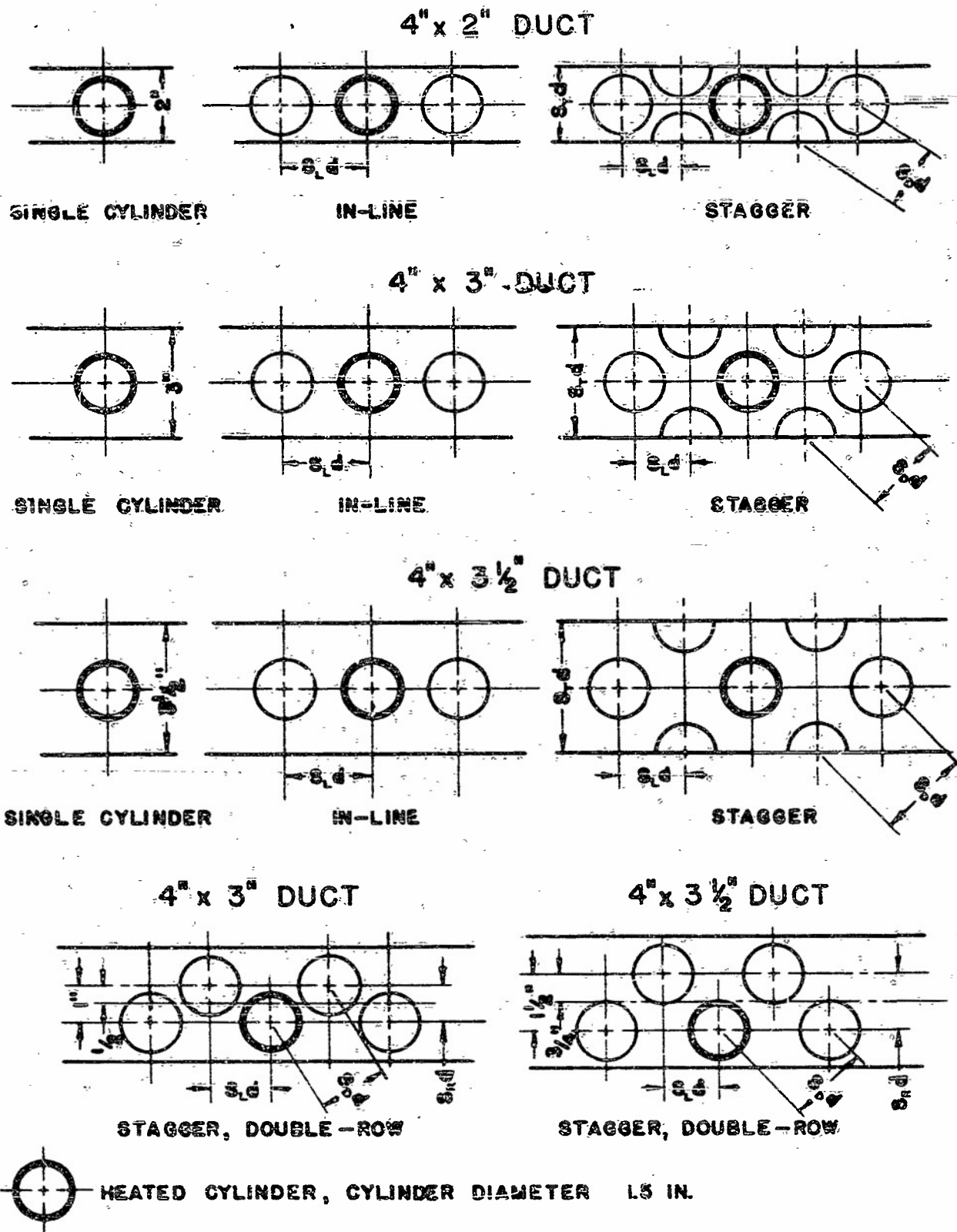


FIGURE 4. SKETCH OF TEST CONFIGURATIONS

Table I. Test Configurations

a. Test Cylinder A in Steel Ducts		
Duct Width, inches	Configuration	S_T
5	Single	2.000
4	Single	2.667
6	Single	4.000

b. Test Cylinder B in Aluminum Ducts					
Duct Width, inches	Configuration	S_L	S_T	S_D	S_R
2	Single		1.333		
	In-line	1.083 1.250 1.500 2.000			
	Staggered	0.957 1.058 1.345		1.167 1.250 1.500	
3	Single		2.000		
	In-line	1.083 1.250 1.500 2.000			
	Staggered	0.576 1.000		1.153 1.413	
	Staggered, double-row	0.855 1.058 1.345		1.083 1.250 1.500	0.667
3.5	Single		2.533		
	In-line	1.083 1.250 1.500 2.000			
	Staggered	0.673 1.167		1.347 1.500	
	Staggered, double-row	0.375 1.000		1.153 1.413	1.000

IV. RESULTS AND DISCUSSION

Nomenclature

A	area, sq ft
C	constant
d	diameter of test cylinder, ft
E	heat input, Btu per hr
F	configuration factor in film Nusselt number equation
G	mass velocity, lb per (sec-sq ft)
h	surface heat transfer coefficient, Btu per (hr-sq ft-°F)
K	radial thermal conductance of test cylinder, Btu per (hr-sq ft-°F)
k	thermal conductivity, Btu per (hr-sq ft-°F per ft)
Nu	Nusselt number, hd/k
n	number of cylinder banks, or exponent, or number of surface locations
q	heat flux, Btu per (hr-sq ft)
Re	Reynolds number, dG/μ
S_T	transverse pitch, cylinder diameters
S_L	longitudinal pitch, cylinder diameters
S_D	diagonal pitch, cylinder diameters
S_R	row pitch, cylinder diameters
S_{LU}	upstream longitudinal pitch, cylinder diameters
S_{LD}	downstream longitudinal pitch, cylinder diameters
T	temperature, °R
t	temperature, °F
w	duct width, ft
Y	relative conductance

- α relative position on surface of cylinder, degrees from the forward stagnation point
- Δp static pressure drop across the configuration, in. of water
- μ absolute viscosity, lb per (ft-sec)
- ρ specific weight, lb per cu ft
- Σ summation of
- σ ratio of specific weights ρ/ρ_0 , or Stephan-Boltzmann constant in radiation equation, 0.173×10^{-8} Btu per [hr-sq ft-(°R)⁴]
- ϕ modification factor
- ψ configuration factor in static pressure drop equation

Subscripts:

- A area, used in F_A for calculation of radiant heat flux
- ave average of point values
- b bulk air condition
- conv convection
- e emissivity, used in F_e for emissivity factor
- f film condition based on film temperature
- i inside surface of Transite shell of test cylinder
- o standard condition, 29.92 in. Hg and 59°F
- rad radiation
- ref reference
- s outside surface of test cylinder
- tr Transite
- x referring to location of surface thermocouple
- μ referring to viscosity

Data Reduction

In all studies of heat transfer by forced convection the universally used parameters for purpose of analysis and correlation have been Reynolds

number, AG/μ , and Nusselt number, hd/k , which are indicative of flow characteristics and heat transfer characteristics, respectively. Theoretically or experimentally determined expressions relating the two dimensionless moduli are generally sought to present and interpret the results of investigations. Examination of these two moduli shows that they contain (1) the heat transfer coefficient, h , a function of the heat flux and the temperature difference between the surface and the fluid stream, (2) the mass velocity, G , a function of the flow rate and the cross section of the flow passage, (3) a characteristic dimension, d , and (4) the physical properties of the flow medium, μ and k , which are subject to variation due to change of temperature.

The purpose of this investigation was the determination of peripheral variations of Nusselt number of a heated cylinder in single or multiple configurations. Therefore, the experimental study was undertaken principally to produce information which yielded values of point heat flux on the cylinder surface as a function of angular position relative to flow direction. The test models and particularly cylinder B used for this experimental investigation were designed to permit the measurement of local temperature drop across an outer insulating shell with radial heat flow from an internal heat source. The point heat flux was calculated for any position by the temperature drop across the shell and a known point thermal conductance of the shell, based on the assumption that tangential heat flow was negligible and that only radial heat flow took place. The point heat flux thus obtained made possible the calculation of the point heat transfer coefficient, based on the difference between local surface and air temperature.

In the calculation of Nusselt number and Reynolds number, the diameter, d , of the test model was used as the significant dimension. The mass velocity, G , based on gross cross-sectional area, was determined conventionally by calculation of air flow from the orifice meter readings.

In view of the large temperature differences which were encountered in the experimental study, it was found necessary to determine the reference temperature for the evaluation of the physical properties of air to be used in the calculation of Nusselt number and Reynolds number. The choice was to be made among the commonly employed reference temperatures, i.e. surface temperature, bulk temperature and film temperature, the latter being the mean value of surface and bulk temperature. A criterion for determining the reference temperature was furnished in the correlation of results. For this purpose, a number of preliminary plots of both the average Nusselt number over the entire circumference determined by graphical integration, and the point Nusselt number at the forward stagnation point versus Reynolds number were made for a single heated cylinder in 2-, 3-, and 3.5-inch test ducts. In all the plots, different reference temperatures were used for the same test runs and the correlations were compared. The results of the comparison showed that the use of bulk temperature as reference was definitely inadequate, because in similar test runs with constant air flow, but different heat flow due to different surface temperature, several bulk Nusselt numbers were calculated for the same bulk Reynolds number. The correlations obtained with film reference temperature indicated generally better agreement than those obtained with surface reference temperature. Accordingly, film reference temperature

was used in the final analysis and interpretation of the test data.

Methods of calculating point heat flux, point heat transfer coefficients, and other parameters from the test data are described in Appendix V.

For presentation of the Nusselt number distribution data, it was desired to show, if possible, a single curve for each bulk Reynolds number and configuration. However, the film Nusselt number distribution was not only a function of bulk Reynolds number but also of the surface temperature level which varied with heat input. Investigation of point Nusselt number correlations with point Reynolds number for various angular positions on the surface disclosed a generally applicable relationship, namely,

$$Nu_f = C Re_f^n \quad (1)$$

The exponent n varied from 0.5 to 0.76, depending on the position on the surface. Similarly, preliminary plots of average film Nusselt number versus average film Reynolds number gave the expression

$$\begin{aligned} Nu_{f(ave)} &= C' [Re_{f(ave)}]^{0.62} \\ &= C' [Re_b]^{0.62} [\mu_b / \mu_{f(ave)}]^{0.62} \end{aligned} \quad (2)$$

Thus, a modified form of the average film Nusselt number could be developed which was only dependent upon the bulk Reynolds number. The modified film Nusselt number was expressed as

$$Nu_{f(ave)} [\mu_{f(ave)} / \mu_b]^{0.62}$$

Strictly speaking, the modification factor in the form $[\mu_{f(ave)} / \mu_b]^{0.62}$ was applicable only to average Nusselt number. However, its point values $(\mu_f / \mu_b)^{0.62} = \phi_\mu$ were utilized to correlate point Nusselt numbers at different surface temperatures for constant bulk Reynolds number. The exponent 0.62 was accepted as a representative average value for the entire range of the variation of exponent n in equation (1) for the purpose of simplifying the data correlation, while maintaining its accuracy within acceptable limits. The errors in modified point Nusselt numbers, due to the use of the constant exponent 0.62, were in the range between plus and minus one per cent.

Test Data Summary

Tables II to VIII contain a summary of the principal test data obtained in the investigation. The range of configurations and their dimensions are given. The variation of flow conditions was indicated by the bulk Reynolds number for each run. The individual runs are characterized by the average difference between cylinder surface temperature and cooling air as well as the maximum and minimum film temperature determined from the measured surface temperature distribution. Each run is further identified by a capital letter and a graphical point symbol which corresponds to the designation of the particular run in its graphical presentation in the figure indicated as reference at the bottom

of each column of the data tables.

Peripheral variations of the modified Nusselt number Nu_{ϕ} are presented in Figures 5 to 34 for various cylinder arrangements in ducts of different widths. For cylinder arrangements symmetrical with respect to the heated test model, distributions of Nusselt number are presented for 180 degrees of the periphery only. In this category are single, in-line, and staggered configurations. For cylinder arrangements asymmetrical with respect to the test model, i.e. staggered double-row configurations, distributions are presented for the entire circumference. The cylinder arrangements and the configurations are given as pitch dimensions in terms of the 1.5-inch diameter of the test models. The designation of configurations and arrangements may be more clearly understood by referring to Table I and Figure 4. For each cylinder arrangement, the distributions are shown at several different nominal bulk Reynolds numbers.

Some test runs listed in Tables II to VIII are not contained in the figures because they do not differ appreciably from other runs at nearest Reynolds number. Also, some of the low-Reynolds number data are not plotted because the circumferential variations of the absolute value of point Nusselt number are almost insignificant.

The tables and figures do not contain the test data obtained with in-line configuration and unequal longitudinal spacings. These tests were run for exploratory purposes and sample data are shown in Figures 39, 40 and 41 in connection with the detailed discussion of distribution curves.

Data on pressure gradients and overall pressure drops determined in the experimental investigation are not presented in summarized form. Representative pressure gradients along the duct wall for single and in-line configurations are contained in Figures 35 to 38.

A noticeable general characteristic of all distribution plots in Figures 5 to 24 appears to be the better correlation of runs at equal bulk Reynolds number but different temperature levels for low Reynolds numbers. The spread among test points for the same position becomes more appreciable at higher Reynolds numbers. This may have been due to greater turbulence and local instabilities of air flow. Some of the spread among the test points for a particular curve for a given nominal bulk Reynolds number is undoubtedly due to slight variation of the actual bulk Reynolds number for the runs at different temperature levels. This may be noted from the data in Tables II to VIII where the bulk Reynolds numbers indicated for each curve are nominally equal but may differ in some instances by as much as two per cent.

Table XI. Data Summary for Single and In-Line Cylinders in 2-Inch Dext ($S_g = 1.563$)

Configuration		Single			In-line, $S_g = 1.083$			In-line, $S_g = 1.250$			In-line, $S_g = 1.500$			In-line, $S_g = 2.000$			
Curve	Symbol	Re _p	Δp -b (ave)	t_f (min)	Re _p	Δp -b (ave)	t_f (min)	Re _p	Δp -b (ave)	t_f (min)	Re _p	Δp -b (ave)	t_f (min)	Re _p	Δp -b (ave)	t_f (min)	
A	○	51,700	138	186	138	53,200	116	174	140	32,900	151	192	135	21,150	110	158	137
	□	51,600	189	221	184	53,100	156	199	154					21,250	190	233	145
	◇	51,700	249	253	208									48,100	64	140	128
B	○	41,800	108	170	148	42,300	108	164	136	42,100	150	198	137	14,100	98	154	136
	□	42,000	169	210	179	42,300	158	236	134					14,120	200	214	177
	◇	42,000	282	249	207									42,200	134	178	133
C	○	31,550	87	152	136	32,050	88	148	124	32,150	86	141	121	10,640	106	152	136
	□	31,500	186	210	178	31,600	128	171	140	31,970	119	164	137	10,730	294	255	203
	◇	31,450	266	256	214	31,700	192	213	167	31,850	184	208	167	31,700	140	179	154
D	○	21,100	145	177	155	21,350	116	168	138	21,200	193	212	172	5,345	193	233	175
	□	20,850	220	219	190	21,500	204	230	170					5,330	284	256	218
	◇	21,200	271	281	224									21,030	103	162	145
E	○	15,800	154	188	164	15,900	106	156	138	16,000	210	212	174				
	□	15,800	221	222	195	15,780	214	221	180					15,820	97	151	138
	◇	15,790	298	257	232												
F	○	10,490	146	182	163					10,800	314	266	216				
	□	10,440	230	231	206	10,710	311	281	217					10,640	104	150	140
	◇	10,420	315	275	242									10,610	272	247	218
G	○	5,460	177	190	192	5,295	124	158	140	5,395	298	252	214				
	□	5,450	250	232	225	5,285	314	253	220					5,350	110	152	140
	◇	5,450	322	283	236									5,320	276	248	219
H	○	2,140	204	192	178												
	□	2,140	280	236	220												
	◇	2,125	372	325	255												
Ref.		Figure 8			Figure 9			Figure 9			Figure 10			Figure 11			

Table XII. Data Summary for Single and In-Line Cylinders in 3-Inch Dext ($S_g = 2.000$)

Configuration		Single			In-line, $S_g = 1.063$			In-line, $S_g = 1.250$			In-line, $S_g = 1.500$			In-line, $S_g = 2.000$			
Curve	Symbol	Re _g	Δp -b (ave)	t_f (min)	Re _g	Δp -b (ave)	t_f (min)	Re _g	Δp -b (ave)	t_f (min)	Re _g	Δp -b (ave)	t_f (min)	Re _g	Δp -b (ave)	t_f (min)	
A	○	85,100	114	169	136	74,600	81	143	131	74,050	81	144	134	74,000	79	144	138
	□	86,000	169	204	156	74,000	121	172	152	74,100	121	169	154	73,900	119	168	156
	◇	86,000	220	237	174	74,000	160	198	169	74,000	160	191	171	74,500	162	184	167
B	○	66,490	79	132	126	64,900	90	152	136	64,600	91	147	134	64,350	89	148	139
	□	66,000	190	213	157	63,900	136	186	163	63,900	134	186	164	63,700	134	178	160
	◇	66,600	250	252	180	63,500	182	214	182	63,500	180	210	184	63,400	178	225	183
C	○	53,500	87	152	126	53,400	94	154	138	53,650	94	153	138	53,350	91	154	141
	□	53,300	222	233	175	53,300	160	193	166	53,800	156	191	167	53,500	152	187	164
	◇	53,100	264	269	196	53,500	204	218	181	53,700	210	212	181	53,750	198	206	178
D	○	42,600	96	165	135	43,100	78	142	125	43,200	74	138	123	43,200	72	135	124
	□	42,500	188	220	171	43,000	155	194	161	42,250	150	189	164	42,950	142	177	156
	◇	42,600	268	268	201	43,000	222	235	183	43,000	214	225	183	42,900	202	216	185
E	○	31,950	97	156	132	32,250	83	146	128	31,050	79	143	129	32,200	74	139	128
	□	31,850	206	225	178	31,950	178	208	169	31,950	169	198	170	32,000	180	189	166
	◇	31,850	290	270	208	32,300	242	247	194	32,150	234	237	198	31,800	219	224	192
F	○	21,300	116	172	146	21,350	166	199	166	21,350	159	192	168	21,350	153	183	166
	□	20,950	184	216	179	21,100	214	233	191	21,170	206	224	192	21,200	199	213	186
	◇	21,350	275	273	213	21,520	248	254	202	21,400	259	247	208	21,660	251	244	194
G	○	15,890	164	194	164	10,640	154	188	160	10,720	151	172	155	10,600	146	178	161
	□	15,820	240	239	198	10,640	244	235	199	10,680	237	222	196	10,600	229	221	197
	◇	15,910	314	276	226	10,620	314	273	228	10,650	298	265	228	10,520	294	260	227
H	○	10,690	106	147	130	5,310	135	166	153	5,360	134	162	150	5,335	133	165	152
	□	10,560	260	242	208	5,290	222	217	194	5,380	220	209	191	5,330	210	207	189
	◇	10,510	325	281	240	5,295	347	285	247	5,310	339	273	247	5,310	324	270	243
I	○	5,340	98	140	130												
	□	5,305	229	214	193												
	◇	5,315	352	279	230												
Ref.		Figure 6			Figure 12			Figure 13			Figure 14			Figure 15			

Table IV. Data Summary for Single and In-Line Cylinders in 3.5-Inch Duct ($S_T = 2.333$)

Configuration			Single						In-line, $S_T = 1.034$						In-line, $S_T = 1.240$						In-line, $S_T = 1.500$						In-line, $S_T = 2.000$														
Curve	Symbol	Re ₀	$\Delta p = b(\text{ave})$			$t_f(\text{max})$			$t_f(\text{min})$			Re ₀	$\Delta p = b(\text{ave})$			$t_f(\text{max})$			$t_f(\text{min})$			Re ₀	$\Delta p = b(\text{ave})$			$t_f(\text{max})$			$t_f(\text{min})$			Re ₀	$\Delta p = b(\text{ave})$			$t_f(\text{max})$			$t_f(\text{min})$		
A	○	62,800	108	171	140	62,100	83	153	142	62,500	78	130	140	62,450	78	150	140	62,400	79	145	142	62,400	79	145	142	62,400	79	145	142	62,400	79	145	142	62,400	79	145	142				
	□	62,600	236	250	186	62,350	174	209	183	63,100	175	196	176	63,000	172	195	177	63,000	177	194	180	63,000	177	194	180	63,000	177	194	180	63,000	177	194	180	63,000	177	194	180				
B	○	53,200	118	177	144	51,250	93	158	143	52,000	90	155	144	52,000	86	156	145	51,800	91	156	148	52,000	91	156	148	52,000	91	156	148	52,000	91	156	148	52,000	91	156	148				
	□	53,050	256	264	198	52,200	184	222	189	52,400	200	216	190	52,400	197	214	189	52,400	199	209	192	52,400	199	209	192	52,400	199	209	192	52,400	199	209	192	52,400	199	209	192				
C	○	41,400	126	186	152	41,450	106	171	152	41,500	100	166	152	41,500	100	162	150	41,600	98	158	150	41,600	98	158	150	41,600	98	158	150	41,600	98	158	150	41,600	98	158	150				
	□	41,450	262	268	205	41,600	222	240	200	42,200	213	216	186	42,200	204	210	184	42,200	204	205	188	42,200	204	205	188	42,200	204	205	188	42,200	204	205	188	42,200	204	205	188				
D	○	31,100	139	192	158	31,450	122	174	150	31,450	117	168	151	31,420	110	162	148	31,450	110	160	150	31,450	110	160	150	31,450	110	160	150	31,450	110	160	150	31,450	110	160	150				
	□	31,000	269	273	215	31,450	238	242	196	31,400	234	234	199	31,550	215	218	191	31,600	214	212	193	31,600	214	212	193	31,600	214	212	193	31,600	214	212	193	31,600	214	212	193				
E	○	20,800	156	202	170	20,900	143	186	162	21,200	143	175	155	21,170	154	166	152	21,150	127	165	152	21,150	127	165	152	21,150	127	165	152	21,150	127	165	152	21,150	127	165	152				
	□	20,600	312	274	218	21,000	278	266	218	21,000	278	266	218	21,000	256	241	212	21,000	251	238	216	21,000	251	238	216	21,000	251	238	216	21,000	251	238	216	21,000	251	238	216				
F	○	10,550	176	190	164	10,590	160	190	170	10,540	162	189	172	10,510	140	184	167	10,530	147	180	167	10,530	147	180	167	10,530	147	180	167	10,530	147	180	167	10,530	147	180	167				
	□	10,520	329	276	234	10,580	306	270	234	10,580	308	266	235	10,550	290	258	228	10,600	282	251	228	10,600	282	251	228	10,600	282	251	228	10,600	282	251	228	10,600	282	251	228				
G	○	5,305	202	197	178	5,275	196	197	180	5,300	193	193	176	5,170	182	198	183	5,170	176	194	182	5,170	176	194	182	5,170	176	194	182	5,170	176	194	182	5,170	176	194	182				
	□	5,290	377	292	264	5,260	375	296	268	5,250	369	293	263	5,240	348	285	256	5,240	339	279	256	5,240	339	279	256	5,240	339	279	256	5,240	339	279	256	5,240	339	279	256				
H	○	1,770	218	204	192																																				
	□	1,765	390	296	274																																				
Ref.	Figure 7						Figure 17						Figure 19						Figure 16						Figure 18																

Table V. Data Summary for Staggered Cylinders in 2-Inch Duct

Configuration, staggered		$S_T = 1.333$ $S_L = 0.957, S_D = 1.167$						$S_T = 1.333$ $S_L = 1.633, S_D = 1.240$						$S_T = 1.333$ $S_L = 1.945, S_D = 1.500$							
Curve	Symbol	Re ₀	Δp (ave)			t_f (max)	t_f (min)	Re ₀	Δp (ave)			t_f (max)	t_f (min)	Re ₀	Δp (ave)			t_f (max)	t_f (min)		
A	○	35,700	97	157	138	40,000	99	164	143	38,800	102	164	143	38,800	102	164	143	38,800	102	164	143
	□	35,400	128	176	150	39,950	126	182	154	38,600	134	183	157	38,600	134	183	157	38,600	134	183	157
	◇	35,800	160	194	162	40,000	162	201	166	38,950	170	202	170	38,950	170	202	170	38,950	170	202	170
B	○	31,500	98	161	140	31,200	105	166	144	31,800	109	161	140	31,800	109	161	140	31,800	109	161	140
	□	31,500	190	190	159	31,150	162	200	166	31,750	168	194	163	31,750	168	194	163	31,750	168	194	163
	◇	31,590	176	204	168	31,190	191	216	178	31,750	208	210	173	31,750	208	210	173	31,750	208	210	173
C	○	21,100	123	171	145	20,850	129	182	157	21,200	138	174	150	21,200	138	174	150	21,200	138	174	150
	□	21,050	162	196	163	20,820	170	203	173	21,200	184	200	168	21,200	184	200	168	21,200	184	200	168
	◇	21,050	223	228	185	20,830	213	238	196	21,190	246	237	198	21,190	246	237	198	21,190	246	237	198
D	○	15,610	131	179	153	15,540	135	183	161	15,650	141	186	162	15,650	141	186	162	15,650	141	186	162
	□	15,600	178	207	174	15,580	182	213	182	15,650	194	216	184	15,650	194	216	184	15,650	194	216	184
	◇	15,590	240	241	196	15,500	249	251	208	15,620	258	253	212	15,620	258	253	212	15,620	258	253	212
E	○	10,590	148	180	154	10,400	153	185	160	10,650	162	175	153	10,650	162	175	153	10,650	162	175	153
	□	10,590	202	208	174	10,400	206	215	160	10,610	218	212	162	10,610	218	212	162	10,610	218	212	162
	◇	10,620	272	246	201	10,400	280	282	206	10,605	294	284	213	10,605	294	284	213	10,605	294	284	213
F	○	5,260	175	192	167	5,235	184	202	174	5,310	196	200	175	5,310	196	200	175	5,310	196	200	175
	□	5,245	249	232	198	5,245	262	247	208	5,330	282	246	210	5,330	282	246	210	5,330	282	246	210
	◇	5,195	238	253	215	5,330	304	260	216	5,340	325	268	227	5,340	325	268	227	5,340	325	268	227
G	○	2,109	153	174	158	2,120	162	176	158	2,121	165	191	172	2,121	165	191	172	2,121	165	191	172
	□	2,110	216	206	194	2,131	224	208	182	2,121	234	228	200	2,121	234	228	200	2,121	234	228	200
	◇	2,115	314	257	227	2,115	322	264	228	2,121	380	290	252	2,121	380	290	252	2,121	380	290	252
Ref.		Figure 20						Figure 21						Figure 22							

Table VI. Data Summary for Staggered Cylinders in 3-Inch and 3.5-Inch Ducts

Configuration, staggered		$S_T = 2.000$ $S_L = 0.576, S_D = 1.153$						$S_T = 2.000$ $S_L = 1.000, S_D = 1.413$						$S_T = 2.333$ $S_L = 0.673, S_D = 1.347$						$S_T = 2.333$ $S_L = 1.167, S_D = 1.650$					
		Curve Symbol		Rep	$\Delta s-b(ave)$ $t_f(max)$ $t_f(min)$	Rep		$\Delta s-b(ave)$ $t_f(max)$ $t_f(min)$	Rep		$\Delta s-b(ave)$ $t_f(max)$ $t_f(min)$	Rep		$\Delta s-b(ave)$ $t_f(max)$ $t_f(min)$	Rep		$\Delta s-b(ave)$ $t_f(max)$ $t_f(min)$								
A	○	27,820	128	170	146	73,800	134	168	152	51,750	57	143	134	62,500	73	147	137								
	□	27,810	156	190	160		152	170	160	128	188	164	62,500	162	196	176									
B	○	21,530	114	163	140	64,500	150	178	160	41,300	62	130	139	52,100	81	150	142								
	□	21,500	159	212	174	64,530	175	192	170	41,300	132	191	168	52,050	181	205	185								
C	○	16,100	149	173	138	53,750	164	186	166	40,410	71	152	138	41,850	88	154	143								
	□	15,790	224	254	182	53,950	201	205	182	40,410	140	192	166	42,000	186	204	182								
D	○	10,600	153	150	156	43,150	176	190	167	20,980	85	150	135	31,200	98	162	149								
	□	10,490	236	248	194	43,130	218	216	188	20,950	164	199	168	31,200	192	214	191								
E	○	5,340	69	129	119	32,000	187	206	180	10,300	99	163	146	21,000	116	167	152								
	□	5,305	180	195	169	32,100	238	233	202	10,310	194	218	184	20,980	227	230	202								
F	○	2,190	173	172	152	21,220	209	220	193	5,220	126	177	159	10,330	126	180	165								
	□	2,140	180	188	168	21,000	274	256	222	5,245	244	244	209	10,320	246	246	218								
G	○					10,700	242	226	196	1,745	160	188	172	5,250	154	181	166								
	□					10,630	257	261	224	1,745	303	266	238	5,245	299	262	234								
H	○					5,340	270	238	209					1,780	178	183	171								
	□					5,305	331	274	242					1,770	330	267	246								
I	○					2,175	230	204	188																
	□					2,170	273	280	234																
Ref.		Figure 23				Figure 24				Figure 25				Figure 26											

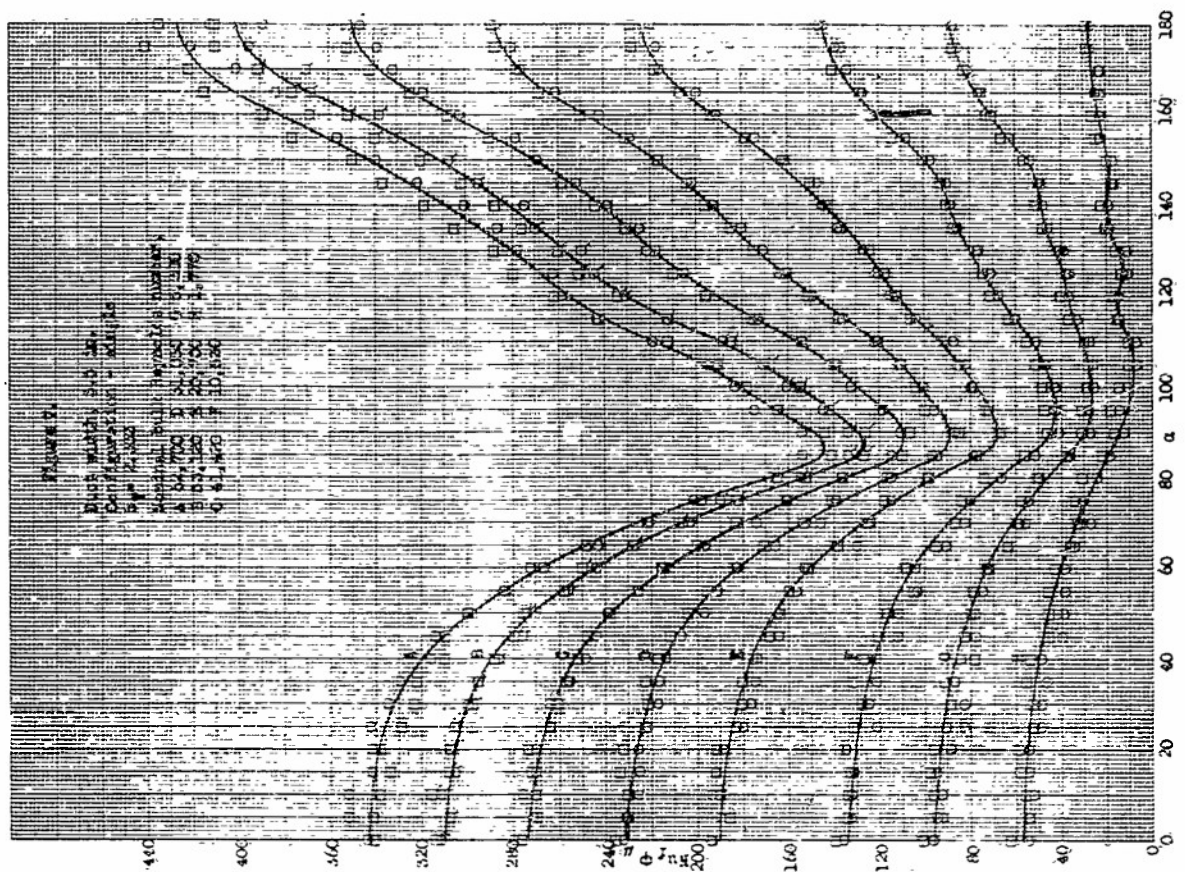
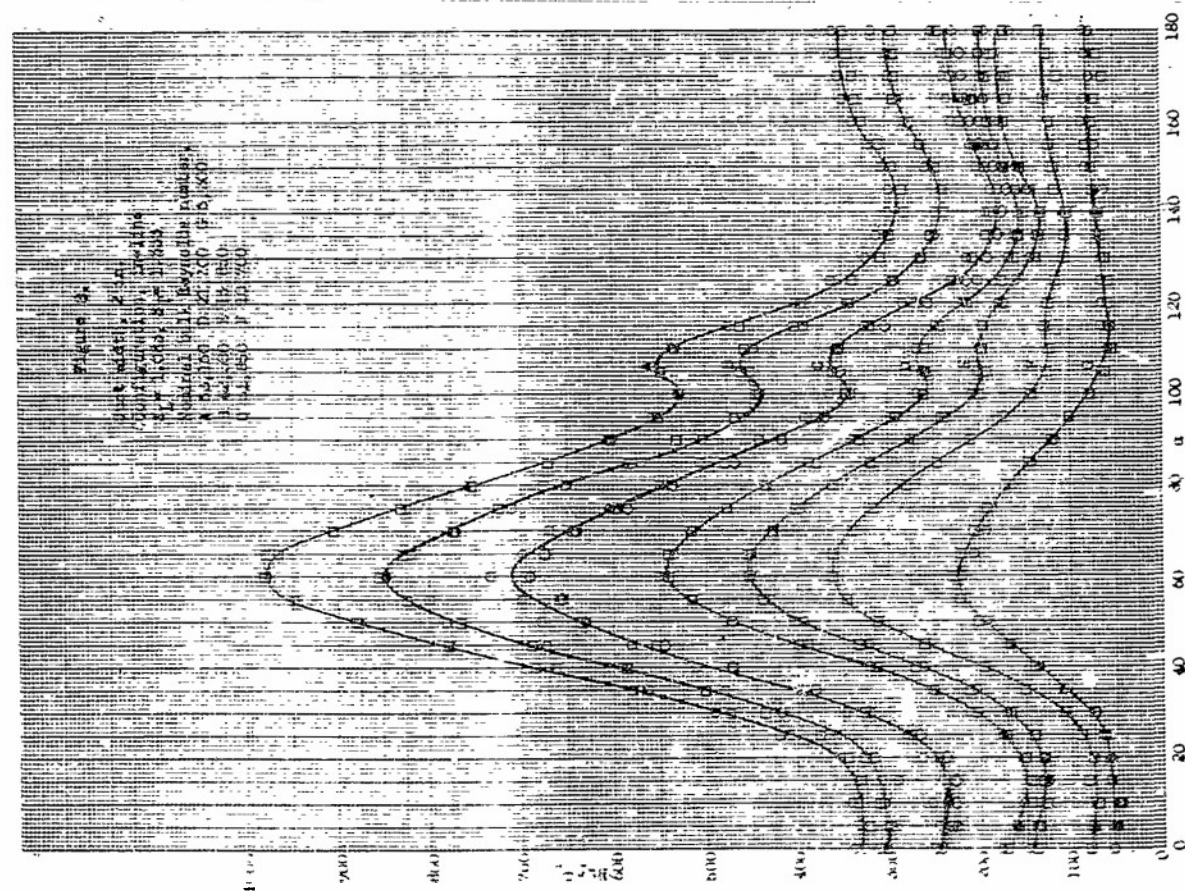
Table VII. Data Summary for Double-Row Staggered Cylinders in 3-Inch and 3.5-Inch Ducts

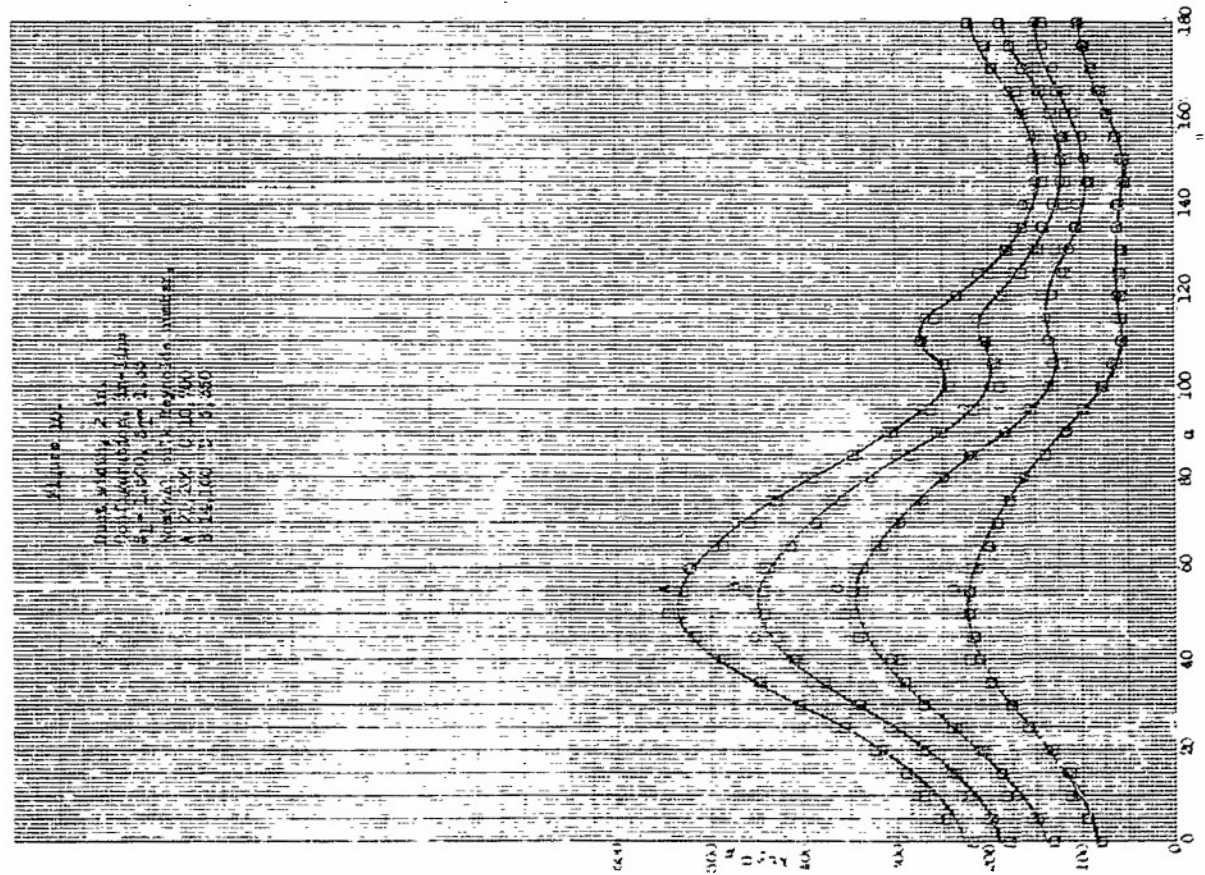
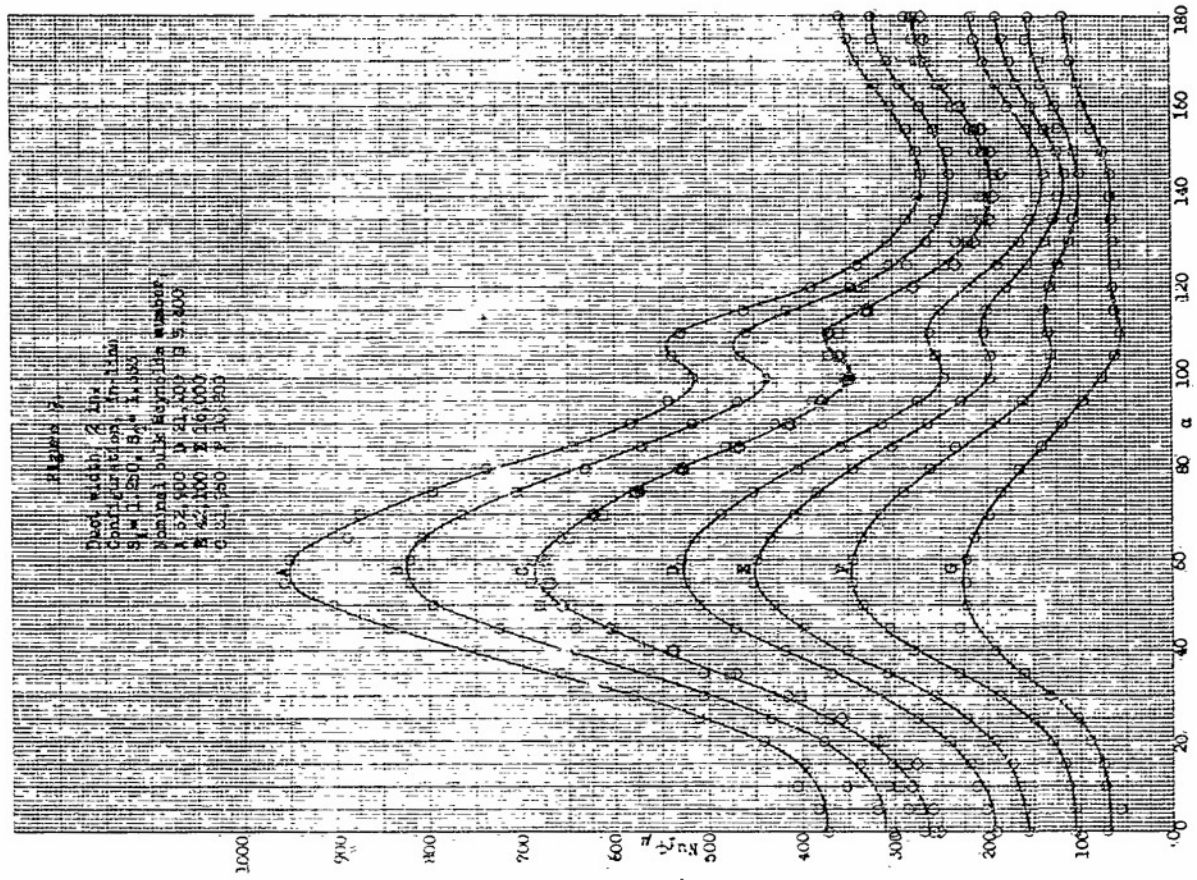
Duct Width			3 Inches												3.5 Inches																	
Configuration, stagger, double-row			$S_T = 0.667$ $S_L = 0.333, S_D = 1.083$						$S_T = 0.667$ $S_L = 1.033, S_D = 1.250$						$S_T = 0.667$ $S_L = 1.343, S_D = 1.500$						$S_T = 1.000$ $S_L = 0.576, S_D = 1.153$						$S_T = 1.000$ $S_L = 1.000, S_D = 1.413$					
Curve	Symbol	Side	Rep	$\Delta s-b(ave)$	$t_f(max)$	$t_f(min)$	Rep	$\Delta s-b(ave)$	$t_f(max)$	$t_f(min)$	Rep	$\Delta s-b(ave)$	$t_f(max)$	$t_f(min)$	Rep	$\Delta s-b(ave)$	$t_f(max)$	$t_f(min)$	Rep	$\Delta s-b(ave)$	$t_f(max)$	$t_f(min)$	Rep	$\Delta s-b(ave)$	$t_f(max)$	$t_f(min)$	Rep	$\Delta s-b(ave)$	$t_f(max)$	$t_f(min)$		
A	○	L	38,400	122	191	147	54,000	151	179	144	73,300	112	169	140	41,950	79	150	130	52,500	74	144	128	38,400	122	191	147	54,000	151	179	144		
	○	R	38,600	112	169	148	54,000	128	169	152	73,300	108	165	149	42,000	75	148	132	52,300	76	147	142	38,600	112	169	148	54,000	128	169	152		
	□	L	38,400	149	208	157	53,450	158	200	158	74,450	150	188	150	41,950	126	180	150	52,500	146	186	157	38,400	149	208	157	53,450	158	200	158		
	□	R	38,400	158	186	160	53,490	156	188	168	74,300	153	182	160	41,900	120	178	153	52,500	150	190	166	38,400	158	186	160	53,490	156	188	168		
B	○	L	32,000	124	183	137	43,000	136	183	150	64,050	132	178	143	31,400	96	163	132	42,100	87	148	130	32,000	124	183	137	43,000	136	183	150		
	○	R	31,850	117	166	144	43,000	137	177	159	64,000	136	174	156	31,400	93	163	135	42,100	89	152	136	31,850	117	166	144	43,000	137	177	159		
	□	L	31,950	156	206	151	43,100	169	205	162	64,100	164	196	153	31,300	180	218	165	42,300	172	194	164	31,950	156	206	151	43,100	169	205	162		
	□	R	31,800	145	182	157	43,100	170	193	174	64,500	167	188	166	31,400	178	216	168	42,300	174	201	172	31,800	145	182	157	43,100	170	193	174		
C	○	L	21,450	144	191	145	31,800	147	190	154	53,500	150	190	152	20,750	108	178	147	31,600	100	153	137	21,450	144	191	145	31,800	147	190	154		
	○	R	21,450	134	168	145	31,820	148	183	163	53,550	154	182	162	20,780	108	174	148	31,600	101	161	144	21,450	134	168	145	31,820	148	183	163		
	□	L	21,610	184	216	158	31,950	184	217	174	53,000	186	214	170	21,000	240	247	185	31,600	204	214	180	21,610	184	216	158	31,950	184	217	174		
	□	R	21,350	174	190	158	31,950	187	205	184	53,050	190	208	183	21,000	226	244	185	31,600	210	225	192	21,350	174	190	158	31,950	187	205	184		
D	○	L	10,500	176	210	168	21,190	166	204	169	42,530	181	210	169	10,400	136	185	154	21,050	114	162	140	10,500	176	210	168	21,190	166	204	169		
	○	R	10,500	180	200	178	21,200	168	198	176	42,500	187	203	180	10,410	138	185	156	21,100	116	166	148	10,500	180	200	178	21,200	168	198	176		
	□	L	10,500	210	230	180	21,300	214	229	183	42,530	223	234	186	10,370	282	268	210	21,050	249	236	196	10,500	210	230	180	21,300	214	229	183		
	□	R	10,500	214	220	195	21,200	219	226	196	42,700	229	226	198	10,370	278	272	212	21,050	250	243	207	10,500	214	220	195	21,200	219	226	196		
E	○	L	5,255	199	221	184	10,410	205	228	192	31,600	193	223	183	5,245	160	189	162	10,310	129	182	160	5,255	199	221	184	10,410	205	228	192		
	○	R	5,300	207	208	183	10,410	204	226	200	31,600	200	220	196	5,225	160	190	168	10,320	123	175	163	5,300	207	208	183	10,410	204	226	200		
	□	L	5,250	236	248	202	10,410	240	230	207	31,650	245	230	204	5,250	312	274	228	10,280	282	270	228	5,250	236	248	202	10,410	240	230	207		
	□	R	5,255	256	236	207	10,410	240	246	216	31,610	250	247	216	5,230	313	272	228	10,280	274	265	231	5,255	256	236	207	10,410	240	246	216		
F	○	L	2,142	189	195	164	5,250	233	236	196	21,230	219	225	187	1,751	176	191	170	5,245	168	194	171	2,142	189	195	164	5,250	233	236	196		
	○	R	2,175	185	182	162	5,285	232	226	203	21,300	221	223	197	1,770	180	188	170	5,260	166	187	173	2,175	185	182	162	5,285	232	226	203		
	□	L	2,119	305	263	219	5,305	252	234	216	21,400	282	257	209	1,761	372	296	258	5,310	320	282	242	2,119	305	263	219	5,305	252	234	216		
	□	R	2,165	298	245	212	5,300	285	254	228	21,300	286	255	222	1,759	370	293	262	5,310	313	272	246	2,165	298	245	212	5,300	285	254	228		
G	○	L					2,122	208	210	182	10,470	270	259	213					1,751	204	197	177										
	○	R					2,120	209	206	190	10,500	268	250	222					1,782	202	190	177										
	□	L					2,120	330	280	240	10,510	319	286	252					1,773	398	300	267										
	□	R					2,121	330	272	247	10,500	313	274	240					1,770	385	291	266										
H	○	L									5,345	296	255	210																		
	○	R									5,330	289	246	220																		
	□	L									5,295	369	294	242																		
	□	R									5,295	354	283	251																		
I	○	L									2,121	252	227	197																		
	○	R									2,120	244	223	206																		
	□	L									2,139	397	300	258																		
	□	R									2,139	390	293	255																		
Fig. 27			Figure 28						Figure 29						Figure 30						Figure 31											

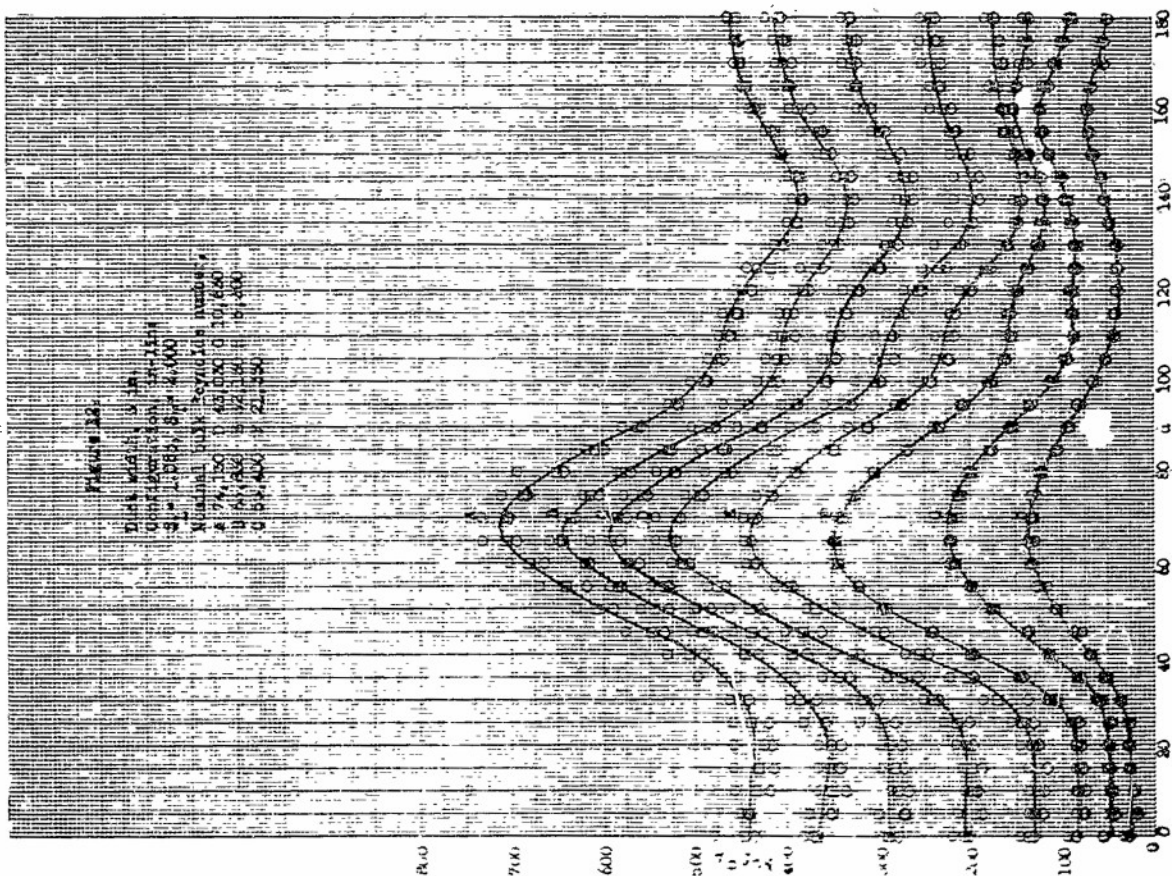
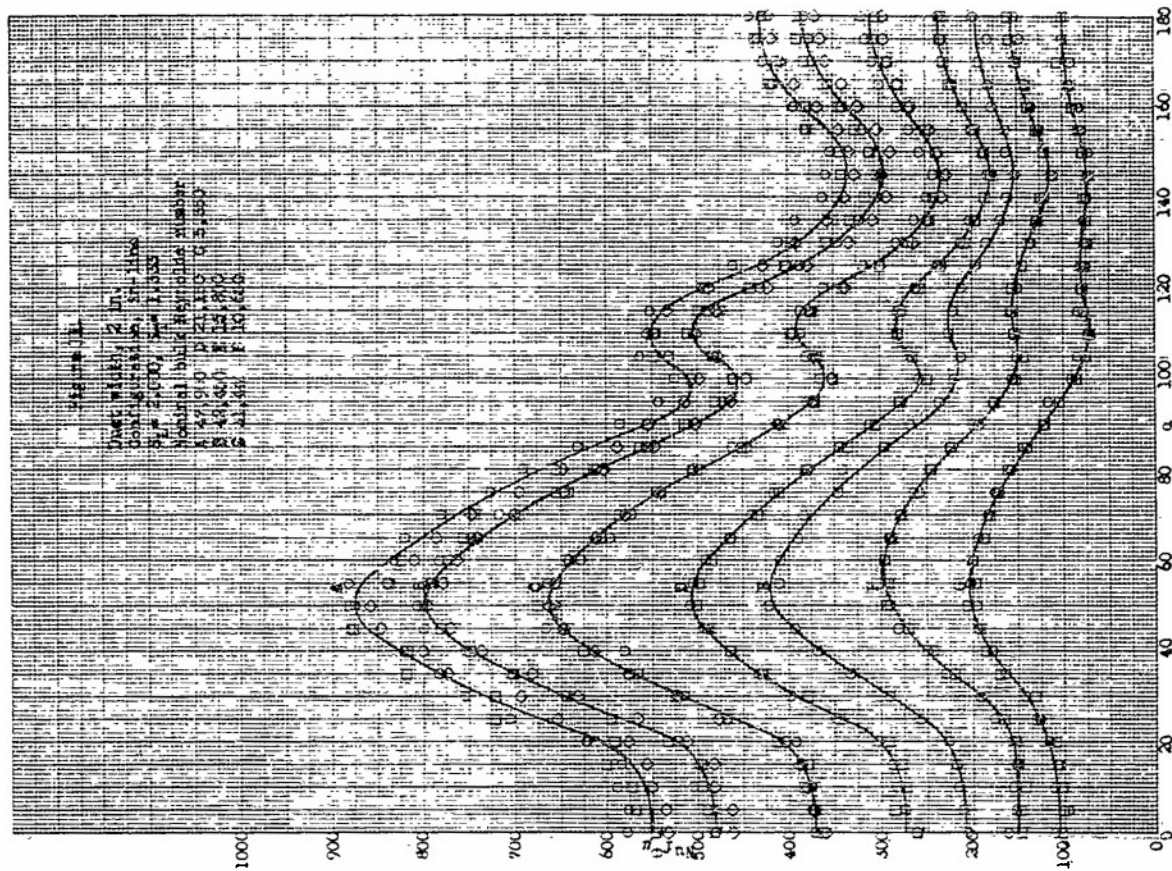
Table VIII. Data Summary for Single Cylinder in 3-Inch, 4-Inch and 6-Inch Duct ($S_T = 2.000, 2.666, 4.000$)

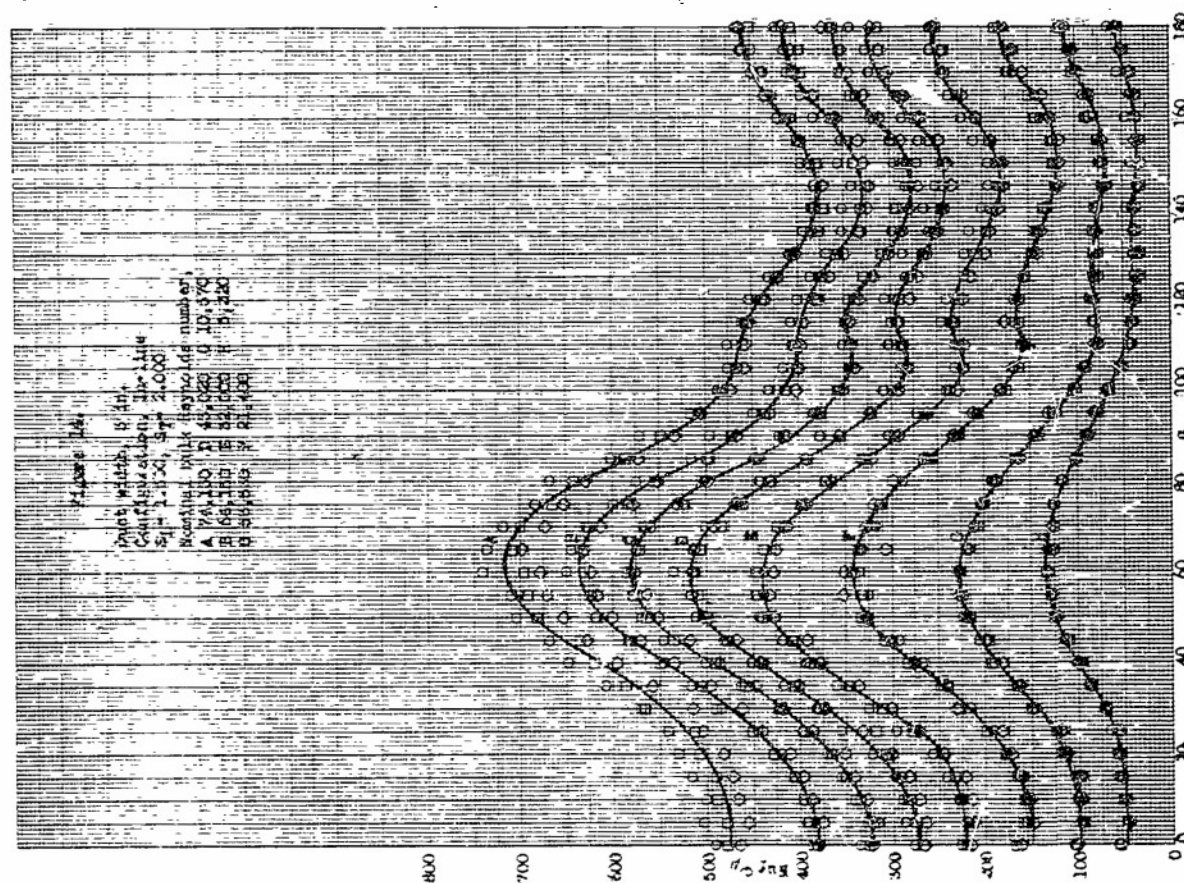
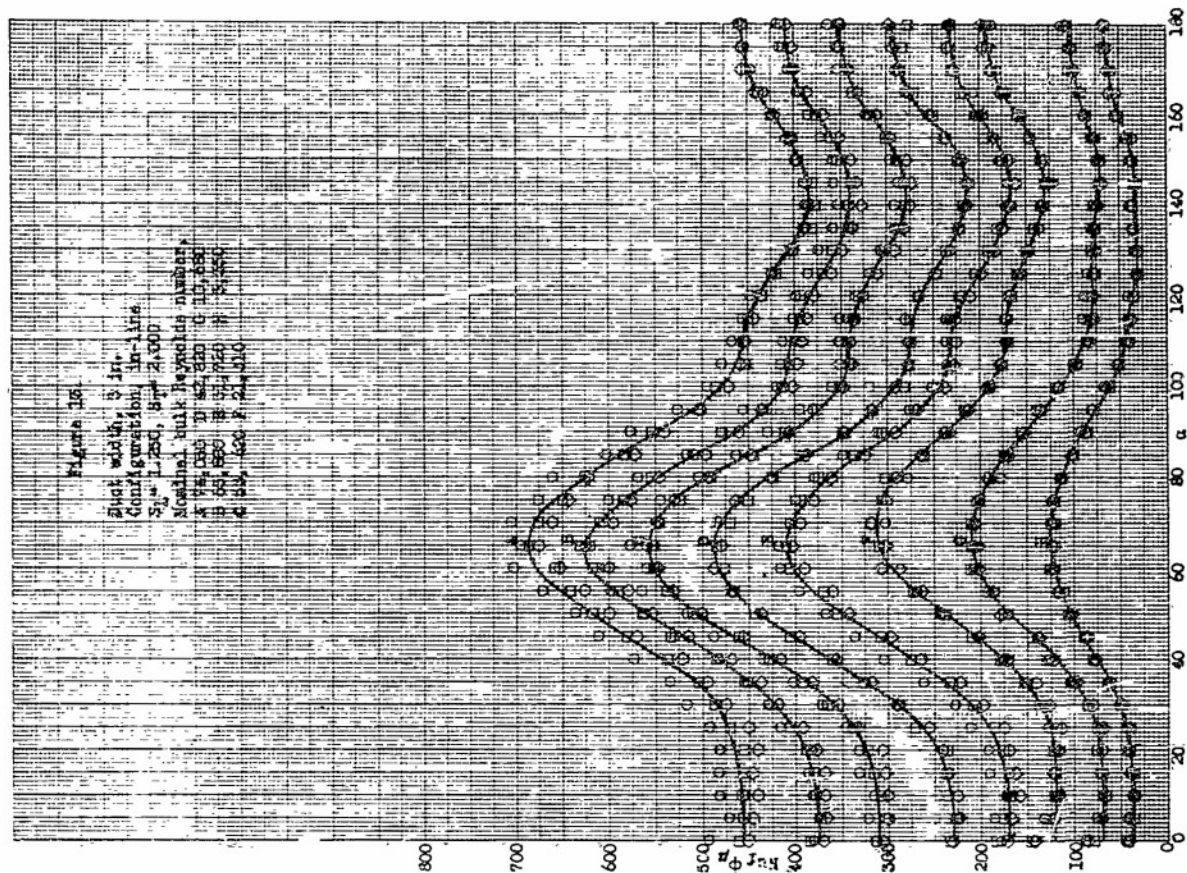
Configur		a	Single, $S_T = 2.000$			Single, $S_T = 2.667$			Single, $S_T = 4.000$				
Curve	Symbol	Rep	$\Delta s-b(ave)$			$\Delta s-b(ave)$			$\Delta s-b(ave)$				
			$t_f(max)$	$t_f(min)$		$t_f(max)$	$t_f(min)$		$t_f(max)$	$t_f(min)$			
A	○	63,710	219	222	190	62,425	32	143	133	42,000	144	197	166
	□									42,230	244	262	209
B	○	53,400	223	228	192	52,250	133	183	163	31,535	134	206	173
C	○	42,050	236	248	198	41,550	138	193	171	21,930	248	265	202
D	○	31,560	36	131	116	31,600	144	197	167	10,380	244	242	191
	□					31,445	246	266	215				
E	○	21,135	260	256	194	20,900	59	144	127				
	□					20,950	144	197	160				
	◇					20,950	246	261	200				
F	○	10,450	237	256	204	10,350	244	256	205				
Ref.		Figure 32			Figure 33			Figure 34					

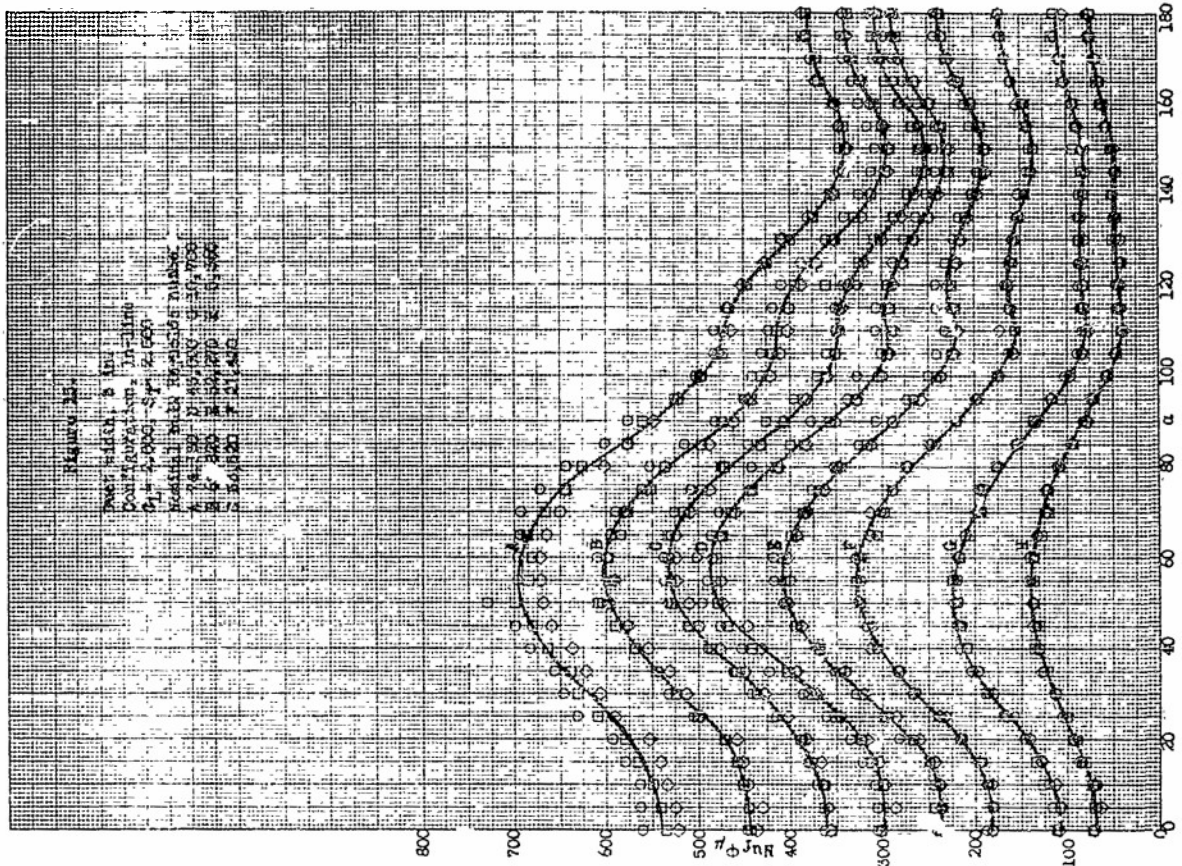
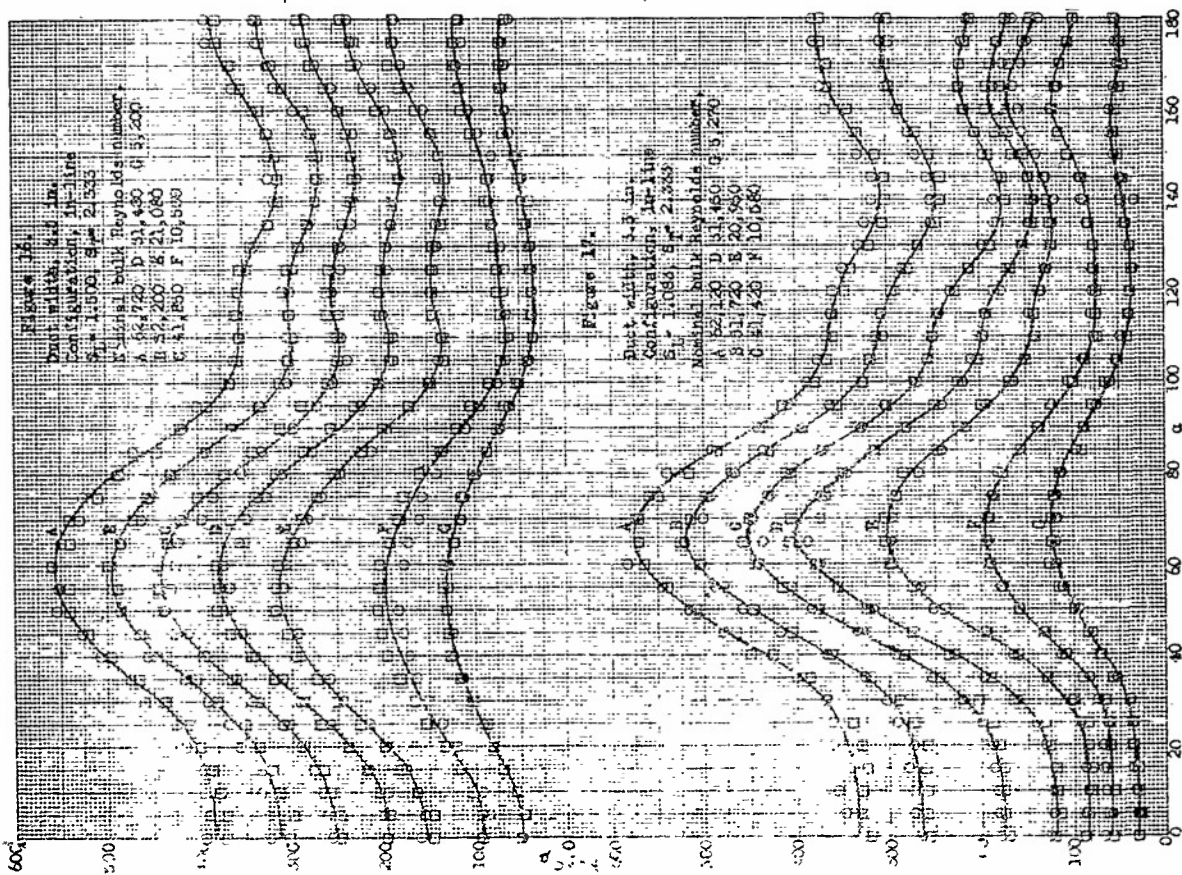
Note: These data were obtained with test cylinder A located in the steel test ducts. As mentioned in the text, the reliability of these data is doubtful. However, for purpose of comparison with reference data, these results are qualitatively acceptable.

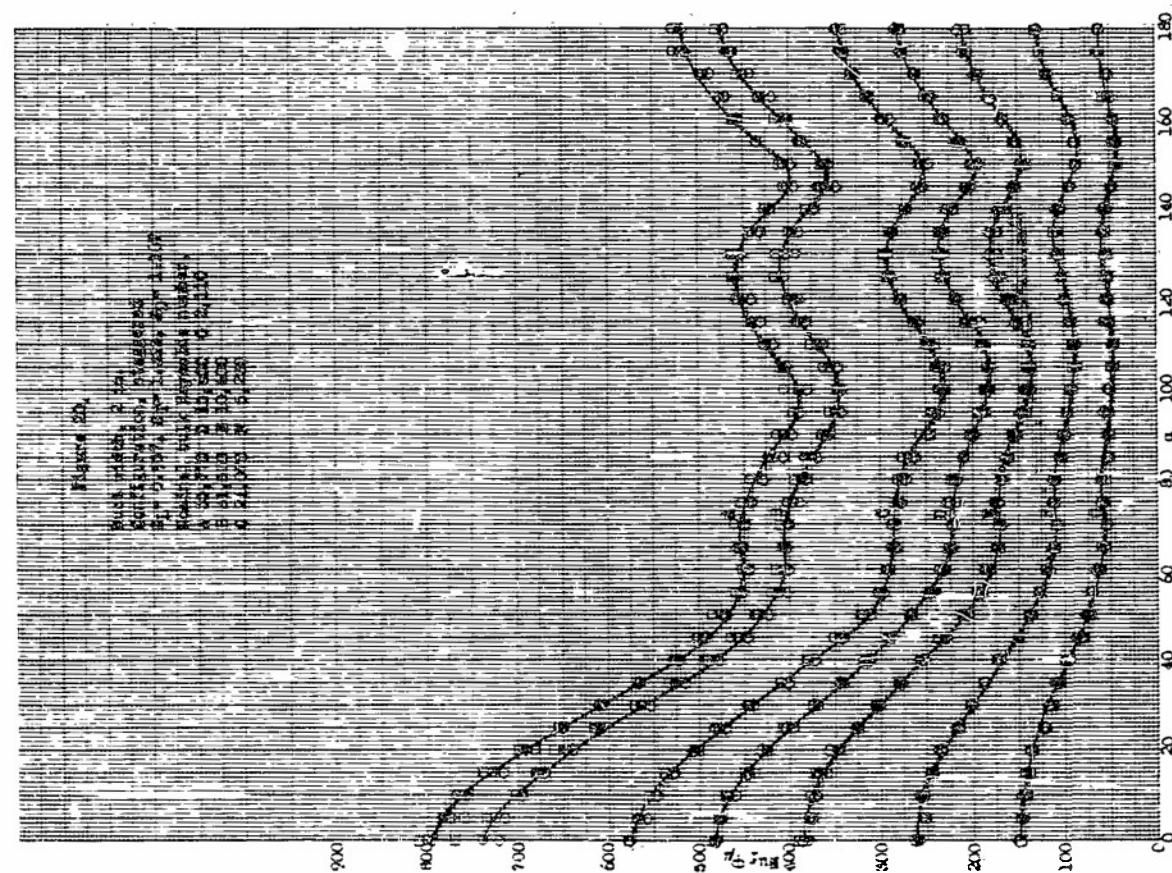
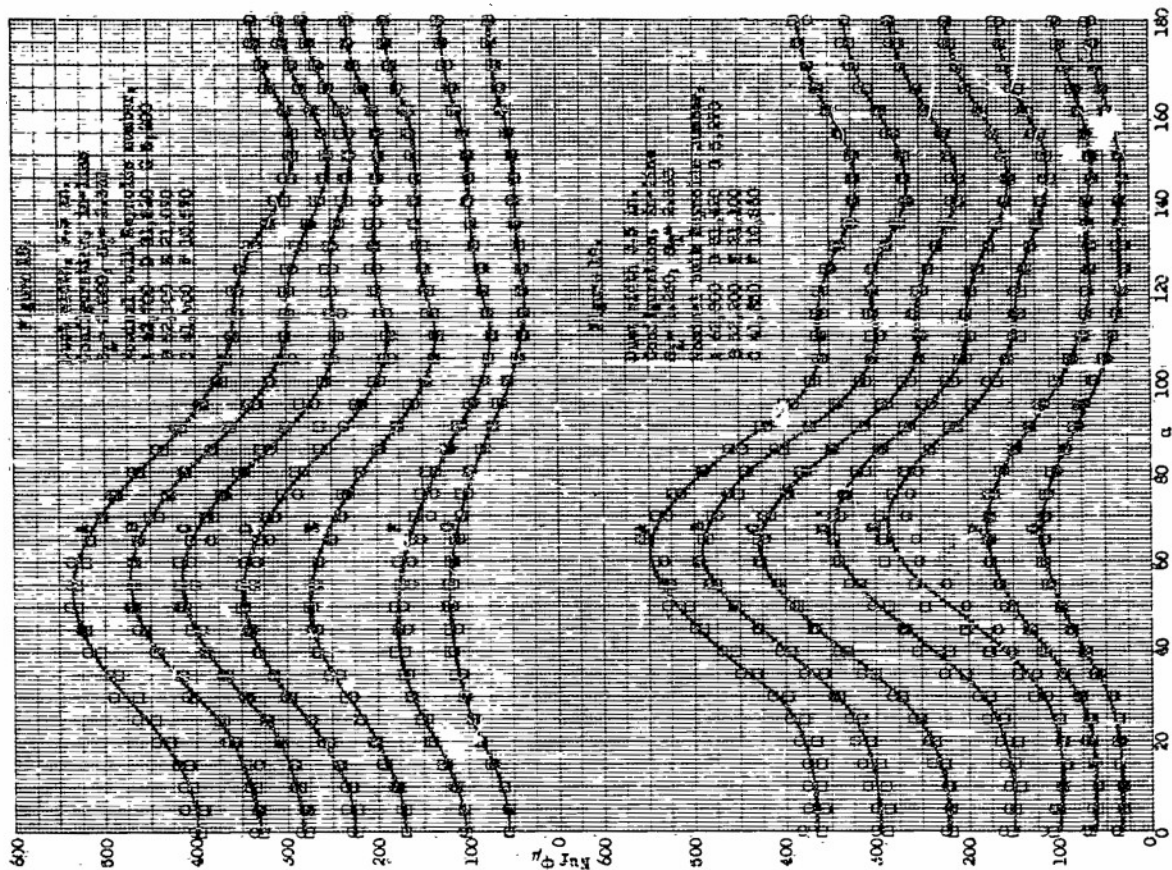


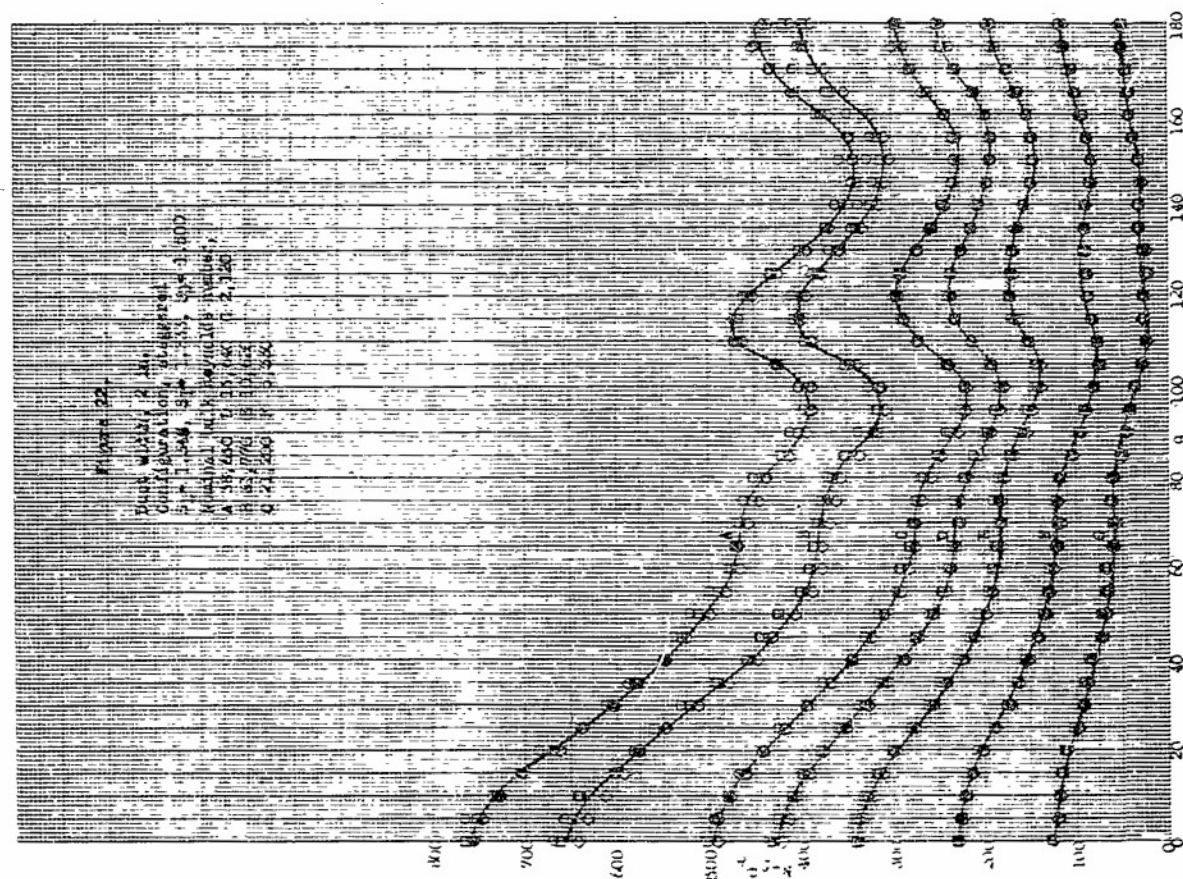
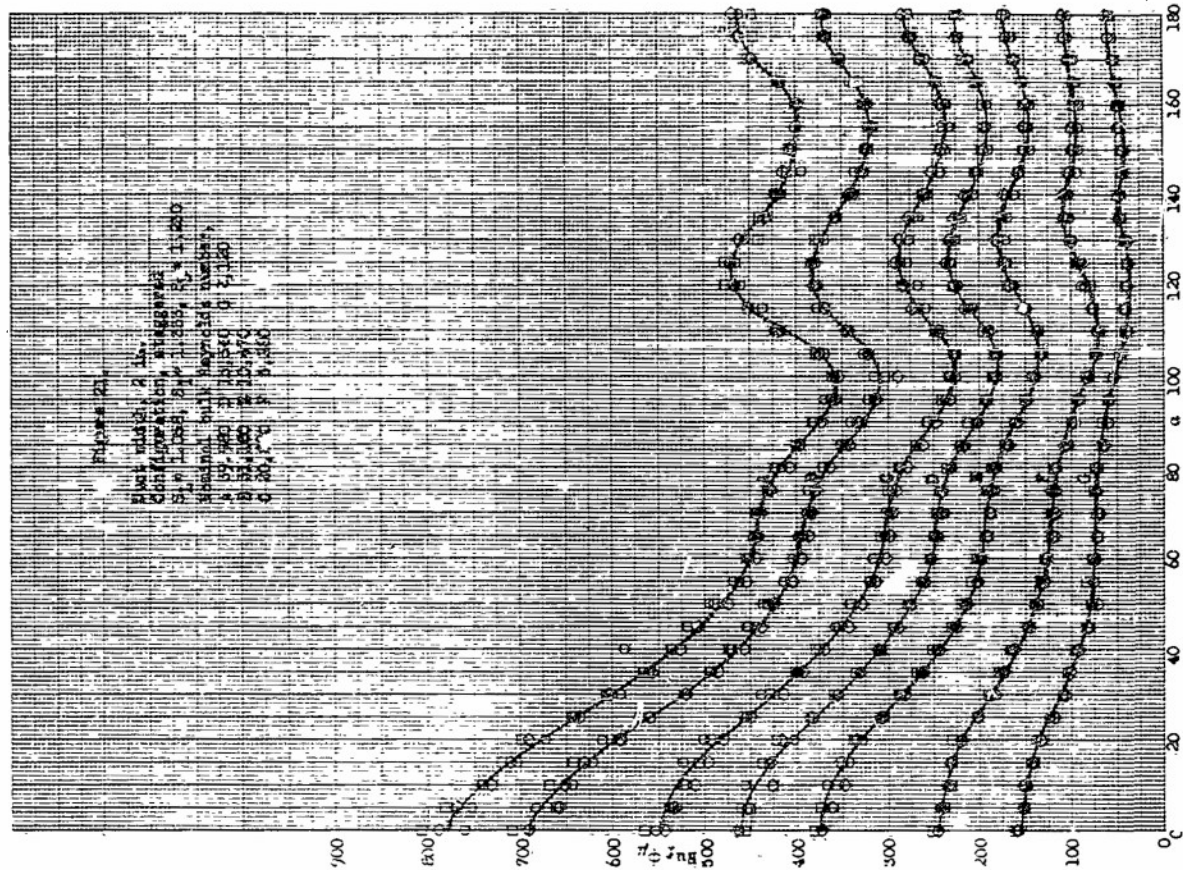


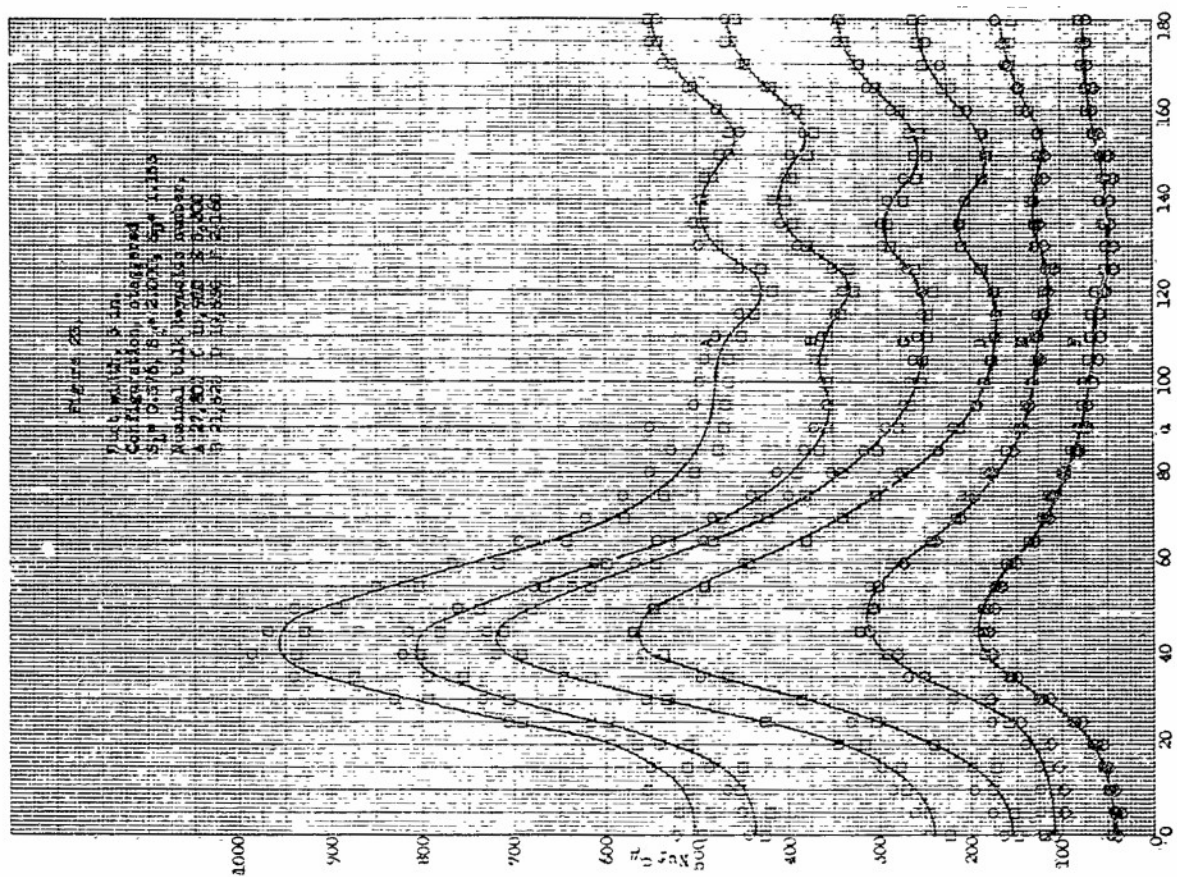
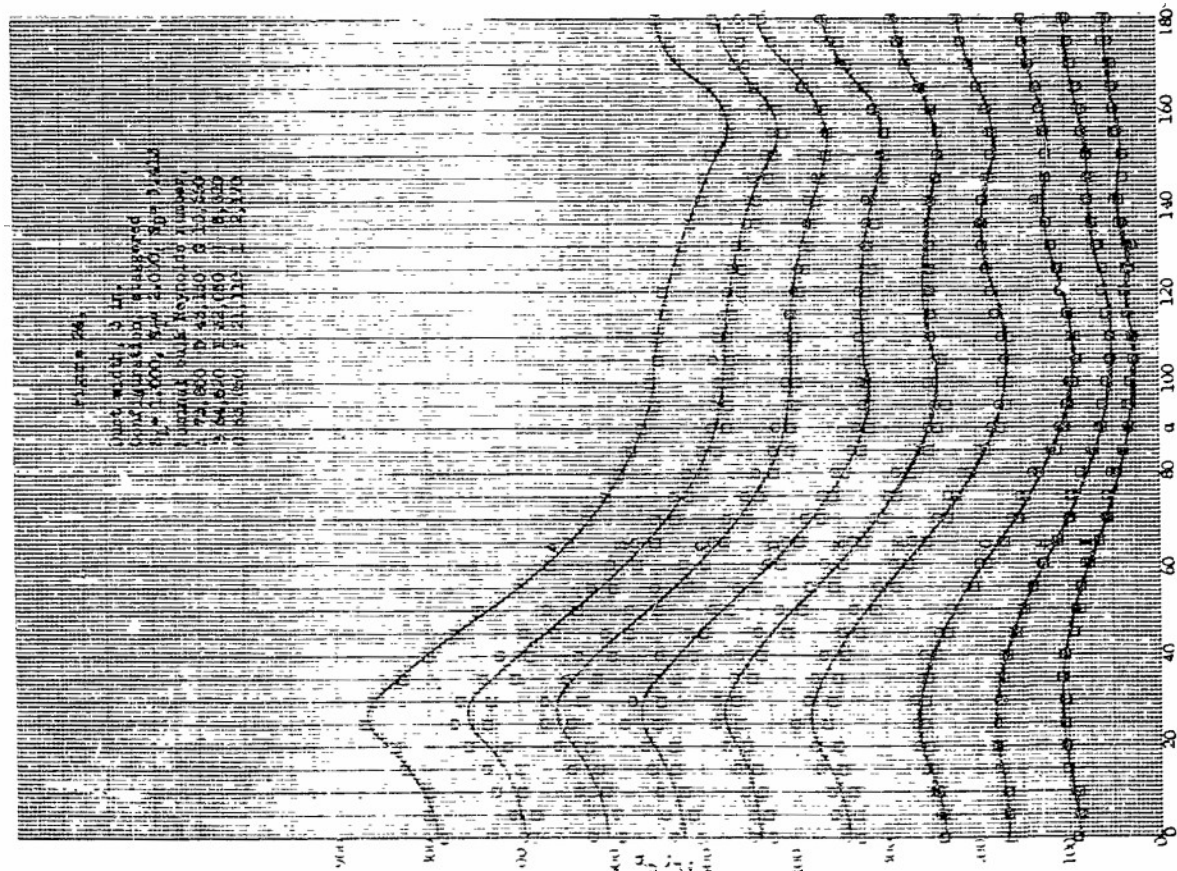


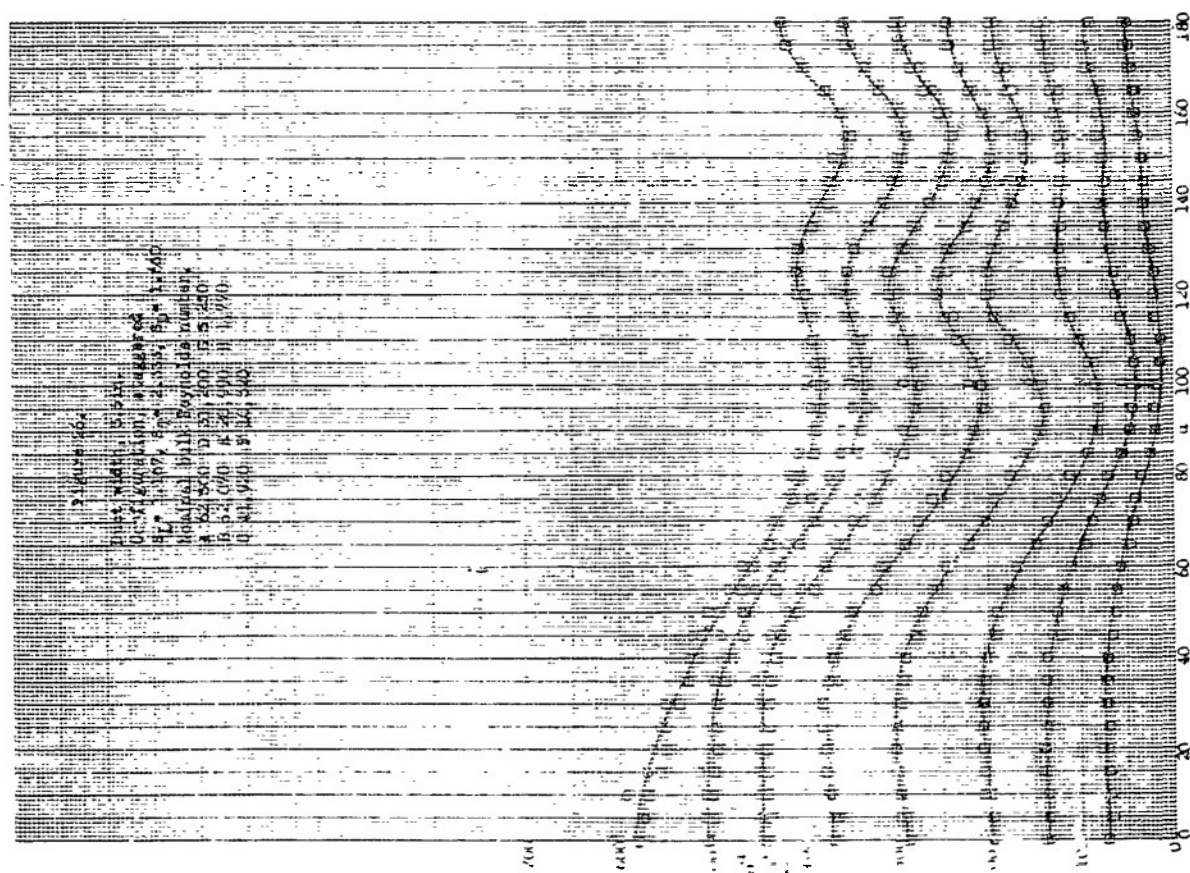
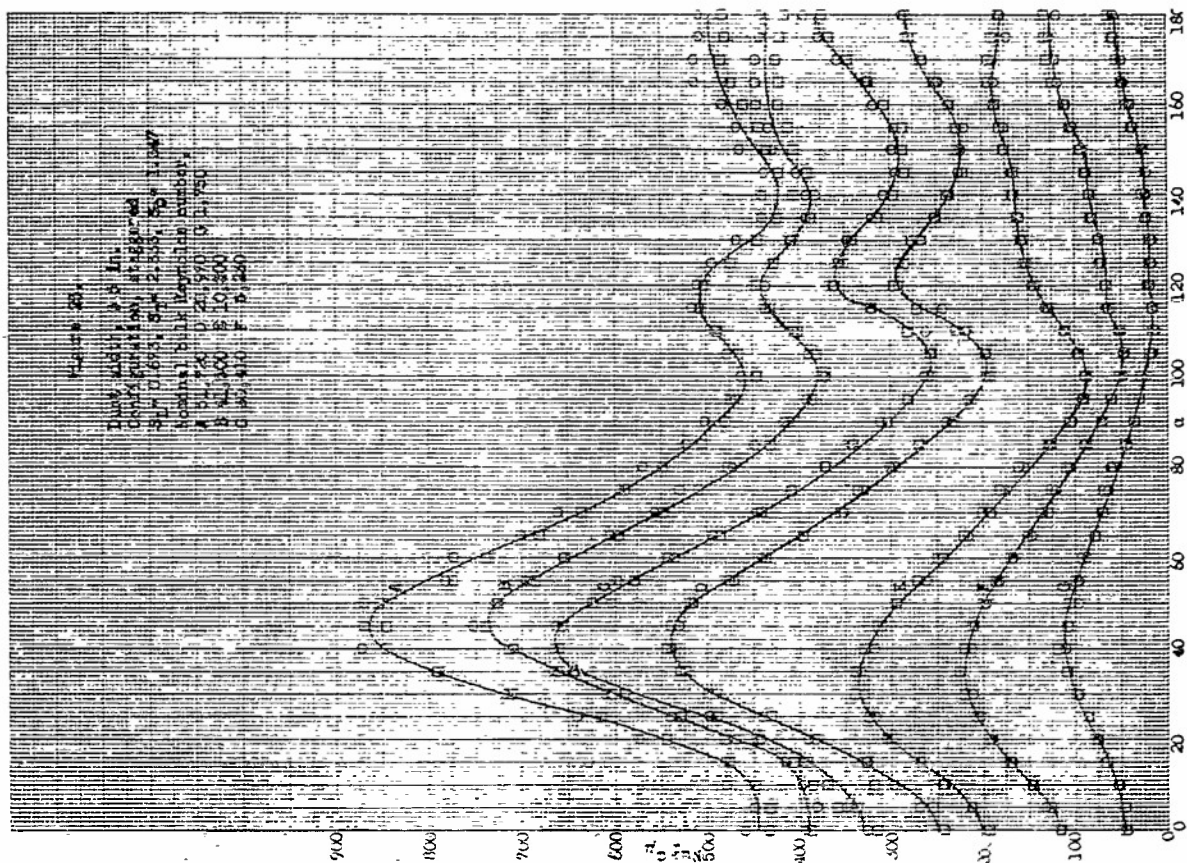


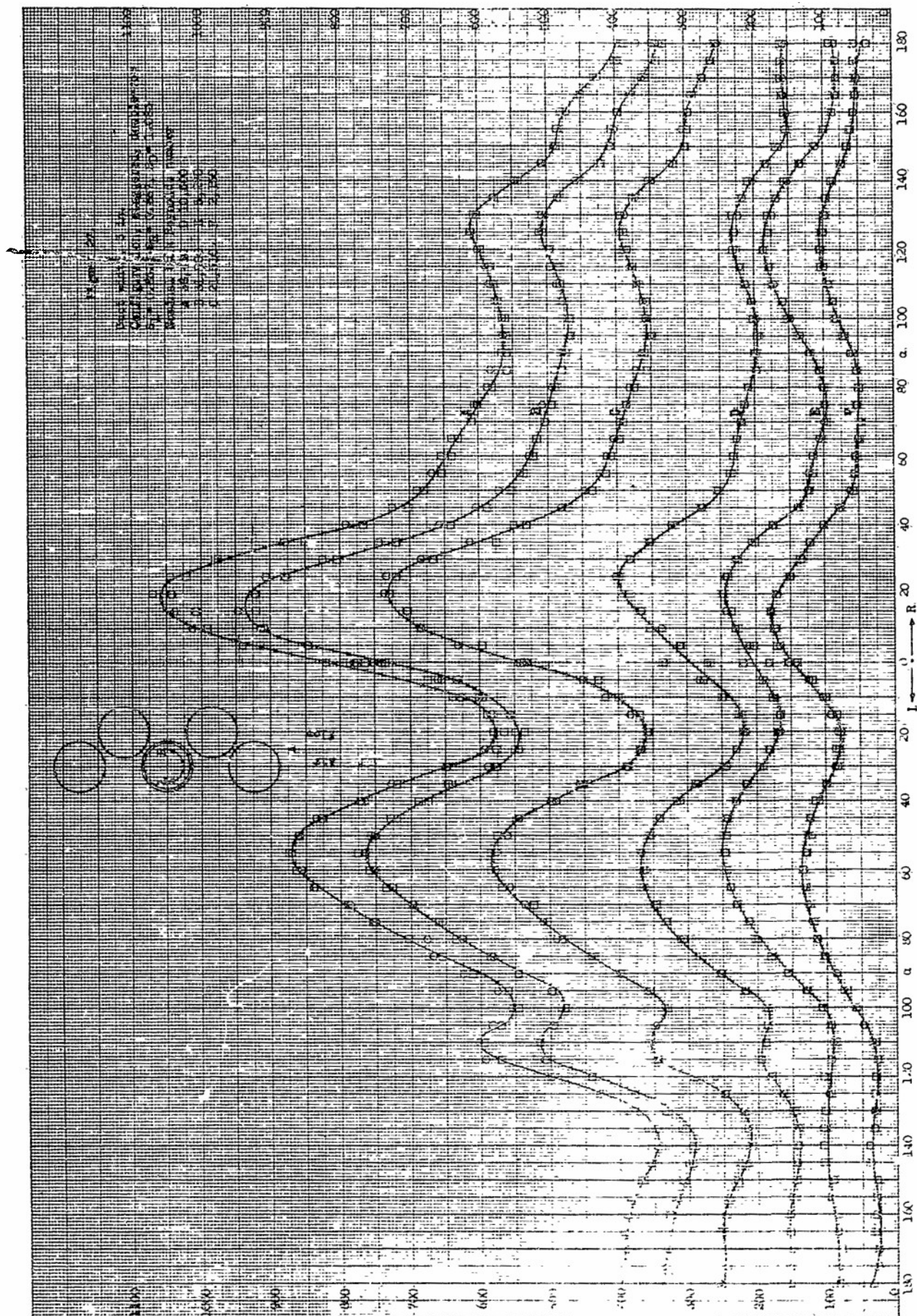


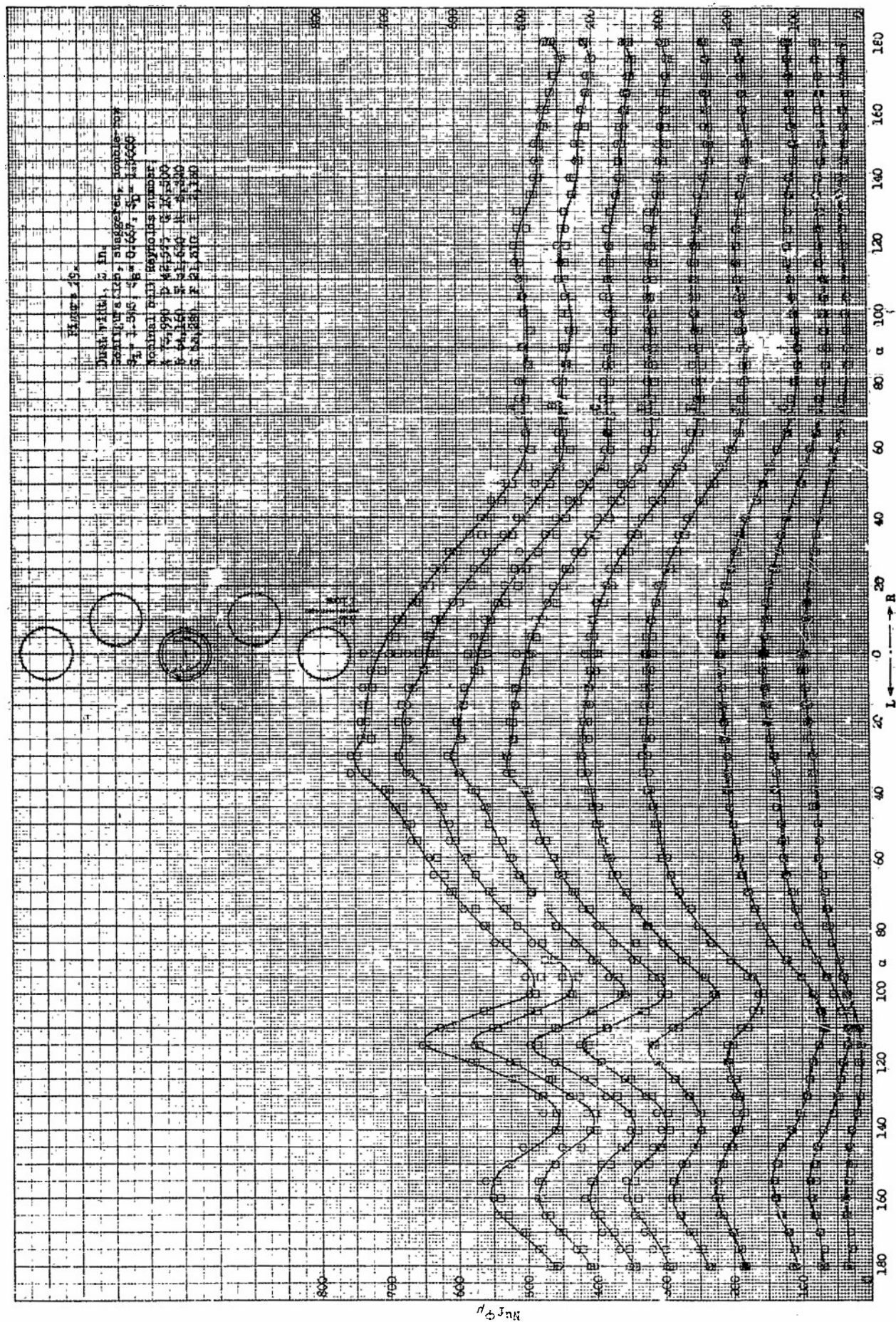


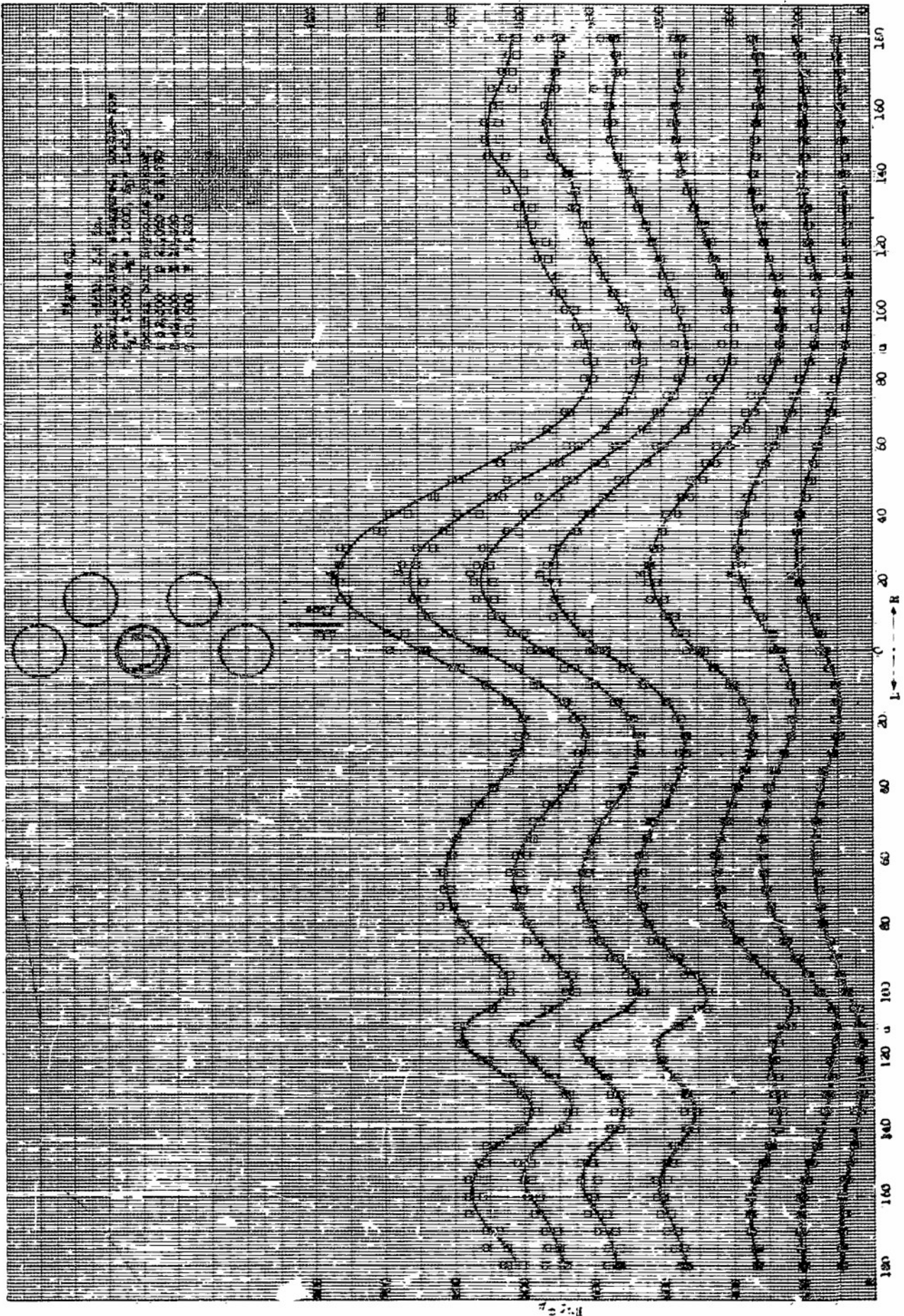


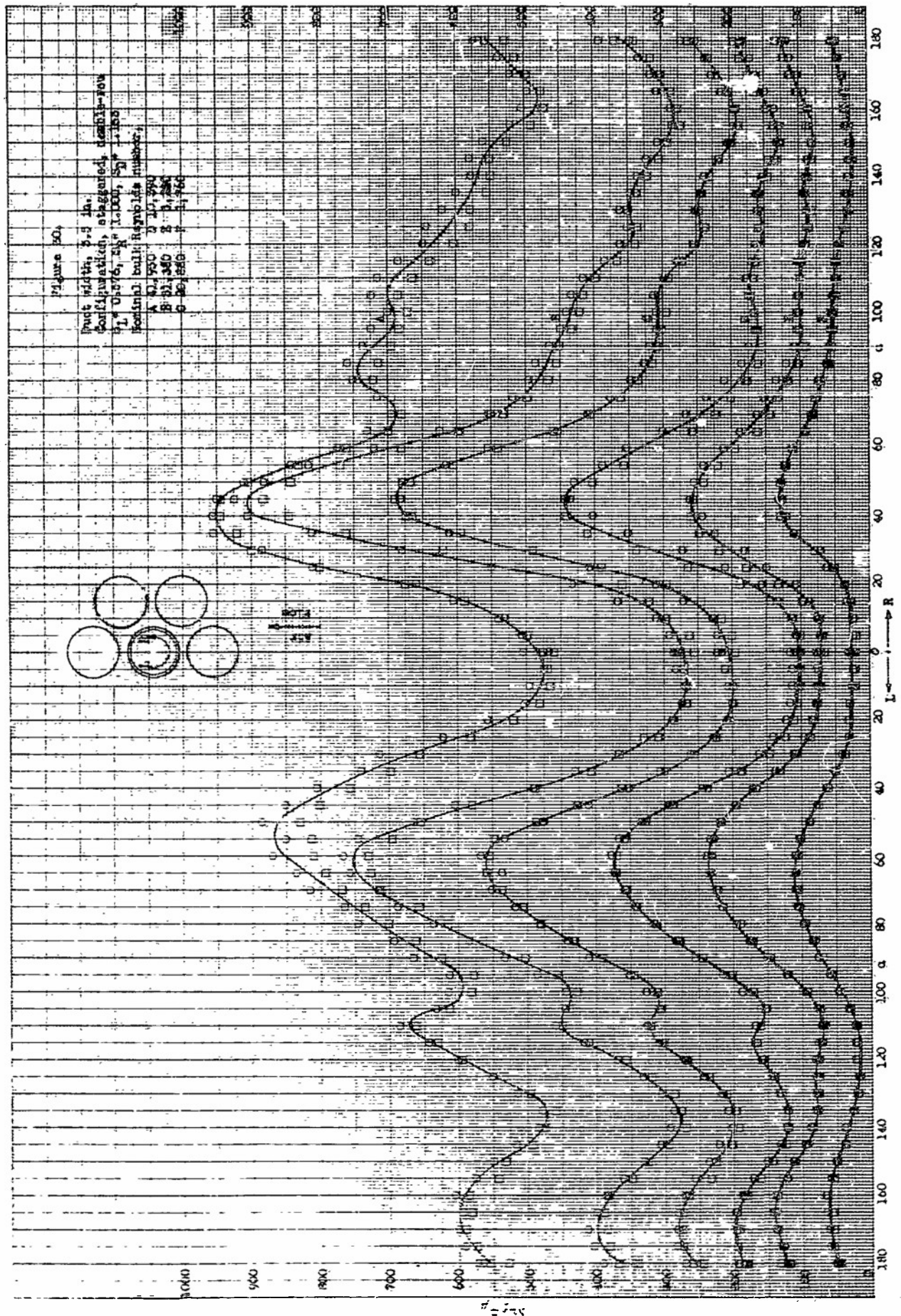


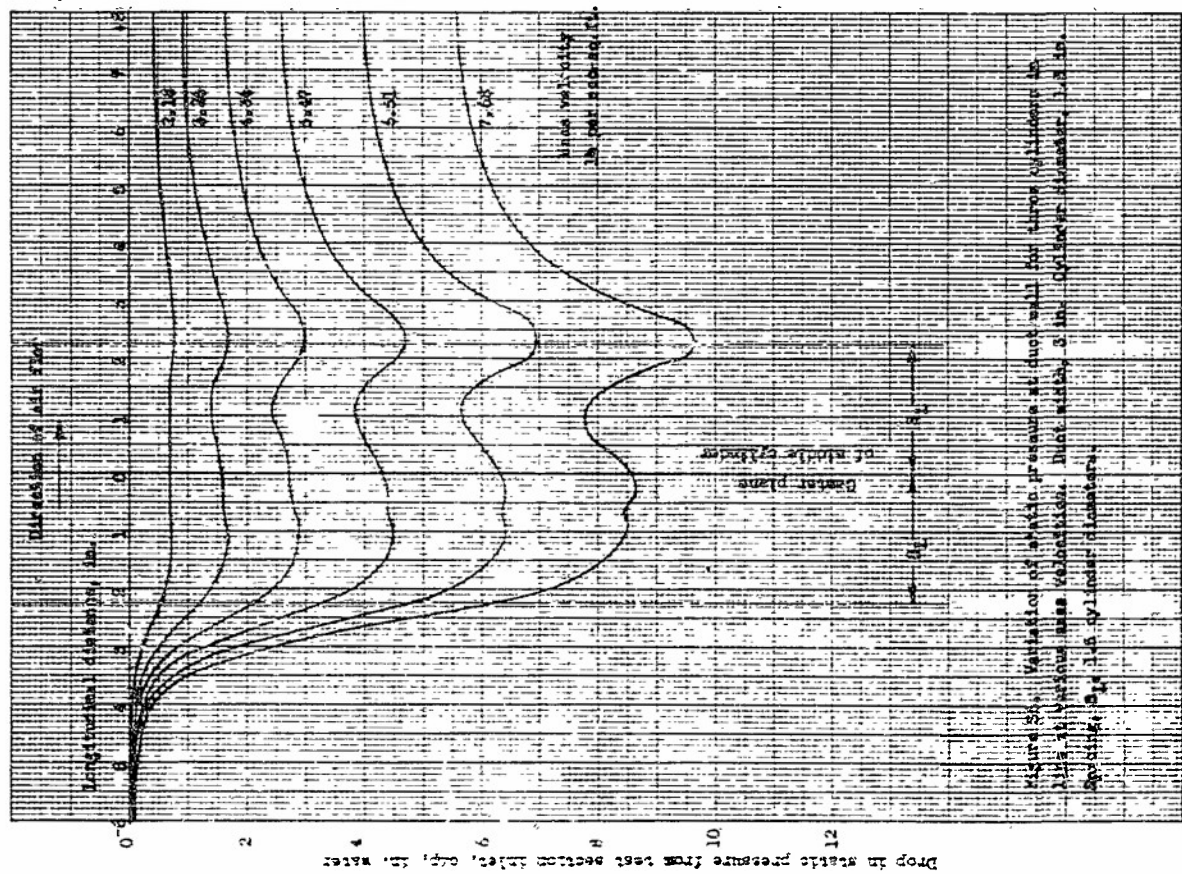
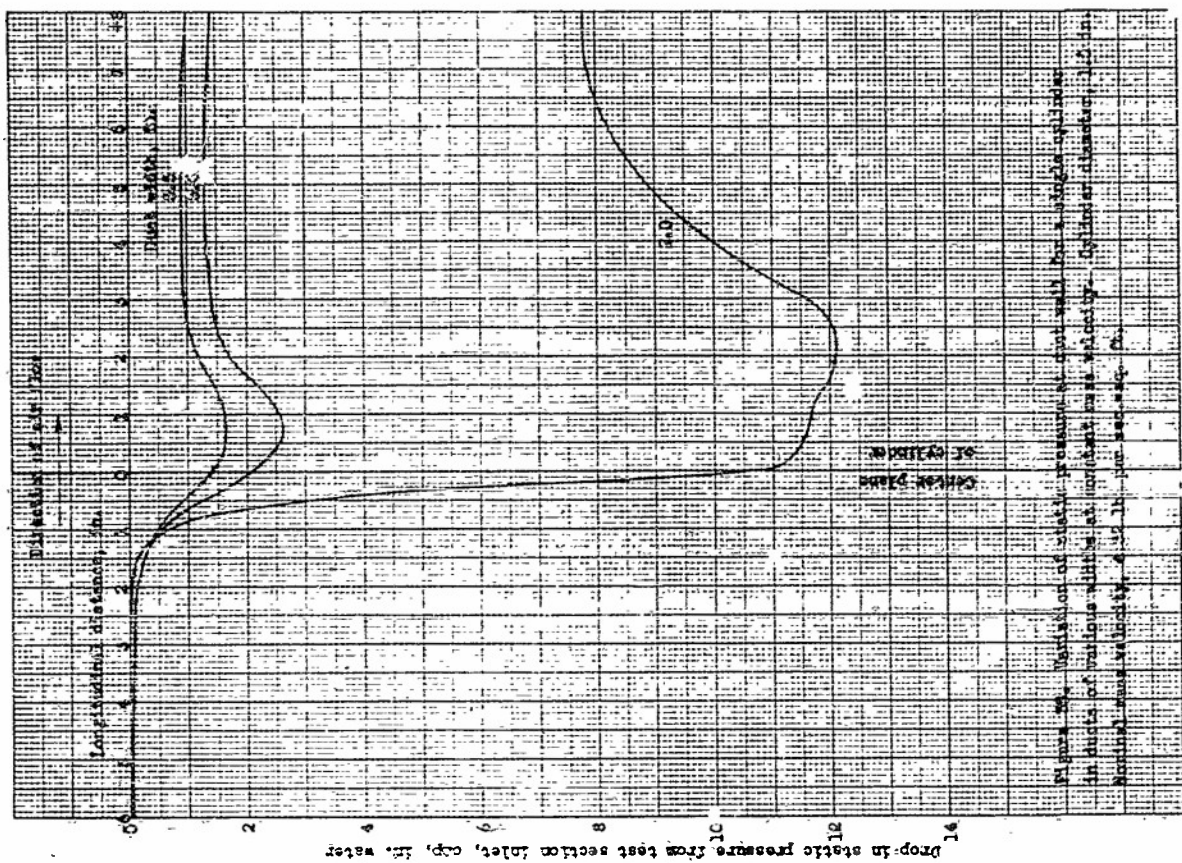












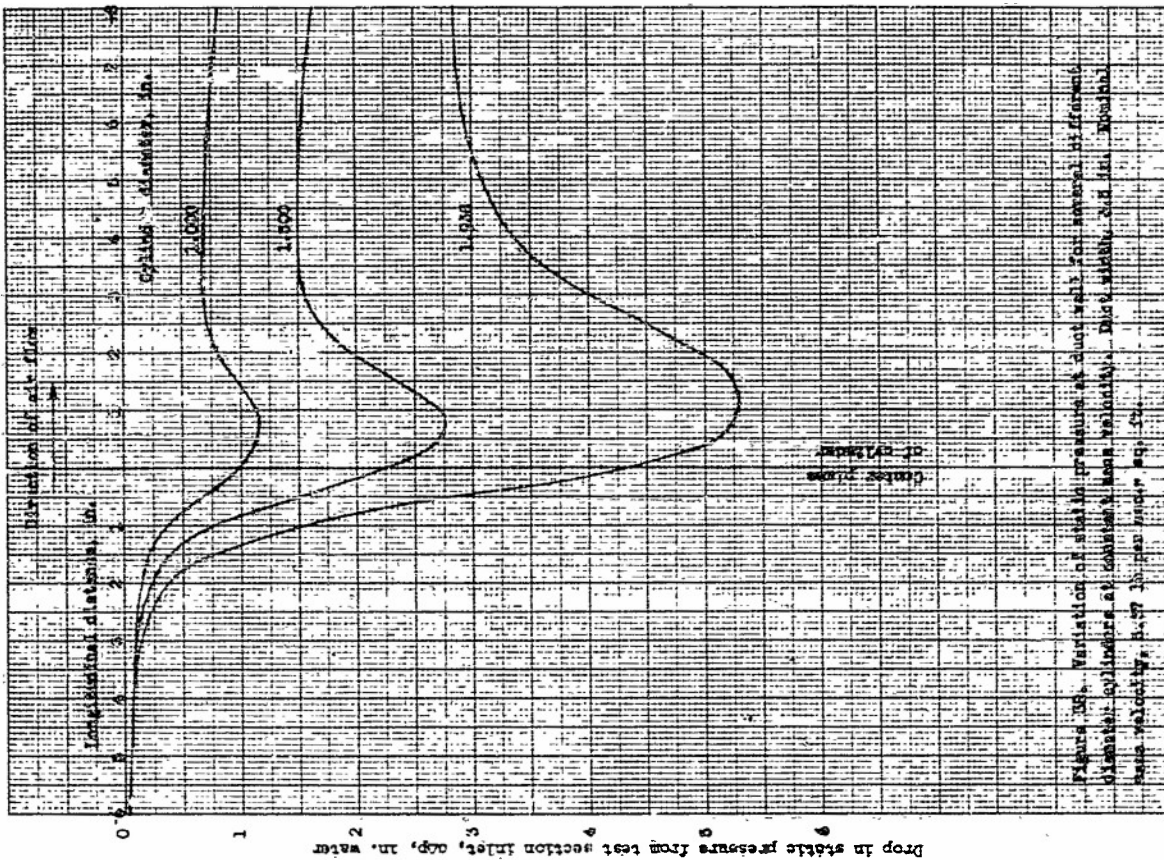


Figure 36. Variation of static pressure at duct wall for several different diameters of cylinders at constant mass velocity. Duct width, 2.0 in. Mass velocity, 1.47 lb per sq. ft. per sec.

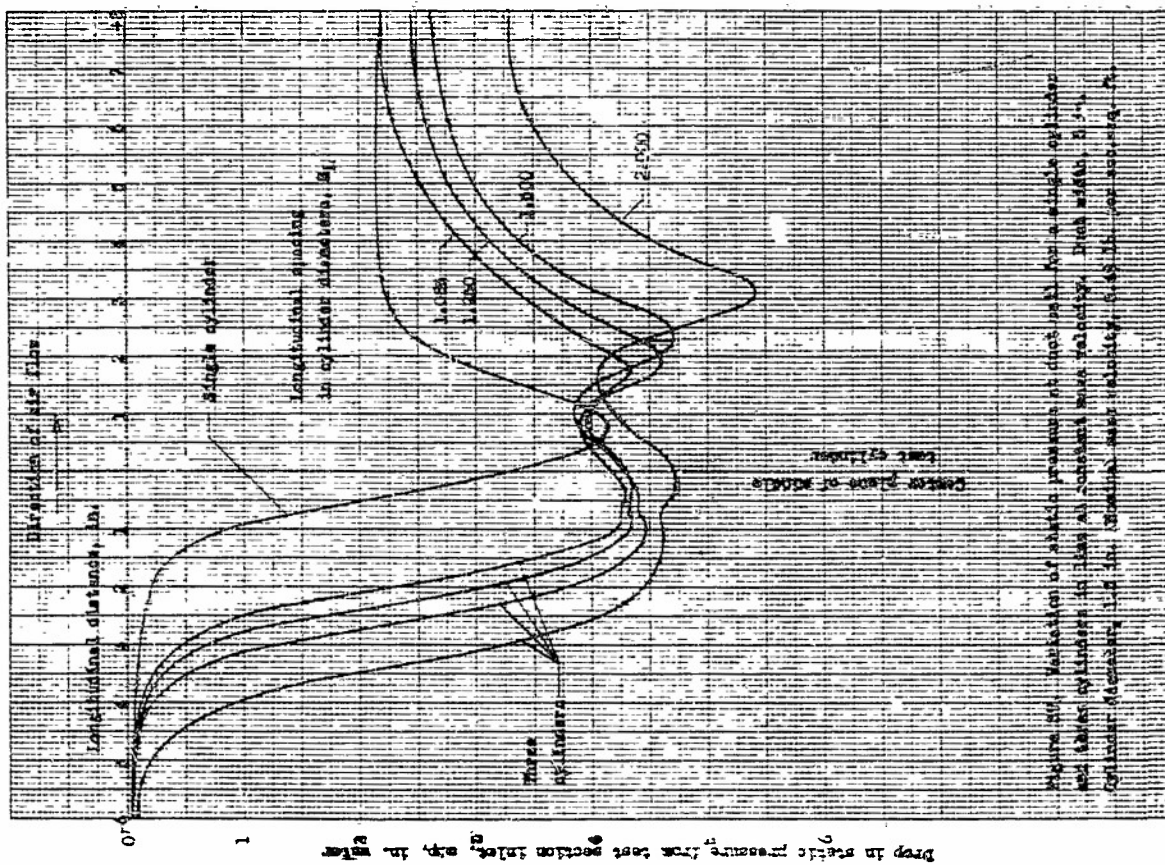


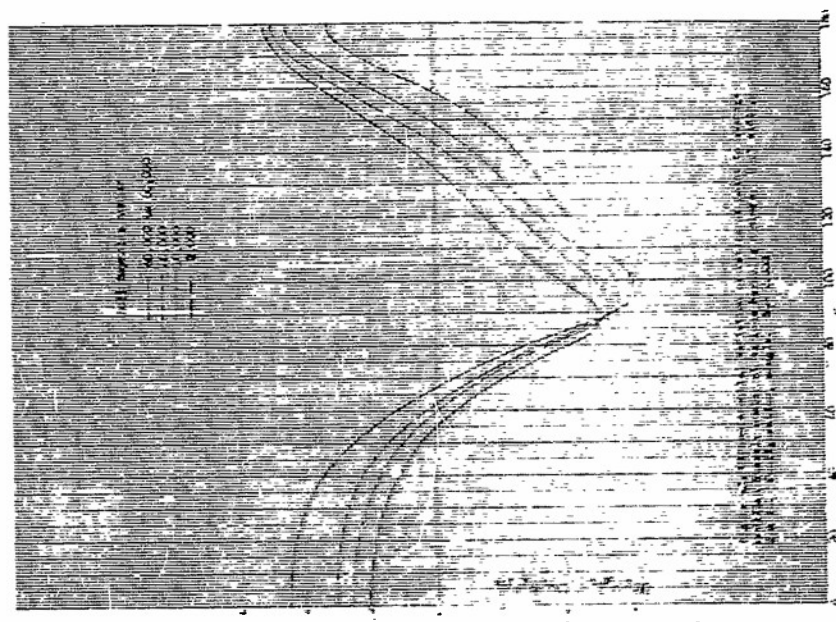
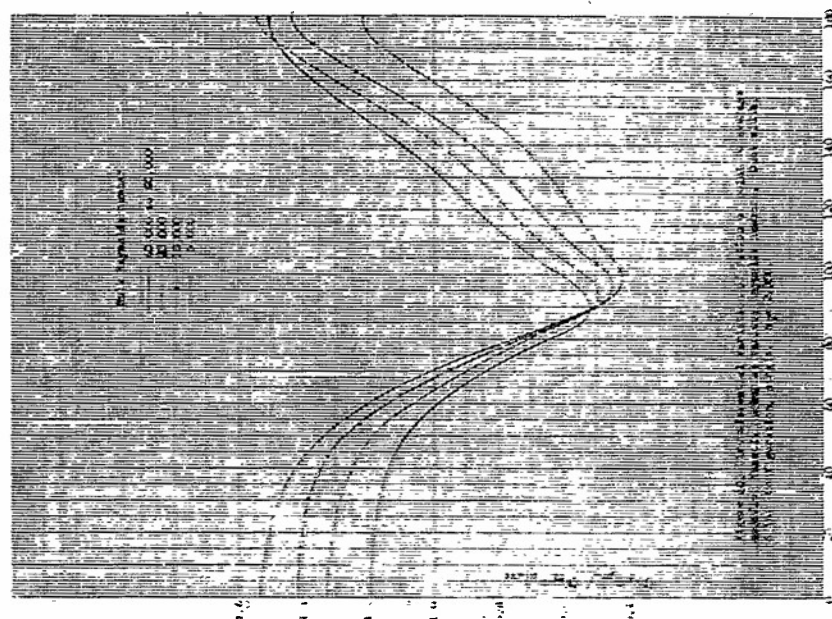
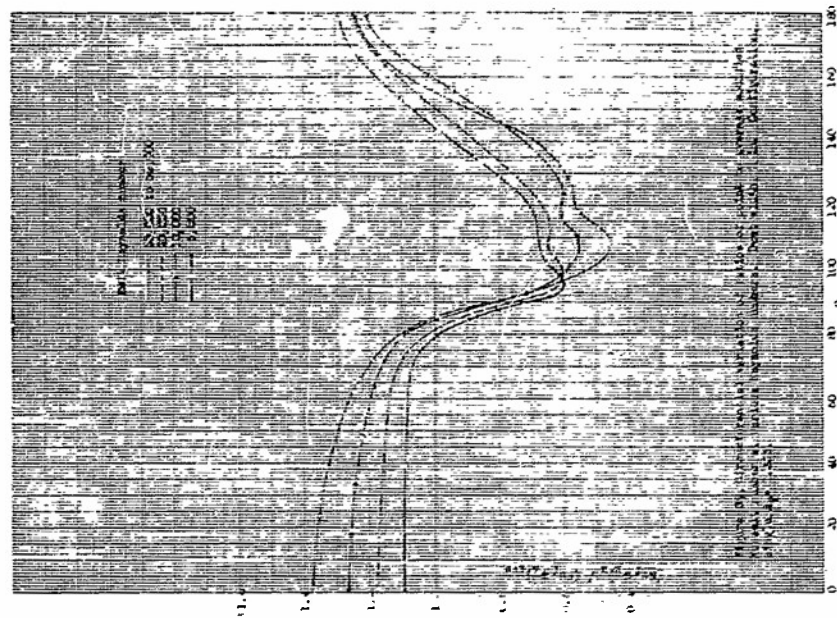
Figure 37. Variation of static pressure at duct wall for a single cylinder and three cylinders in plan at constant mass velocity. Duct width, 2.0 in. Mass velocity, 1.47 lb per sq. ft. per sec.

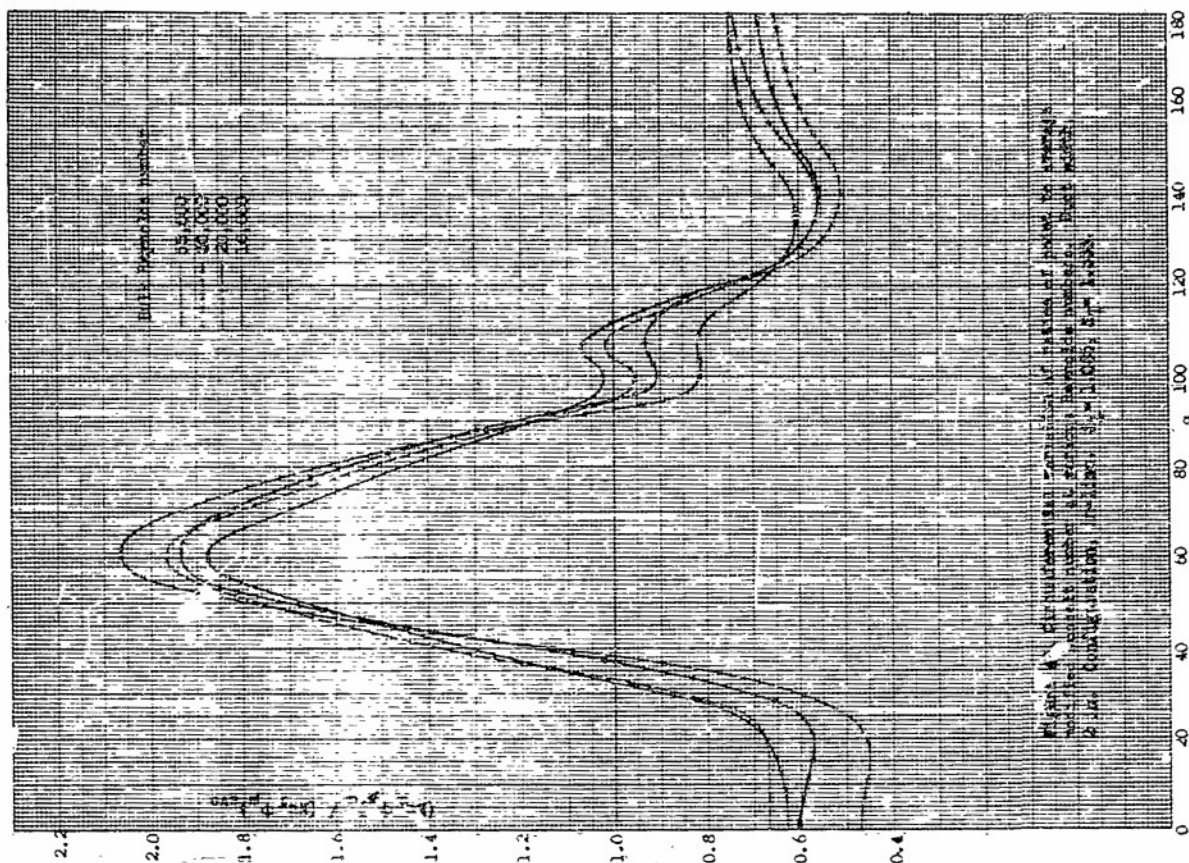
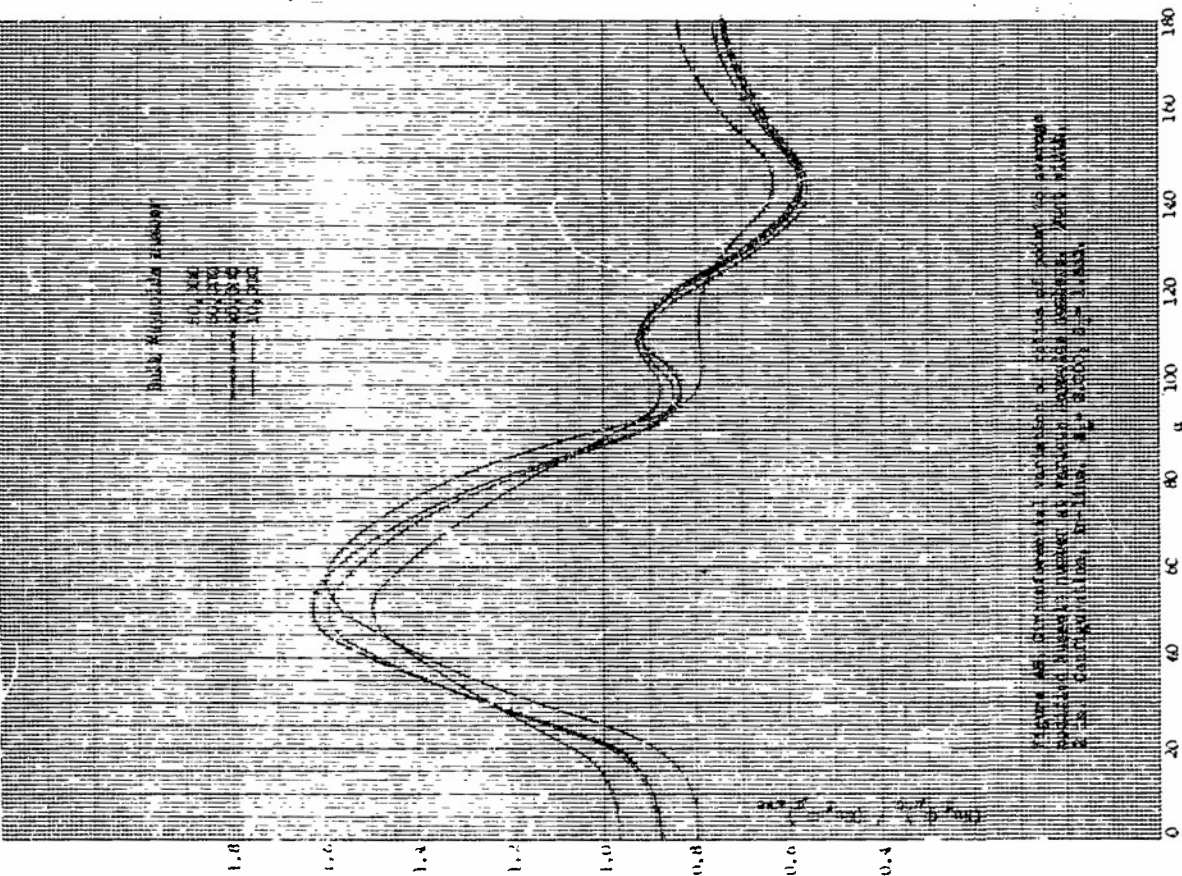
Peripheral Distribution

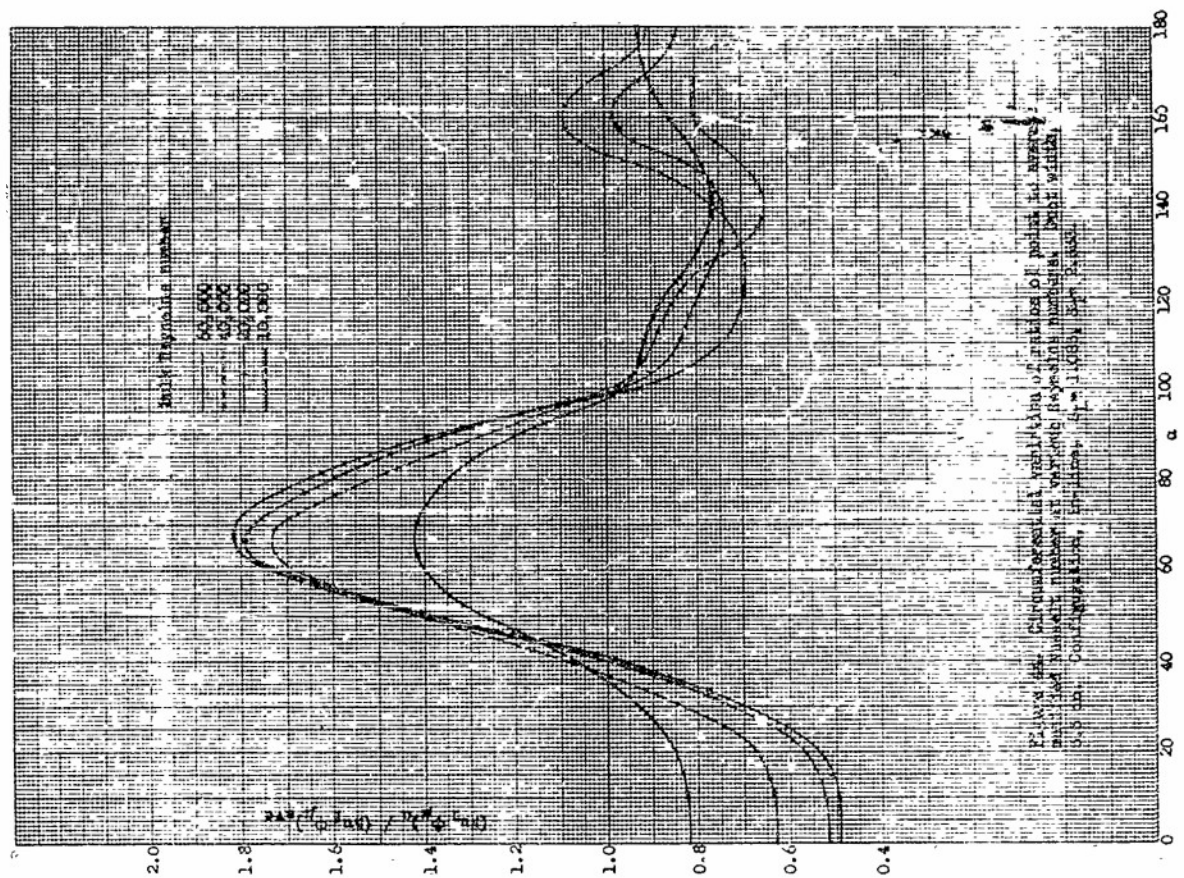
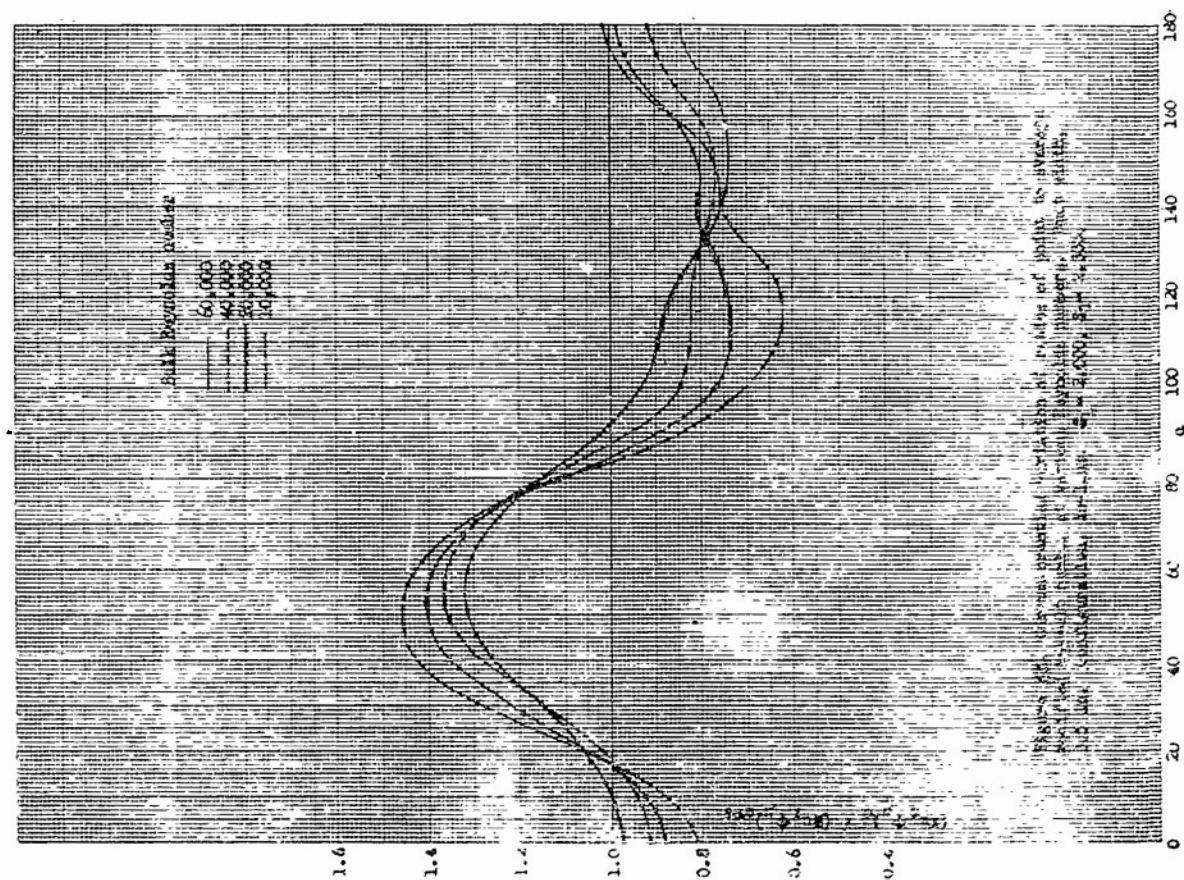
General inspection of the distribution curves in Figures 5 to 34 for all cylinder arrangements shows that they are fundamentally of different patterns. The modified point film Nusselt number and consequently the point heat transfer coefficient on the cylinder surface may vary ± 60 to 100 per cent from the average value. The locations of maximum and minimum heat transfer coefficients on the cylinder surface also vary with different arrangements. However, for a given arrangement the distribution curves at different flow rates are essentially similar to one another.

The relative circumferential variation of Nusselt number, as well as the influence of bulk Reynolds number and configuration on the distribution are shown effectively by distribution plots of the ratio of point-to-average Nusselt number. Figures 39 to 51 contain representative ratio plots for the configurations investigated. These ratios may also be interpreted as point-to-average heat dissipation ratios or as relative point unit heat transfer coefficients. The variation of these ratios is shown to be greatest for in-line configuration and least for single configuration.

In general, the variations of the ratios of point-to-average modified Nusselt number follow the same trend as the Nusselt number distributions. The ratio plots emphasize several distinctions which are not readily apparent from an inspection of the Nusselt number distributions; namely, that the range of the ratio variation increases with a decrease in Reynolds number and a decrease in configuration pitch and that at higher Reynolds numbers the ratio variation tends to become independent of flow rates. For all multiple cylinder arrangements the range of ratio variation increases with decreasing duct width. The opposite applies for single cylinders. Also for single cylinders, the range of ratio variation appears to be only slightly affected by a change of duct width from 3 to 3.5 inches.







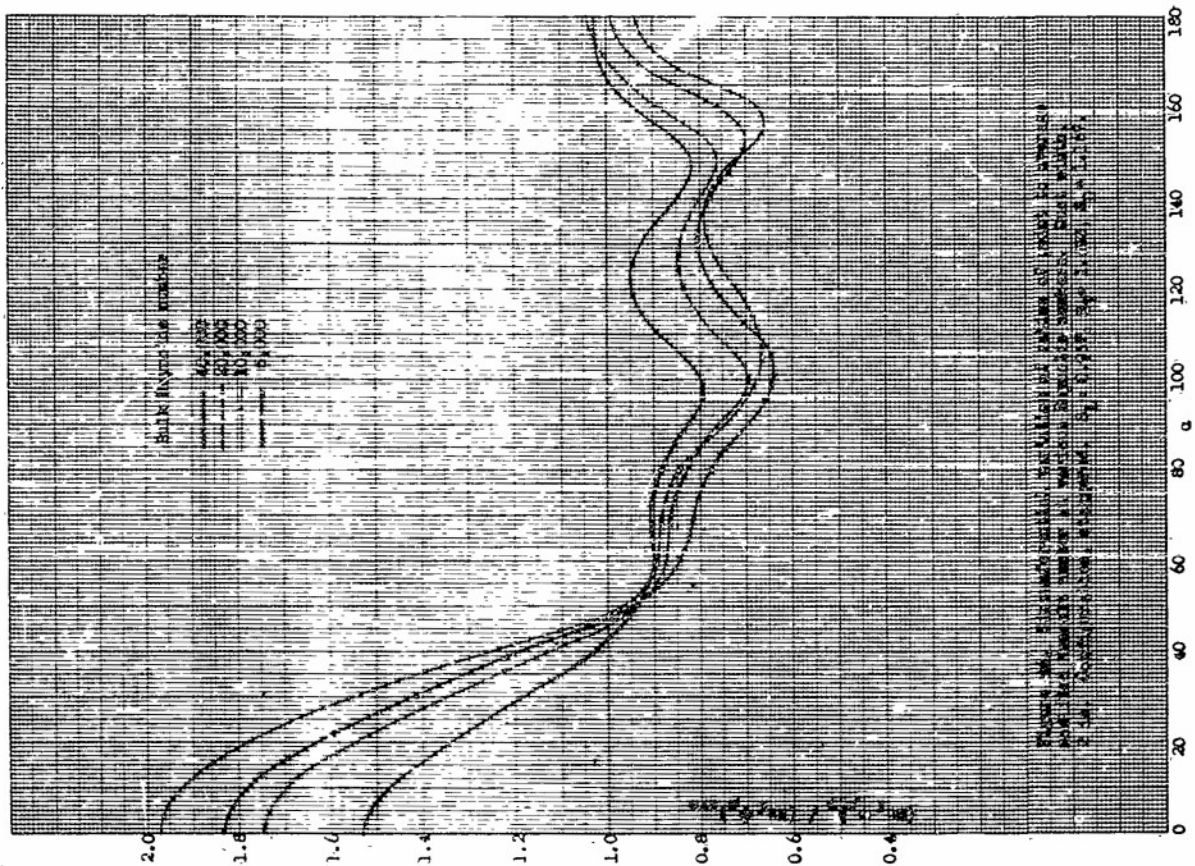


Figure 46. Bulk Rheology Modulus vs. Angle α for various frequencies. Bulk Modulus is a function of frequency, ω , and angle, α . The curves are for $\omega = 45, 100, 200, 500$.

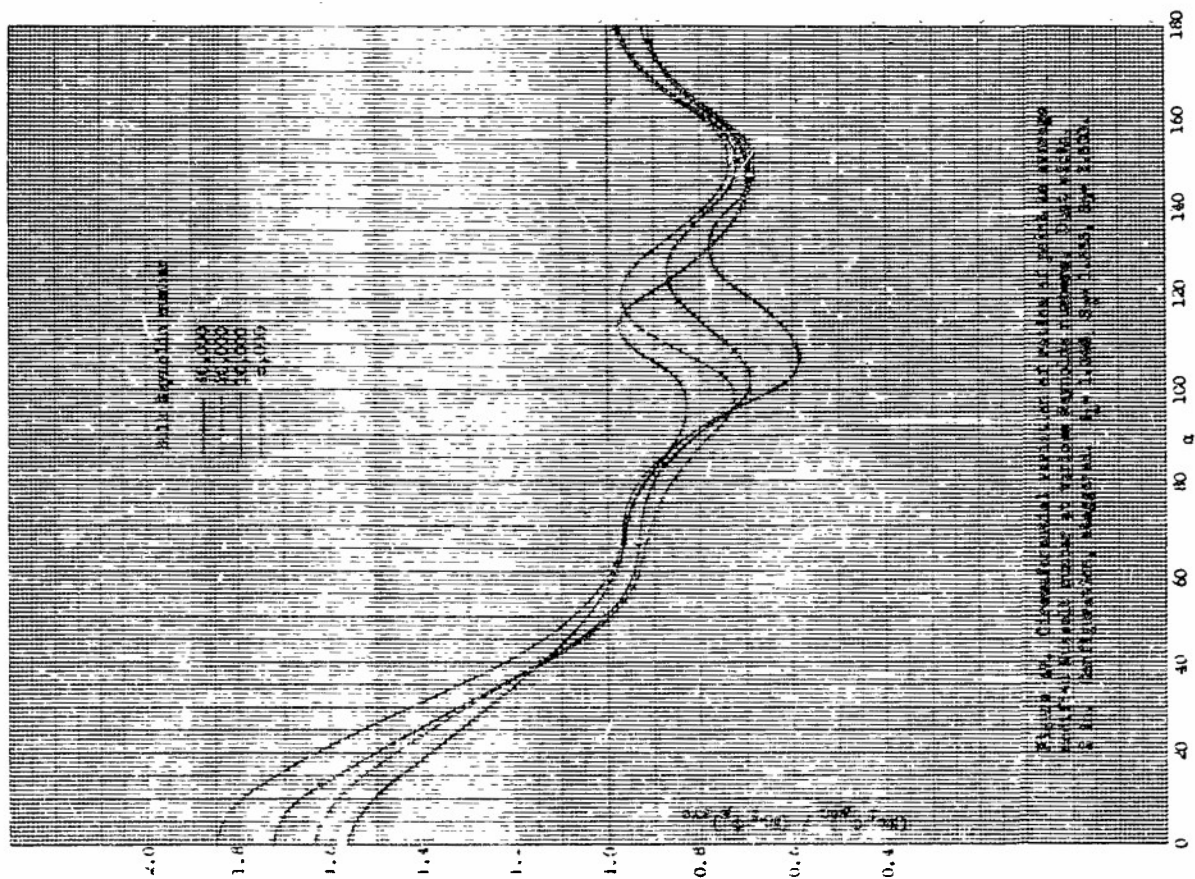
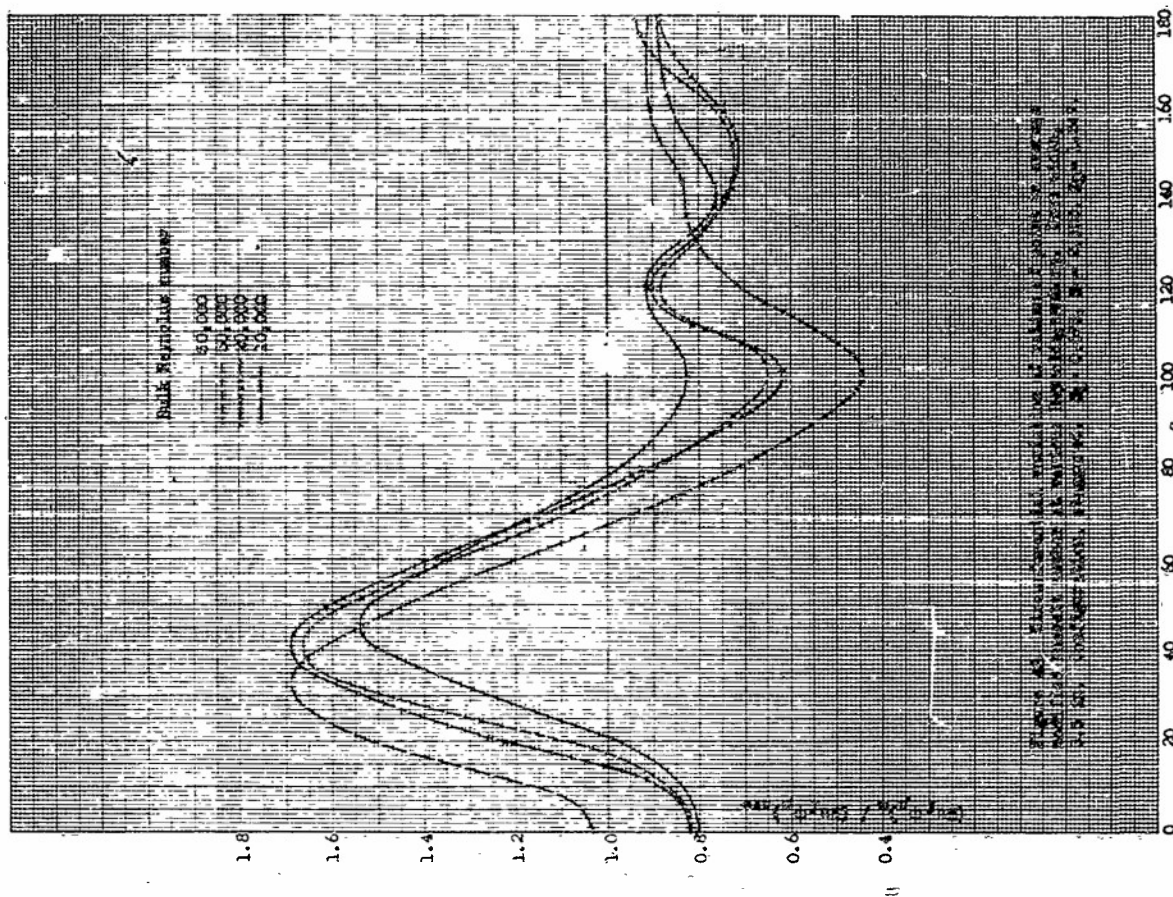
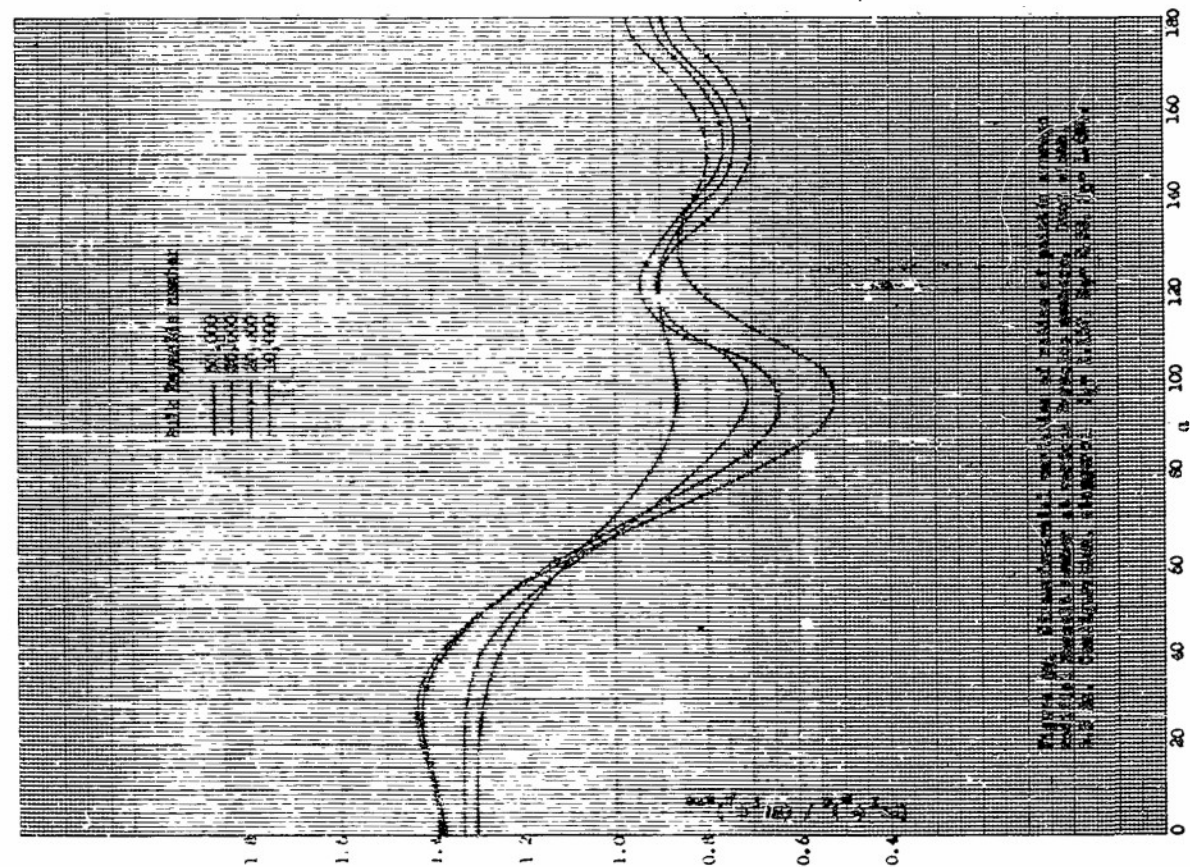
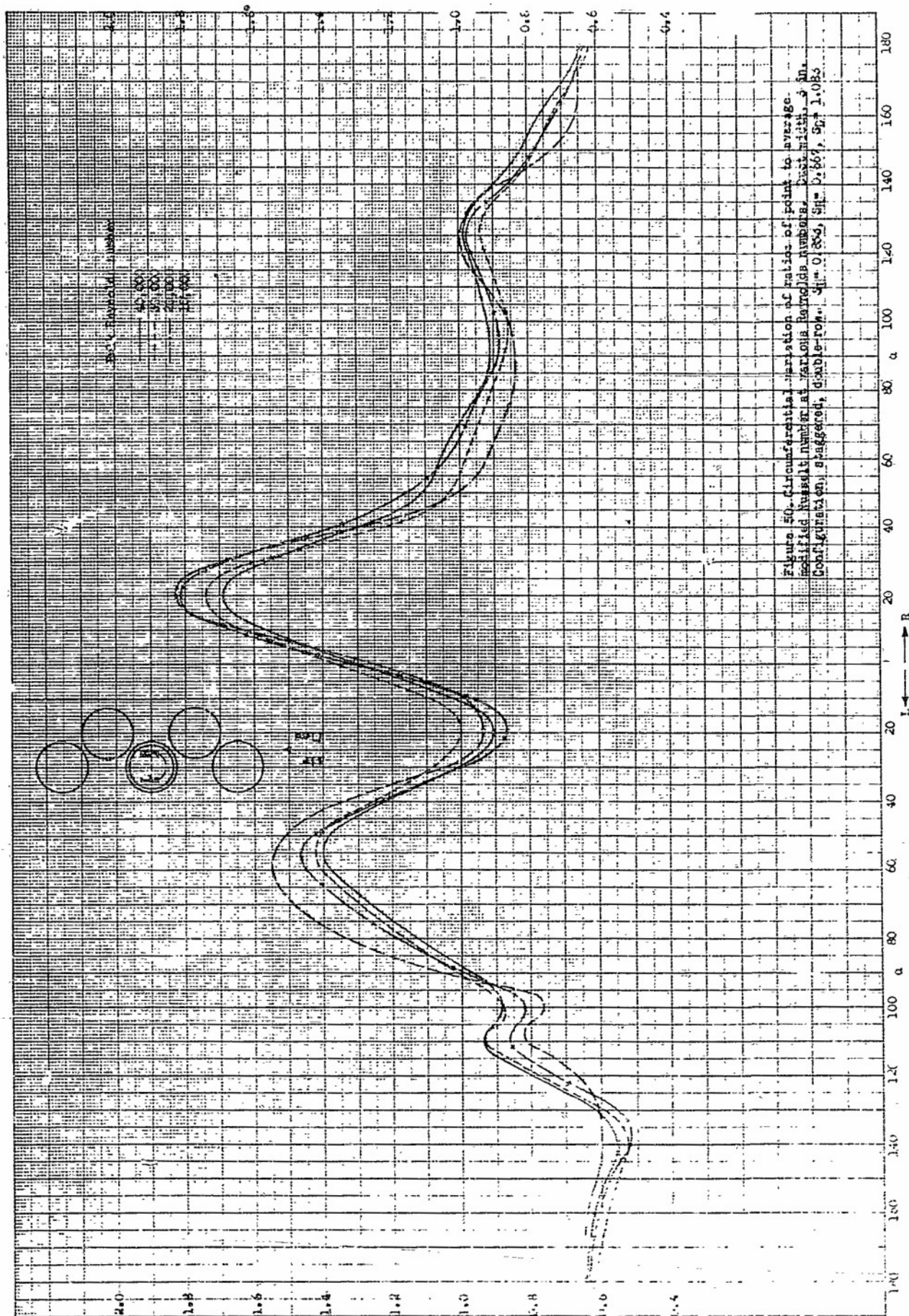
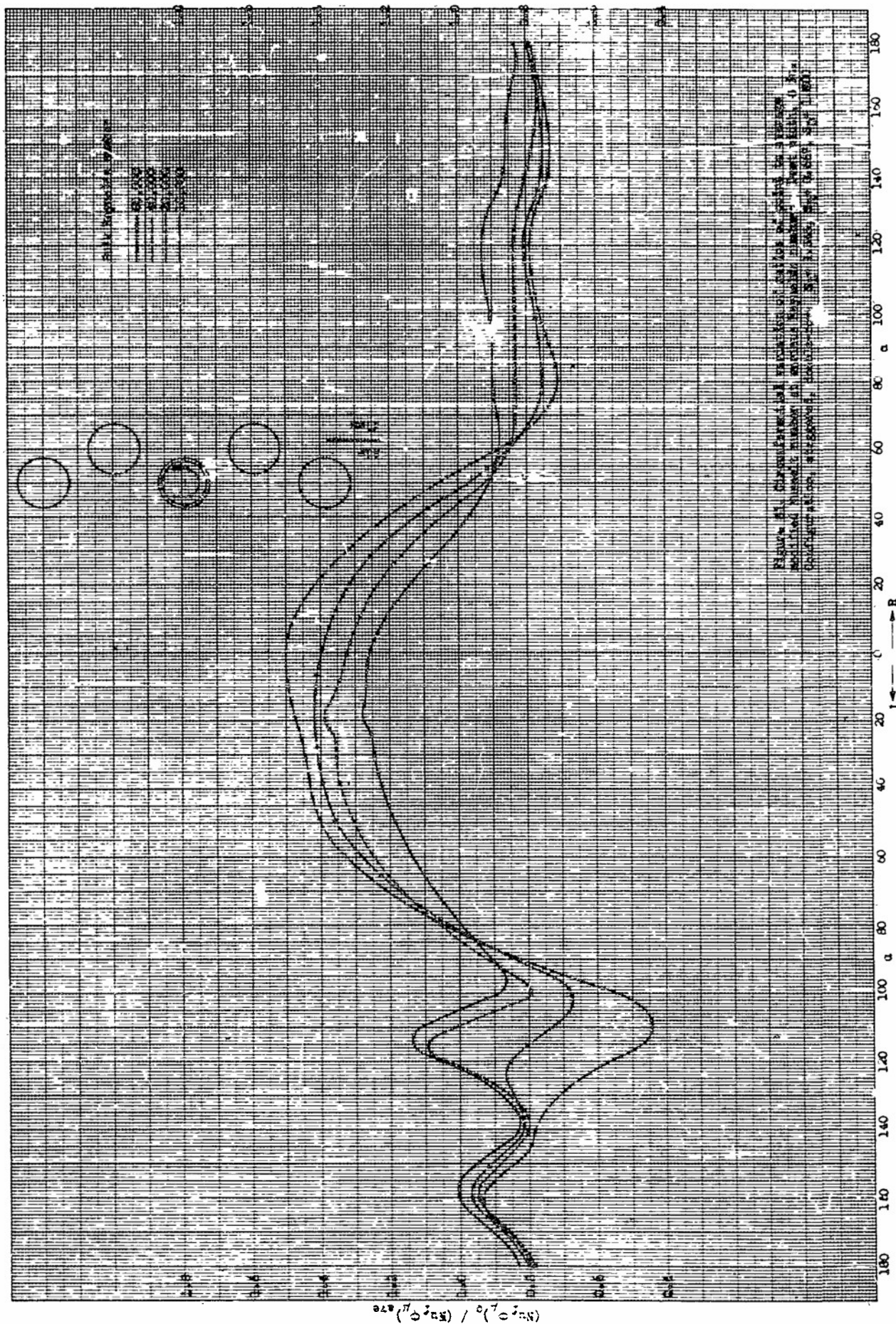


Figure 47. Circumferential Modulus vs. Angle α for various frequencies. Circumferential Modulus is a function of frequency, ω , and angle, α . The curves are for $\omega = 45, 100, 200, 500$.







1. Single Cylinders

The modified Nusselt number distributions for a single 1.5-inch diameter test cylinder located in 2-, 3-, and 3.5-inch wide ducts, shown respectively in Figures 5, 6, and 7, indicate several singularities. For bulk Reynolds numbers below 10,000 corresponding to a nominal velocity of approximately 15 feet per second, the maximum point Nusselt number, and hence the maximum surface heat transfer coefficient, occurs at the forward stagnation point of the cylinder ($\alpha = 0$ degrees). For Reynolds numbers above 10,000, the maximum Nusselt number occurs at the rear stagnation point ($\alpha = 180$ degrees). The minimum values of Nusselt number occur at approximately 100 to 110 degrees from the stagnation point for the lowest bulk Reynolds numbers and shift to approximately 87 to 97 degrees from the stagnation point at the higher bulk Reynolds numbers.

The variation of point Nusselt number in the peripheral region near the stagnation point is almost negligible. This region of uniform heat transfer extends to 60 degrees either side of the stagnation point for the 2-inch wide duct and to 20 degrees either side of the stagnation point for the 3.5-inch wide duct.

In the wider duct, the distributions resemble those obtained in free stream tests. In the narrow duct, the uniformity of heat transfer over the forward one-third of the periphery must be ascribed to the flow-containing effect of the duct.

A significant feature observed in Figures 5, 6, and 7 is the shift in the location of the minimum Nusselt number with duct width and Reynolds number. According to Fage and Falkner, as cited by Schmidt and Wenner (11), the location of the minimum Nusselt number is associated with transition from laminar to turbulent flow in the fluid layer adjacent to the surface. Therefore, it appears that lower Reynolds number and narrower duct width which contribute to the restoration of undisturbed flow conditions downstream by virtue of smaller dynamic inertia and a greater containing effect on the main stream tend to retard the occurrence of transition.

The effect of this retardation is reflected by the fact that the ratio of the average Nusselt number of the downstream half to the average Nusselt number of the entire cylinder increases with the Reynolds number. Schmidt and Wenner (11) have shown that when artificial turbulence is introduced by means of an axial interference wire on the upstream surface of the cylinder, the location of the minimum Nusselt number shifts approximately 20 degrees upstream and the average Nusselt number of the back half of the cylinder is raised appreciably. Thus, the reduced ratio of average Nusselt number of the downstream half to the average Nusselt number of the entire cylinder at lower velocity appears to be the consequence of weak turbulence due to retarded transition caused by decreased velocity.

The effect of velocity or Reynolds number on the location of the minimum Nusselt number and on the relative magnitude of point heat transfer coefficients is shown in Figures 39 to 41 where the ratios of point-to-average Nusselt numbers over the entire circumference are shown at several Reynolds numbers for single cylinders in 2-, 3-, and 3.5-inch . . .

wide aluminum test ducts, respectively. It is of interest to note that for each duct width, the ratio-variation is greater for lower than for higher Reynolds numbers and remains relatively constant for Reynolds numbers greater than 30,000. At this Reynolds number the maximum range of point-to-average heat transfer coefficient ratio for the 2-inch wide duct is from 0.6 to 1.29, while for the 3.5-inch wide duct the variation is from 0.49 to 1.52. The corresponding relationships for a Reynolds number of 5000 are 0.46 to 1.38 for the 2-inch wide duct and 0.38 to 1.45 for the 3.5-inch wide duct.

2. In-Line Cylinders

The Nusselt number distributions for four in-line arrangements, each located in a 2-inch, a 3-inch, or a 3.5-inch wide duct are shown in Figures 8 to 19. These distributions differ quite markedly from those obtained for a single cylinder. In general, the maximum value of modified Nusselt number occurs approximately 60 degrees from the stagnation point while the minimum value occurs either at the stagnation point or approximately 140 degrees from it. The magnitudes of the modified Nusselt number in these locations are approximately the same in ducts of same width at the same Reynolds number, irrespective of spacing.

A second maximum value of the modified Nusselt number occurs at approximately 110 degrees from the stagnation point of the test model in a 2-inch wide duct. The magnitude of the second maximum is considerably lower than that of the first. In ducts of 3- and 3.5-inch widths an inflection of the distribution curves appears at approximately 110 degrees from the stagnation point.

The different Nusselt number distribution curves should be expected from studies of cylinder arrangements and flow direction. In the case of the single cylinder, the air stream impinges directly and normally on the forward stagnation point where the boundary layer starts to form and produces a relatively higher heat transfer coefficient. However, in the case of several cylinders arranged in line, the stream flowing through the relatively narrow opening between the upstream cylinder and the duct wall impinges on the upstream half of the downstream test cylinder at a location other than the forward stagnation point. The flow at the narrowest opening between the upstream cylinder and the duct wall is essentially parallel to the duct axis but is deflected toward the duct centerline in the region upstream of the test cylinder, resulting in impingement approximately 60 degrees from the stagnation point. Also the impingement occurs at a higher local velocity than in the case of the single cylinder at equal Reynolds number. This is also apparent from the relative magnitudes of Nusselt numbers for the in-line and the single configurations at the same Reynolds number and duct width. For example, in a 2-inch wide duct at a Reynolds number of 15,800 the maximum modified Nusselt number occurring at the stagnation point of a single cylinder is 177, while the maximum modified Nusselt number for in-line cylinders occurs between 50 and 60 degrees from the stagnation point and has a value in the range from 420 to 453 for cylinder spacings in the range from 2,000 to 1,023 diameters. This also indicates that neither the location of the maximum heat transfer coefficient nor its magnitude, the latter presumably dependent on the impingement velocity, are appreciably affected by cylinder spacing.

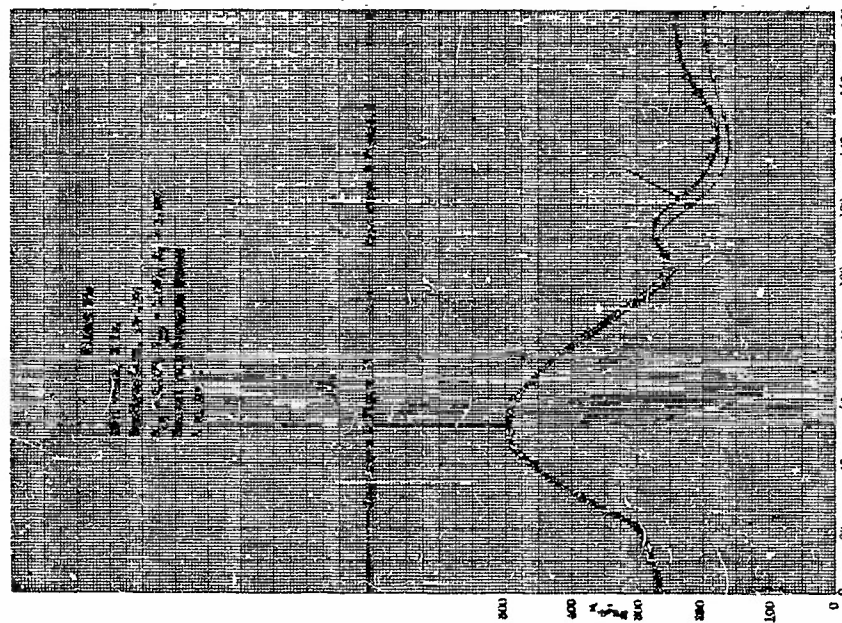
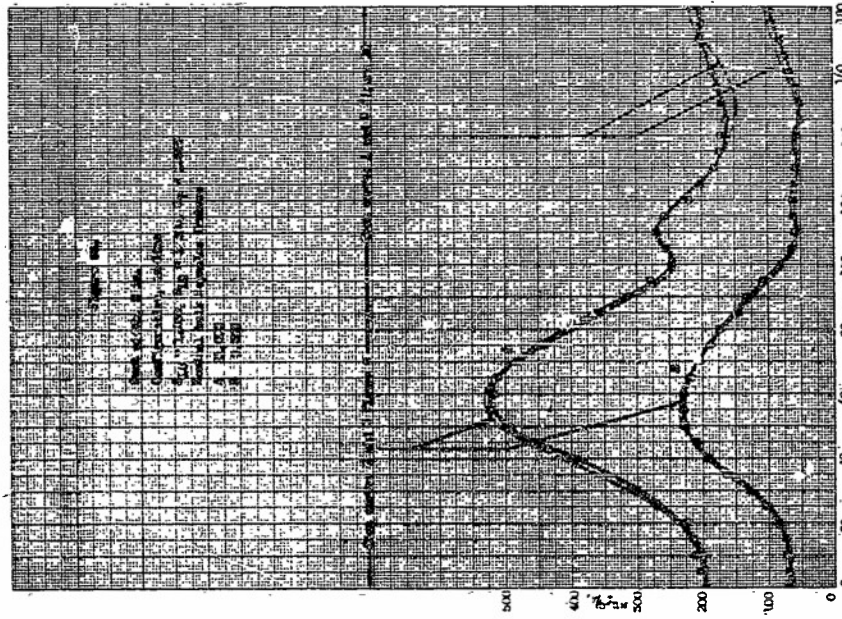
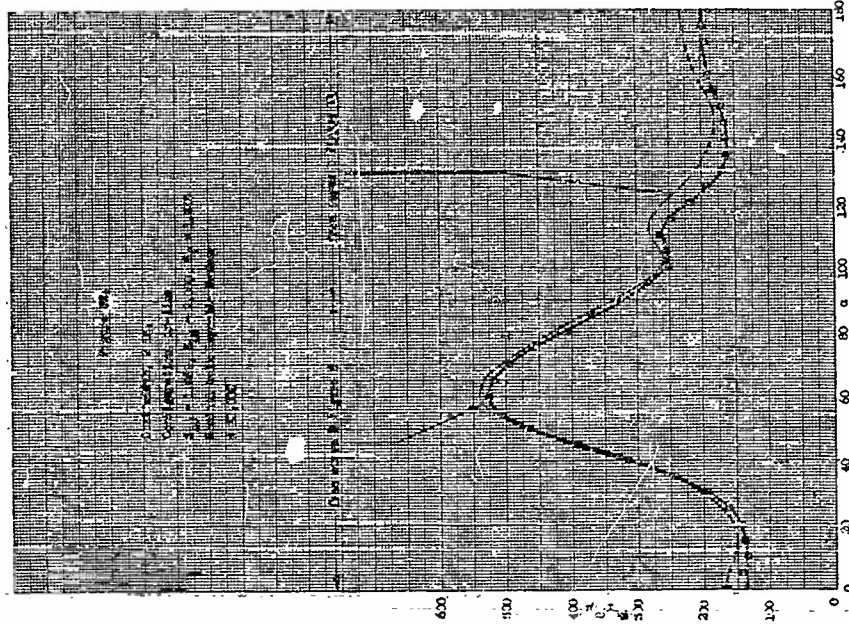
The location of the maximum heat transfer coefficient appears to be somewhat affected by duct width. For example, at equal spacing of 1.083 diameters, the location of the maximum Nusselt number is shifted from 60 degrees for 2-inch duct width to 67 degrees for 3.5-inch duct width. The effect of variation in spacing is the same in the wider duct and causes a shift in the location of the maximum point of up to 10 degrees.

When comparing the values of the maximum Nusselt numbers at different duct widths for equal Reynolds number, an appreciable change is noted. For example, the mean value of the maximum Nusselt numbers at a Reynolds number of 10,700 for all the spacings used in the 2-inch wide duct is approximately 340. The comparable value at a Reynolds number one per cent lower in the 3.5-inch wide duct is approximately 187.

Representative variations of point-to-average ratios of heat transfer coefficients for the in-line configurations are shown in Figures 42 to 45 for two spacings, each in the 2-inch and the 3.5-inch wide ducts. Curves for three cylinders arranged in line with longitudinal spacings of 1.083 and 2.000 cylinder diameters in the 2-inch wide duct are shown in Figures 42 and 43 respectively. Curves for these same configurations are shown in Figures 44 and 45 for the 3.5-inch wide duct. These arrangements represent combinations of least and greatest spacings and duct widths. The ratio variations of the intermediate in-line arrangements fall approximately proportionately within those of the described arrangements. In general, ratio variations are greater at lower than at higher Reynolds numbers. It may also be noted that for a given longitudinal spacing the ratio variations are greater for the 2-inch wide duct than for the 3.5-inch wide duct and that for each duct width the ratio variations are greater for the closer spacings than they are for the wider spacings. For example, at a Reynolds number of 30,000 and a longitudinal spacing of 1.083 diameters, the variation is 0.50 to 1.96 for the 2-inch wide duct while for the same spacing in the 3.5-inch wide duct the variation is about from 0.55 to 1.75. At the same Reynolds number for three cylinders in-line in the 2-inch wide duct, for a longitudinal spacing of 2.00 cylinder diameters the variation is from 0.56 to 1.59.

The indicated variations show that the effect of duct width on the relative distribution of Nusselt number is not very great, although noticeable, and tends to reduce the variation with increase of duct width. The effect of spacing is somewhat greater and evidences itself in reduced variation for increased spacings. In comparison to the variations obtained for single cylinders, those for multiple cylinders are greater. They do not differ materially in respect to minimum ratios but may be up to 50 per cent greater in respect to maximum ratios. This again points to the sizable spot cooling effect produced by the impinging air flow originating at the minimum cross-sectional flow area between the duct and the upstream cylinder.

Figures 52 to 54 show several representative variations of point Nusselt number for three cylinders in line with unequal longitudinal upstream and downstream spacings. The distribution curves display close resemblance and comparable magnitudes to those with even spacings in a duct of the same width. Remarkable similarities are observed when the



frontal distribution and rear distribution are compared individually with corresponding distributions of in-line cylinder arrangements with even spacings equal to the upstream and the downstream spacings, respectively. This comparison indicates that the distribution for unequal spacings can be considered as a composite of two distributions for even spacings and that, consequently, the former distribution may be estimated with reasonable accuracy by combining half distributions obtained for equal spacings.

3. Staggered Cylinders

As shown in Figures 20 to 22 the three staggered configurations in the 2-inch wide duct have similar profiles and indicate that the maximum Nusselt number occurs at the stagnation point and that minimum values of approximately equal magnitudes occur at about 100 degrees and 150 degrees from the stagnation point. The two distributions for staggered cylinders obtained in the 3-inch wide duct are widely different. The data for the closer spacing shown in Figure 23 indicate a maximum value of Nusselt number at approximately 45 degrees from the stagnation point and a minimum value at about 120 degrees. The maximum Nusselt number for the wider spacing shown in Figure 24 occurs at 27 degrees while the minimum value shifts from 105 degrees at low Reynolds numbers to 155 degrees at higher Reynolds numbers. The two staggered configurations in the 3.5-inch wide duct also differ markedly as shown in Figures 25 and 26. The maximum Nusselt number for the closer spacing occurs at 35 degrees to 45 degrees from the stagnation point while the minimum is 100 degrees. The distribution for the wider spacing is comparatively flat with a maximum Nusselt number at the stagnation point and a minimum at either 95 degrees or 155 degrees. The distributions for the closer spacing in both 3- and 3.5-inch wide ducts show a fundamental pattern similar to that of the in-line configuration except that the maxima occur at 45 degrees and not at 60 degrees from the stagnation point as is the case for the in-line configuration. It is of interest to note that in these arrangements with closer spacing, two maxima of equal magnitude occur at 40 degrees to the right and the left of the stagnation point, while only one maximum, namely at the stagnation point, occurs for other spacings.

Examination of the locations of the maximum Nusselt number in Figures 20 to 26 and their relative values gives a qualitative indication of the existing flow characteristics. In the narrow duct, 2-inch wide, the occurrence of the maximum Nusselt number at the stagnation point indicates that the effect of the cylinders in the upstream bank, located symmetrically relative to the center-line is to create a jet which impinges at the stagnation point. This results in a maximum Nusselt number which is greater the smaller the spacing between banks is. For longitudinal spacings from 0.937 to 1.345 diameters and a bulk Reynolds number of 10,600 the maximum Nusselt number decreases from 385 to 340. The values of the Nusselt number in the downstream half of the cylinder are considerably less affected.

The jet effect is also illustrated by comparison of the Nusselt number at the stagnation point in the staggered arrangement with that obtained for a single cylinder. The respective values, as obtained from Figures 20 and 5 for a Reynolds number of 10 600 are 385 and 148.

The convergence of flow effected by the upstream bank is a function not only of longitudinal spacing but also of the transverse spacing

which in the present investigation is synonymous with duct width. This is illustrated by comparison of the distribution obtained for the 3- and 3.5-inch ducts with those of the 2-inch duct. The fact that in the wider duct and at the smaller longitudinal spacings as shown in Figures 23 and 25 two maxima occur indicates that actually two separate jets are formed whose velocity and convergence are dependent on the transverse spacing. Again, the absolute values for the narrower duct are appreciably greater and the location of the maxima is shifted slightly toward the stagnation point for the narrower duct. The convergence of the jets is indicated by comparison of Figures 23 and 24 which show the relative magnitudes of the maximum value and its position to change appreciably with longitudinal spacing. For example, at a Reynolds number of 10,550 and a longitudinal spacing of 0.576 diameter, as shown in Figure 23, the maximum Nusselt number occurs at 45 degrees from the stagnation point and has a value of 563 as compared to a Nusselt number of 155 at the stagnation point. Compared with this, at a Reynolds number of 10,660 and a longitudinal spacing of 1.00 diameter, as shown in Figure 24, the maximum Nusselt number occurs at 25 degrees from the stagnation point and has a value of 263 as compared to a Nusselt number of 235 at the stagnation point. This tendency of the flow to converge into a single jet of more uniform velocity is further substantiated by the shapes of the distribution curves in Figure 26 for a 3.5-inch wide duct and a longitudinal spacing of 1.167 diameters at which the convergence appears to have been completed since an essentially constant Nusselt number distribution is obtained in the peripheral region extending 30 degrees either side of the stagnation point.

Variations of point-to-average ratio of Nusselt number for the staggered configuration located in the 2-inch and the 3.5-inch wide ducts are shown in Figures 46 to 49. The effect of longitudinal spacing is obtained by comparison of Figures 46 and 47, both for the 2-inch duct but of different longitudinal spacings of 0.957 and 1.345 diameters, respectively. At a Reynolds number of 30,000, the ranges of the ratio variation are almost identical and are from 0.75 to 1.65 and from 0.71 to 1.60, respectively. The effect of longitudinal spacing on the range of ratio variation becomes more appreciable in ducts of greater width. As shown in Figures 48 and 49 for the 3.5-inch wide duct at the longitudinal spacings of 0.673 and 1.167 diameters, the ranges of ratio variation at the same Reynolds number of 30,000 are from 0.65 to 1.66 and from 0.70 to 1.33, respectively. Thus, it becomes apparent that the least range of ratio variation is obtained with configurations of largest longitudinal and transverse spacings.

4. Staggered, Double-Row Cylinders

Nusselt number profiles for the staggered, double-row configuration are presented in Figures 27 to 51 and have relatively little similarity with profiles of other configurations. The profiles are non-symmetrical about the center plane of the heated test cylinder. However, even though the distributions of Nusselt numbers over the two halves of the cylinder are not similar, the average values of Nusselt number for each half are approximately equal. Generally, the average values of Nusselt number of the right, or inner half, directed toward the duct's center line is slightly greater than that of the left or outer half. There is also little similarity between profiles obtained with different spacings. The shape

of the Nusselt number profiles is considerably changed when the cylinder spacings are altered.

From the configuration, it is noticed that the cylinder arrangement with respect to the right or inner half of the test model is nearly identical to the staggered configuration and that the arrangement with respect to the left or outer half is very similar to the in-line configuration. As the heat transfer coefficient distribution is dictated by the flow field which is largely influenced by cylinder arrangement, resemblances of Nusselt number profiles of the right half of the test model to that for the staggered configuration, and of the left half of the test model to that for the in-line configuration would be expected for all spacings. However, only for closer spacings this resemblance is more pronounced. This can be observed by comparing the distribution curves of the right half of the cylinder shown in Figure 30 with the distribution curves shown in Figure 25 and that of the left half of the cylinder shown in the same Figure 30 with the distribution curves shown in Figure 17, all for a duct width of 3.5-inch. Similar comparisons may be made between Figures 14 and 23 for the in-line and the staggered configurations in a 3-inch wide duct and Figure 27. The similarities between the Nusselt number distribution curves as noted above, despite the differences in their magnitudes, yield significant indications of flow similarities. Comparing the right half of the distribution curve for double-row stagger with wide spacing with a corresponding distribution curve for a symmetrical stagger, as shown by Figures 28 and 20 respectively, a less pronounced resemblance than for the closer spacing is observed. This lack of resemblance appears to indicate that in closer spacings the flow fields around the right and the left halves of the test model are less affected by one another than in wider spacings.

Several representative variations of point-to-average ratio of Nusselt number for the staggered, double-row configurations located in a 3-inch wide duct are shown in Figures 50 and 51. At a Reynolds number of 30,000 the variation of the ratio is from 0.53 to 1.74 for a longitudinal pitch of 0.853 diameter and a diagonal pitch of 1.083 diameters. The corresponding variation is from 0.75 to 1.4 for a longitudinal pitch of 1.345 diameters and a diagonal pitch of 1.50 diameters. The Reynolds number effect on the range of ratio variation is not appreciable for closer spacings.

5. Test Data of Cylinder A

Figures 32, 33, and 34 present the Nusselt number distributions obtained with test cylinder A located singly in 3-inch, 4-inch, and 6-inch wide steel ducts, respectively. The reliability of these data is doubtful, as evidenced by comparison of Figures 32 and 13 which show the disagreement between the data obtained with the two test cylinders, each located in a duct of different material, but of the same width. The shape of the curves at the lower Reynolds numbers are similar although the magnitudes differ slightly. However, at the higher Reynolds numbers there is little similarity between the curves. It must be assumed that the data obtained with test cylinder B located in the aluminum ducts are more nearly correct because the cylinder and ducts were more carefully constructed and an improved experimental technique was utilized.

As mentioned in the description of the construction of the test cylinders in Appendix II, cylinder A was hand-finished. This process may have resulted in a non-cylindrical surface with flat spots and irregularities. Both the inner surface and outer surface thermocouples were positioned manually. The outer surface thermocouples were cemented into longitudinal grooves which could account for variations in depth from the surface. Likewise, the thermocouples on the inner shell surface may have varied in depth from the surface. Thus, an air gap may have resulted and the effective thickness of the Transite shell was probably different between various pairs of thermocouples. The outer and inner surface thermocouples may not have been radially opposite to each other and this could also cause an erroneous measurement of temperature difference across the Transite shell at any particular location.

Because of thermocouple failure some of these data were obtained with only one pair of thermocouples. Thus, temperature profiles around the periphery could not be obtained simultaneously at a particular air flow and power setting. The cylinder could be positioned at five-degree increments only by means of the hold-down screws instead of with a vernier and guide ring as provided for cylinder B. Therefore, to obtain a temperature distribution around the cylinder, to be used to calculate the Nusselt number distribution, it was necessary to shut off air flow and power input while the cylinder was removed from the duct and rotated to a new position. This procedure extended the data-taking over a considerable length of time during which ambient conditions may have changed appreciably. Also, each position change required the air flow and power input to be shut off, then re-set, and subsequently, a stabilizing interval to be observed. Needless to say, this resulted in a large experimental scatter due to variation in Reynolds number and power input between individual test points.

However, when the distributions of Figures 32, 33, and 34 are compared to those obtained by Giedt (2) and Schmidt and Wenner (11) a marked similarity may be noted. These reference data were obtained for cylinders of large diameter exposed to essentially free-stream flow which resulted in much greater Reynolds numbers. It is likely that the surface roughness of test cylinder A may have increased the effective Reynolds number appreciably so that qualitatively the Nusselt number distributions may be compared with the reference data. For duct widths greater than two cylinder diameters the flow conditions would approach those realized in a wind tunnel or free stream configuration.

Pressure Gradients in Ducts

Variations of static pressure along the duct wall were obtained for each configuration over the range of experimental air flows as explained in the section on instrumentation in Appendix I. For the staggered configuration the static pressure variation was not measurable because the pressure taps were covered by the half-cylinders installed along the duct wall. For this reason only the total pressure drops across the entire arrangements were obtained.

Representative variations of static pressure along the duct wall obtained with the 1.5-inch diameter test model located in the 2-inch, 3-inch, and 3.5-inch wide ducts, respectively, are shown in Figure 35.

These distributions are for a nominal constant mass velocity of approximately 4.32 pounds per second-square foot which corresponds roughly to a bulk Reynolds number of 42,500 or a flow velocity of 60 feet per second.

Inspection of Figure 35 discloses several significant features. The maximum static pressure drop varies inversely with duct width and is attained at a distance downstream of the center plane of the model. The occurrence of maximum static pressure drop downstream of the center plane indicates a minimum flow cross section similar to a vena contracta. The distance appears to be increasing with decreasing width. As would be expected, complete recovery of the maximum static pressure drop is not realized downstream, where the original flow conditions are believed to have been restored. The percentage of recovery, defined as the ratio of the amount of static pressure recovered to the maximum pressure drop, increased with increasing duct width.

Figure 36 shows the variation of static pressure along the duct wall at several different mass velocities for a typical in-line configuration, consisting of three 1.5-inch diameter cylinders spaced at a longitudinal center-line-to-center-line distance of 2.25 inches which corresponds to 1.5 cylinder diameters. Although these distributions are for the 3-inch wide duct, similar distributions are obtained for the same configuration in ducts of different width and for various longitudinal spacings in the same duct. The minimum static pressure occurs nearly at the center plane of the third downstream-cylinder. This is probably due to the partially confined flow passage upstream, caused by the first two cylinders. Consequently, a more gradual reduction in flow area occurs. Near the upstream-cylinder, the static pressure variation is similar to that for a single cylinder. The static pressure further decreases as the stream flows downstream beyond the center plane of the upstream cylinder. Comparison of variations of static pressure at different mass velocities indicates that the maximum static pressure drop is roughly proportional to the square of the mass velocity and that the percentage of recovery seems to increase with decreasing velocity.

The effect of longitudinal spacings can be observed by comparing the variation of static pressure in a 3-inch wide duct with single cylinder in Figure 35 and the variation for three cylinders in line at a mass velocity of 4.36 pounds per second-square foot in Figure 36. In both cases, the duct widths are the same and the mass velocities nearly equal. The pressure loss for one cylinder is approximately 1.4 inches of water and the pressure loss for three cylinders is approximately 1.03 inches of water which corresponds to a pressure loss of 0.35 inch of water per cylinder, duct width and mass velocity being the same. Thus, if the single-cylinder configuration is considered as a configuration of multiple cylinders longitudinally spaced infinitely apart, the pressure loss per cylinder is reduced to a considerable extent by closer spacing.

The effect of variation of longitudinal spacing on pressure loss is further illustrated in Figure 37, where the longitudinal distribution of static pressure at the duct wall is shown with different longitudinal spacings of three in-line cylinders for a typical test duct. These data

were obtained in a 3-inch wide duct at a constant nominal mass velocity of 5.49 pounds per second-square foot, corresponding to a Reynolds number of 52,000 and a velocity of 75 feet per second and for four different center-line spacings. For comparison, the static pressure distribution for a single cylinder at essentially the same mass velocity is included.

The distribution curves for the in-line cylinders are essentially similar to one another. The maximum static pressure drop appears to be increasing with increase of longitudinal spacing. The pressure loss on a per-cylinder-basis also increases with increasing spacing, with the single-cylinder data as the limit. The percentage of recovery increases with diminishing spacing, as calculations on basis of the shown curve values indicate.

The effect of cylinder diameter on static pressure variation along the wall of the 3.5-inch wide duct is shown in Figure 38 for three cylinders of different diameter. The pressure drop data shown in Figure 38 for a single 1-inch diameter and a 1.938-inch diameter cylinder were used to verify the correlation obtained with the 2.5-inch diameter test cylinder. Comparison of Figure 38 with 35 shows that increasing cylinder diameter produces the same general effect on the pressure distribution as decreasing duct width which would be expected from similarity considerations when the pressure gradient is assumed to be determined by the ratio of cylinder diameter to duct width.

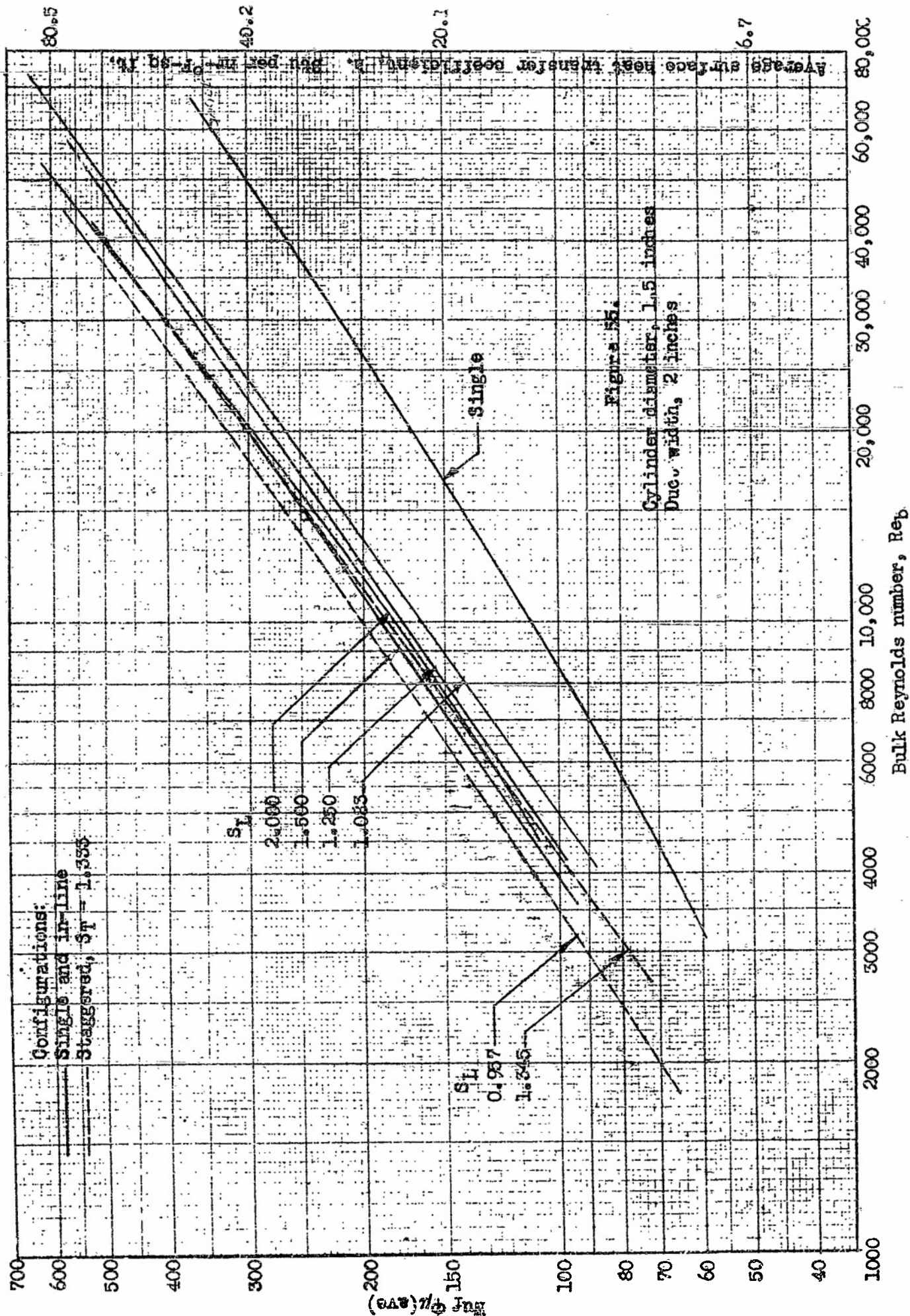
In order to determine the effect of heating on the static pressure distribution at the duct wall, comparative runs were made at constant air flow with the test cylinder heated and unheated. No effect of heating could be detected within the accuracy of the instrumentation, therefore for each configuration only one static pressure distribution was obtained at any given Reynolds number even though the surface temperature of the test cylinder may have varied 200°F or more for the range of heat dissipation used. However, in all instances the temperature rise of the air was small and did not exceed 5°F.

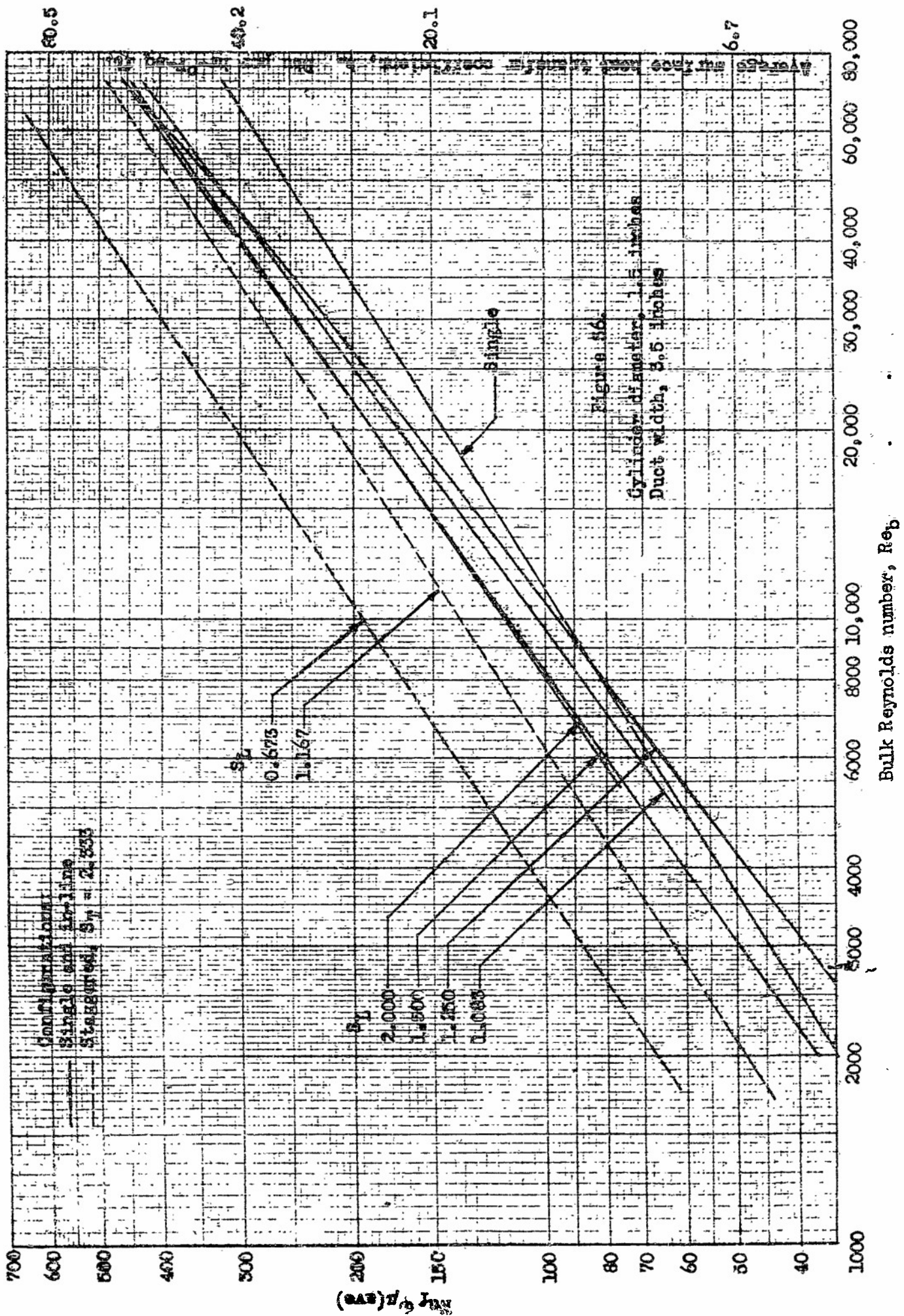
Overall Heat Transfer

1. Effect of Cylinder Arrangement on Nusselt Number

Variations of modified average Nusselt number $Nu_f \phi \mu_{(ave)}$ with bulk Reynolds number for several cylinder arrangements are shown in Figures 55, 56, and 57. The curves indicate the relative effect of cylinder arrangement on the Nusselt number for the physical arrangements described by cylinder diameter, cylinder spacings, and duct width. The quantitative variation of average surface heat transfer coefficients are also described because for the same cylinder diameter, as is the basis of the data, the heat transfer coefficient is directly proportional to the Nusselt number.

Figures 55 and 56 contain curves for single, in-line, and staggered configurations in the 2-inch and 3.5-inch wide duct, respectively. Such curves for a fixed duct width may be compared directly since under this condition a given bulk Reynolds number indicates a constant quantity of air flow irrespective of cylinder arrangement.





The curves in Figure 55 indicate an appreciable increase of heat transfer by use of multiple-cylinder arrangement. The increase over the single cylinder in the 2-inch duct is in the order of 50 to 70 per cent. Among the in-line arrangements, a longitudinal spacing corresponding to 1.5 cylinder diameters appears to produce the greatest heat transfer. However, the range of variation of the values obtained for longitudinal spacings between 1.083 and 2.00 cylinder diameters is only approximately 15 per cent. The order of curves of constant longitudinal spacings indicates the existence of an optimum value within the investigated range which, however, may be greater or smaller than 1.5 cylinder diameters.

With staggered arrangements in the 2-inch wide duct, greater heat transfer than with the in-line arrangements may be obtained. The greatest values indicated in Figure 55 are for the staggered configuration with a longitudinal spacing of 0.95 cylinder diameter. For this arrangement a qualitative increase of 20 per cent over the mean value for the in-line configurations is indicated.

The nature of the curves in Figure 56 for the 3.5-inch wide duct is similar to that of the curves in Figure 55 for the 2-inch wide duct. However, an outstanding difference is that the increase of heat transfer with multiple in-line spacings over the single cylinder is not as appreciable as for the 2-inch wide duct. For the range of longitudinal spacings investigated, the variation in heat transfer is of about the same order as for the narrower duct, although the curves appear to have a tendency to converge at the higher Reynolds number. Again, the existence of an optimum spacing is indicated. Like in Figure 55, the highest values of heat transfer are shown for the staggered spacing. However, in contrast, the increase over the in-line spacing is very appreciable. The maximum values of heat transfer obtained for a staggered arrangement with a longitudinal spacing of 0.675 diameter are approximately 100 per cent greater than the mean of those for the in-line arrangements. Quantitatively the heat transfer coefficients obtained for the spacing are equal to the maximum values obtained for the staggered arrangement in the 2-inch wide duct with 0.95-diameter longitudinal spacing. Consequently, the values for the in-line arrangements in the 3.5-inch wide duct differ appreciably from those in the 2-inch wide duct. For equal Reynolds number, signifying the same air velocity, the heat transfer coefficients in the wider duct are approximately 40 per cent lower.

For comparison, the heat transfer coefficients and Nusselt numbers obtained with a double-row staggered configuration in a 3-inch and a 3.5-inch wide duct are plotted. For reference purposes, Figure 57 also contains values for a single cylinder in each of the ducts. It is evident that heat transfer from a single cylinder in the wider duct and at the same Reynolds number is somewhat lower. At a Reynolds number of 10,000 the difference is in the order of 10 per cent. The double-row staggered configurations show heat transfer coefficients up to 150 per cent greater than the single cylinders. The magnitude of the heat transfer coefficients is appreciably affected by variations in spacing. In the 3-inch wide duct, for a range of diagonal spacings from 1.083 to 1.50 cylinder diameters, the heat transfer coefficient is reduced by approximately 35 per cent. Like in the symmetrically staggered arrangements, for which the data are given in Figures 55 and 56, the largest heat transfer is obtained at the smallest diagonal spacing. The range of diagonal spacings for the 3.5-inch wide duct is smaller and covers only the values of 1.153 and 1.413-cylinder diameters. The difference

between the heat transfer indicated by the two curves is only in the order of 15 per cent.

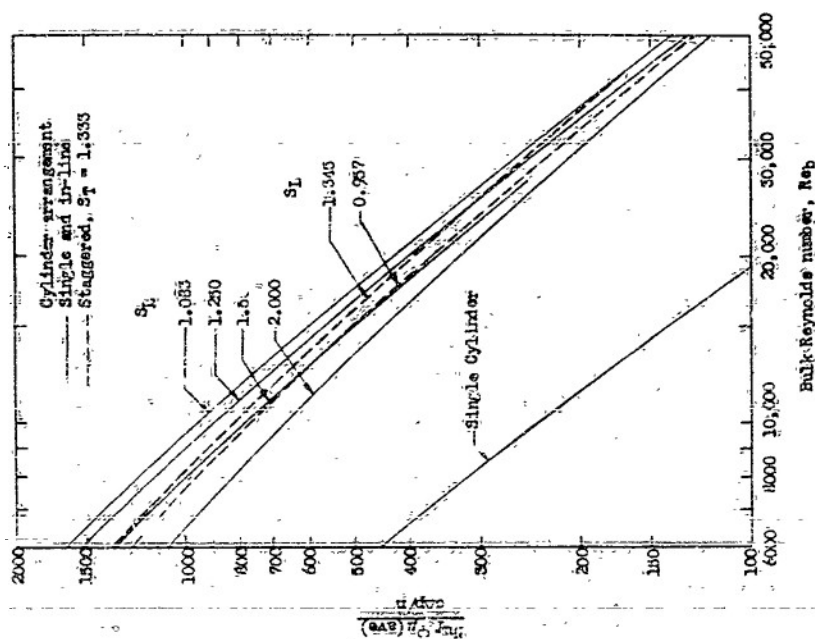
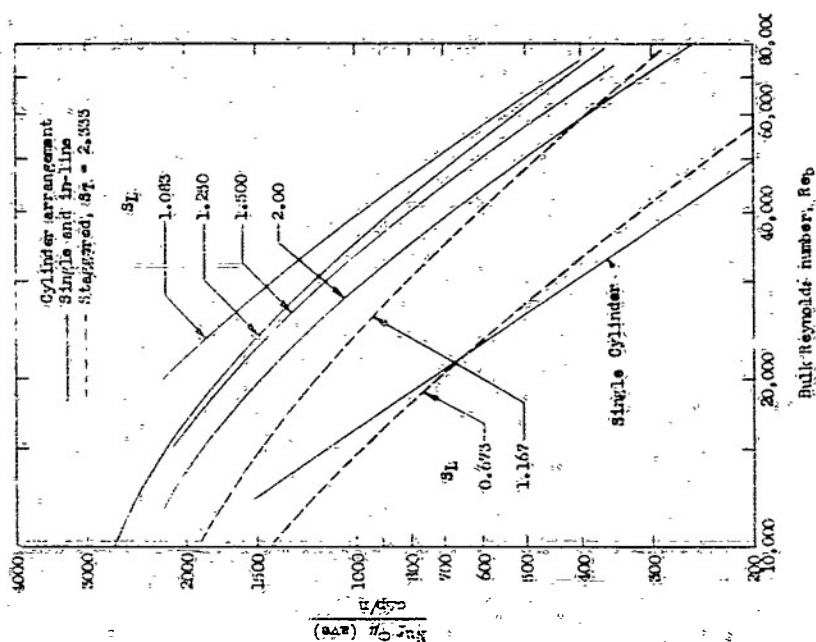
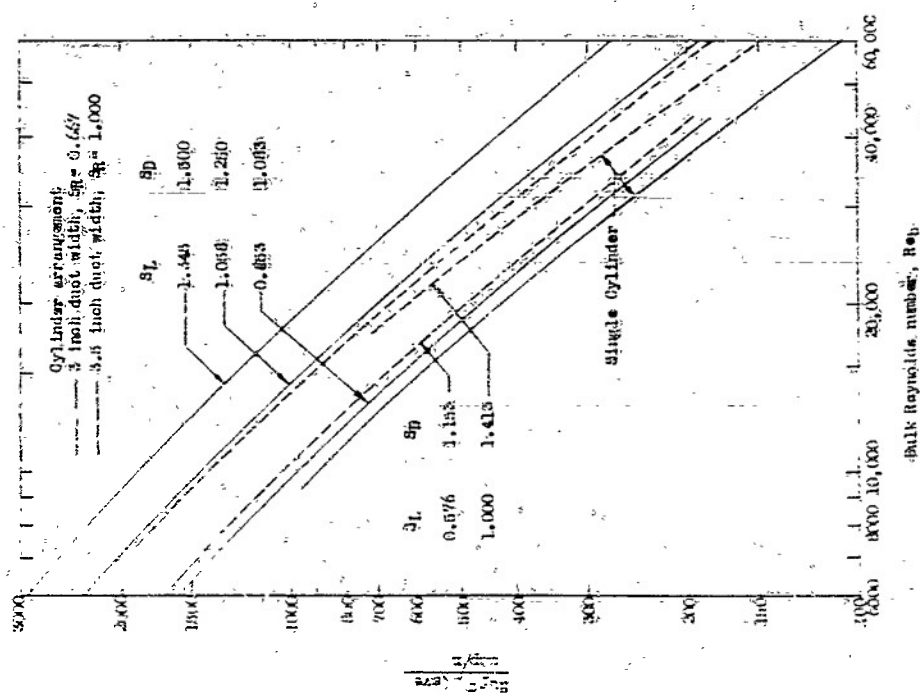
It is noteworthy that the curves for the double-row staggered configurations shown in Figure 57 represent, for any given Reynolds number, heat transfer coefficients of decreasing magnitude with increasing diagonal spacing, irrespective of the duct width. Also, the slopes of the lines expressing the variations of heat transfer coefficient with Reynolds number are, while similar, not equal for the various configurations investigated. Therefore, it appears that for purpose of general correlation the slopes would not be constant but would be dependent on spacing as well as Reynolds number.

2. Nusselt Number and Pressure Drop Relation

Re-interpretation of the average heat transfer curves in Figures 55, 56, and 57 on the basis of energy requirements for indicated heat transmission is of importance to describe more completely the effects of cylinder arrangement and air flow velocity. The ratio of average modified Nusselt number to corrected pressure drop per cylinder, at a given Reynolds number and fixed duct width, is a direct indication of the heat transfer obtained per unit of energy input to the air stream, necessary to produce the given velocity of flow. Thus the efficiency of heat exchange for the various arrangements may be evaluated. Also, the effect of Reynolds number on heat transfer per unit energy requirement may be illustrated.

Figure 58, like Figure 55, contains curves for single, in-line, and staggered cylinder arrangements in the 2-inch wide duct. It is apparent that the efficiency of heat exchange is greatest at the lowest air velocity. However, it should be noted that the total heat exchange obtainable from a given surface for a specified temperature difference decreases with air velocity in the manner shown by Figures 55, 56, and 57. Applied to the cooling of electronic components which must dissipate a fixed quantity of heat from a given surface, reduction in cooling air velocity results in increased temperature rise of the surface.

Greatest heat transfer efficiency at lowest air velocity is also indicated by the curves in Figure 59, similar to Figure 58, but for a 3.5-inch wide duct, and by Figure 60 for double-row staggered arrangements in ducts 7 and 3.5 inches wide. The values shown for different ducts may be compared on the basis of equal flow rate. Since the flow rate is proportional to the product of Reynolds number and duct width, comparable points are obtained at Reynolds numbers related to each other inversely to the duct widths. For example, the curve-value obtained in Figure 58 corresponding to an in-line longitudinal spacing of 1.50-cylinder diameters at a Reynolds number of 35,000 is 200. For the same flow rate, the Reynolds number in Figure 59 must be 20,000 since the duct width is related to that of Figure 58 as 3.5 to 2.0. Therefore, the curve-value obtained in Figure 59 and corresponding to an in-line longitudinal spacing of 1.50-cylinder diameters is 1700. This shows the ratio of heat transfer per unit power requirement to be most favorable for the widest air passage if the air flow rate is fixed. Another basis of comparison would be equal air flow velocity which is attained at the same Reynolds number.



Under this condition, the ratio of heat transfer to unit power requirement is determined by dividing corresponding curve-values by their respective duct widths. For example, the above-mentioned curve-value of 1700 at a Reynolds number of 20,000 in Figure 59, divided by the duct width of 3.5 inches, gives a comparative value of 486. The corresponding value in Figure 58, at the same Reynolds number of 20,000 and the longitudinal spacing of 1.50-cylinder diameters, is found to be 400 which when divided by the duct width of 2 inches gives a comparative value of 200. Thus, on the basis of equal flow velocity as well, the wider air passage, in the range considered, appears to be more favorable if the ratio of heat transfer per unit energy requirement is an important criterion.

The curves in Figure 58 for various configurations in a 2-inch wide duct indicate similar relationships as those in Figure 55 in respect to the effect of configuration. The multiple configurations exhibit values for the heat transfer-pressure drop ratio which are rather closely related and appear to differ only over a range of approximately 30 per cent. The values are, however, vastly different from those for the single cylinder, being at the same Reynolds number on the average more than 200 per cent greater. This is appreciably different from the relationships for heat transfer only, as indicated in Figure 55. Also in respect to relative position the curves in Figure 58 differ from those in Figure 55. For the in-line arrangements no optimum longitudinal spacing appears to be indicated. Instead, the values of the heat transfer-pressure drop ratio increases with reduced longitudinal spacing. The highest values shown in Figure 58 are for the in-line arrangement with a longitudinal spacing of 1.083-cylinder diameter. Those for the staggered arrangements equal closely the average values for the in-line arrangement but differ in their order from those in Figure 55 in that the values for the larger longitudinal spacing are greatest.

Like in Figure 56, the curves in Figure 59 for the heat transfer-pressure drop ratios of various configurations in the 3.5-inch wide duct appear to indicate a considerable spread of values. No great inferiority of the single cylinder is apparent. The order of in-line configurations in respect to magnitude of the heat transfer-pressure drop ratio is opposite to magnitude of longitudinal spacing. The greatest values are shown for the smallest longitudinal spacing of 1.083-cylinder diameters. The staggered configurations have values considerably lower than the in-line configurations, the lowest being those for a longitudinal spacing of 0.673-cylinder diameter which differ but slightly from those for the single cylinder. Thus, the heat transfer-pressure drop ratios for the various configurations in the 3.5-inch wide duct are related among each other differently than the heat transfer coefficients. Among the latter, those for the staggered configuration and a longitudinal spacing of 0.673-cylinder diameter are greatest and are about 100 per cent greater than those for the single cylinder, as shown in Figure 56.

In Figure 60, like in Figure 57, double-row staggered configurations are compared with single cylinders in two different ducts of 3- and 3.5-inch widths respectively. The curves for the heat transfer-pressure drop ratio indicate lower values for smaller diagonal spacings. The values for the single cylinder in the 3-inch wide duct are up to 10 per cent lower

than those for the smallest diagonal spacing of 1.083-cylinder diameters. The values for the single cylinder in the 3.5-inch wide duct are about 20 per cent greater than those for the smaller diagonal spacing of 1.153-cylinder diameters. The entire range of values indicated for equal Reynolds number is about 100 per cent of the minimum values and is comparable to the range of heat transfer values in Figure 57.

V. CORRELATION OF RESULTS

Peripheral Distribution and Point Values

The circumferential variation of point Nusselt number around a single cylinder in a free air stream was studied by various investigators. Comparison of their data discloses considerable disagreement, as pointed out in References (11) and (13). However, data in the literature for the single cylinder in free air flow are qualitatively comparable and offer a basis for comparison of the data obtained in the present investigation for evaluation of the duct effect.

Nusselt number distributions as obtained for the single cylinder in 2-, 3-, and 3.5-inch wide ducts are shown in Figure 61 for a bulk Reynolds number of 52,000. For comparison, the distribution curve for the same Reynolds number and for free stream conditions as reported by Schmidt and Wenner (11) is also included. The duct effect is quite apparent. It evidences itself in increased point Nusselt numbers with reduced duct widths. Also, the effect appears to be more pronounced on the distribution of the upstream half of the cylinder. The location of the minimum Nusselt number is slightly affected by duct width. It shifts about 10 degrees downstream on the periphery for a variation from free stream to 2-inch duct width.

Schmidt and Wenner's data compare favorably with Squire's theoretical solution for the Nusselt number at the stagnation point

$$Nu = 1.01 \sqrt{Re} \quad (3)$$

Data obtained in the present investigation may be compared on the basis of Squire's equation to evaluate the duct effect as a function of dimensional relationships. For equal film Reynolds numbers, Nusselt numbers at the stagnation point of single cylinders in ducts are found to be greater than for free stream conditions. Also, in general the Nusselt numbers are observed to be increasing with decreasing duct width. The factor $\sqrt{1 + d/w}$, where d/w represents the ratio of cylinder diameter to duct width, correlates satisfactorily the experimental data with Squire's equation, as shown in Figure 62. The form of the correlation factor is such that it reduces to unity for the free stream condition where w is infinite. The correlation factor must not exceed the value of 1.414 since this would correspond to a ratio of cylinder diameter to duct width of unity which means that no flow area past the cylinder is available.

Overall Heat Transfer

The different relationships between average Nusselt number and bulk Reynolds number as shown in Figures 55, 56, and 57 serve to illustrate the configuration effects in individual ducts. General correlation of heat transfer in different configurations and ducts is feasible by expressing the average film Nusselt number as a function of film Reynolds number and the characteristic dimensions of the configuration. The average film Nusselt number is the average of the point Nusselt numbers. The film Reynolds number is evaluated on the basis of the mean of the average surface temperature and the bulk air temperature. In correlating the data,

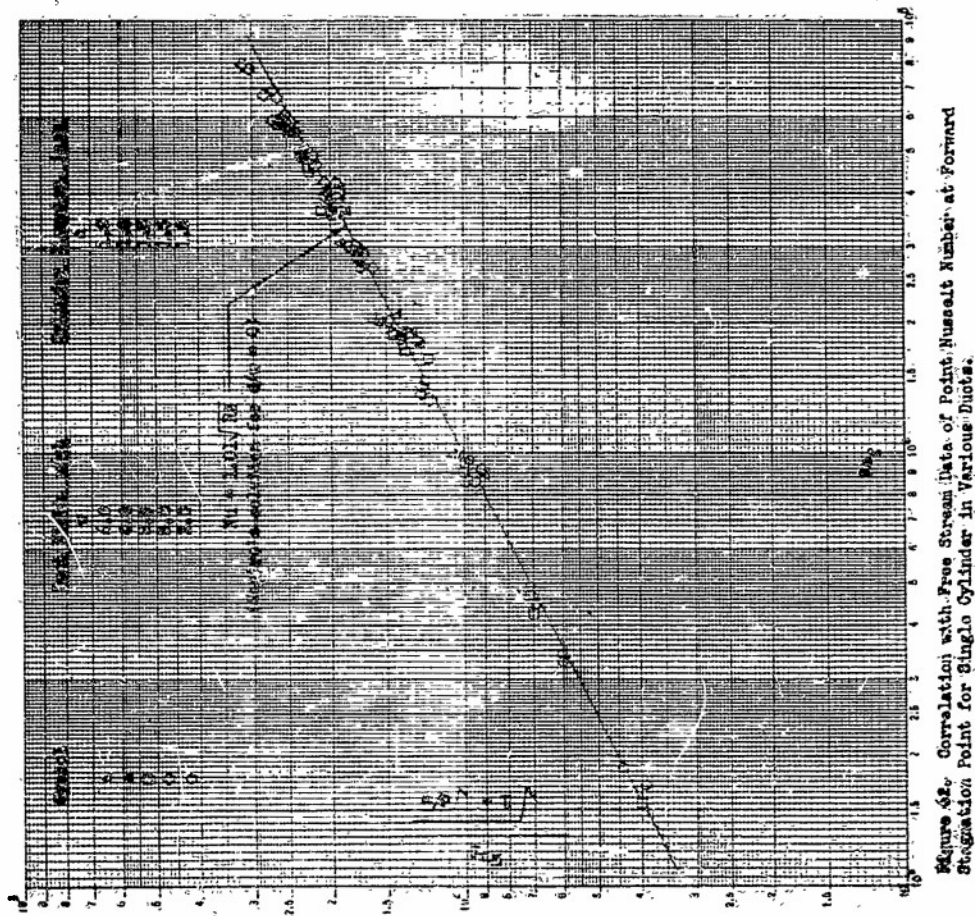


Figure 62. Correlation with Free Stream Data of Point, Nusselt Number at Forward Stagnation Point for Single Cylinder in Various Ducts.

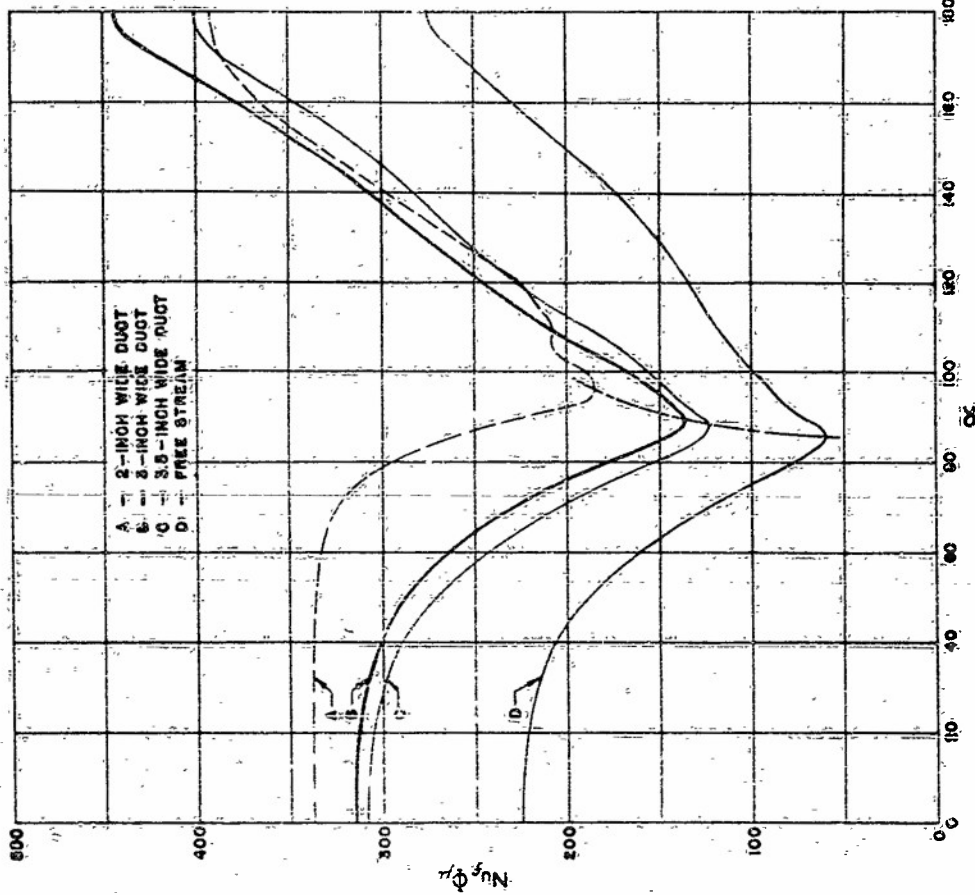


Figure 61. Effect of Duct Width on Nusselt Number Distribution for a Minimal Bulk Reynolds Number of 2000.

McAdams' (9) average line drawn from results obtained by several experimenters with single cylinders in a free air stream may serve as a reference for comparison.

The general form of the correlation equation would fit the curve drawn by McAdams and would have the equation

$$Nu_f(ave) = C \cdot F [Re_f(ave)]^n \quad (4)$$

The values of the constant C and the exponent n are functions of the Reynolds number and may be closely approximated by the following values:

$Re_f(ave)$	C	n
1,000 - 6,000	0.409	0.531
6,000 - 30,000	0.212	0.606
30,000 - 100,000	0.139	0.806

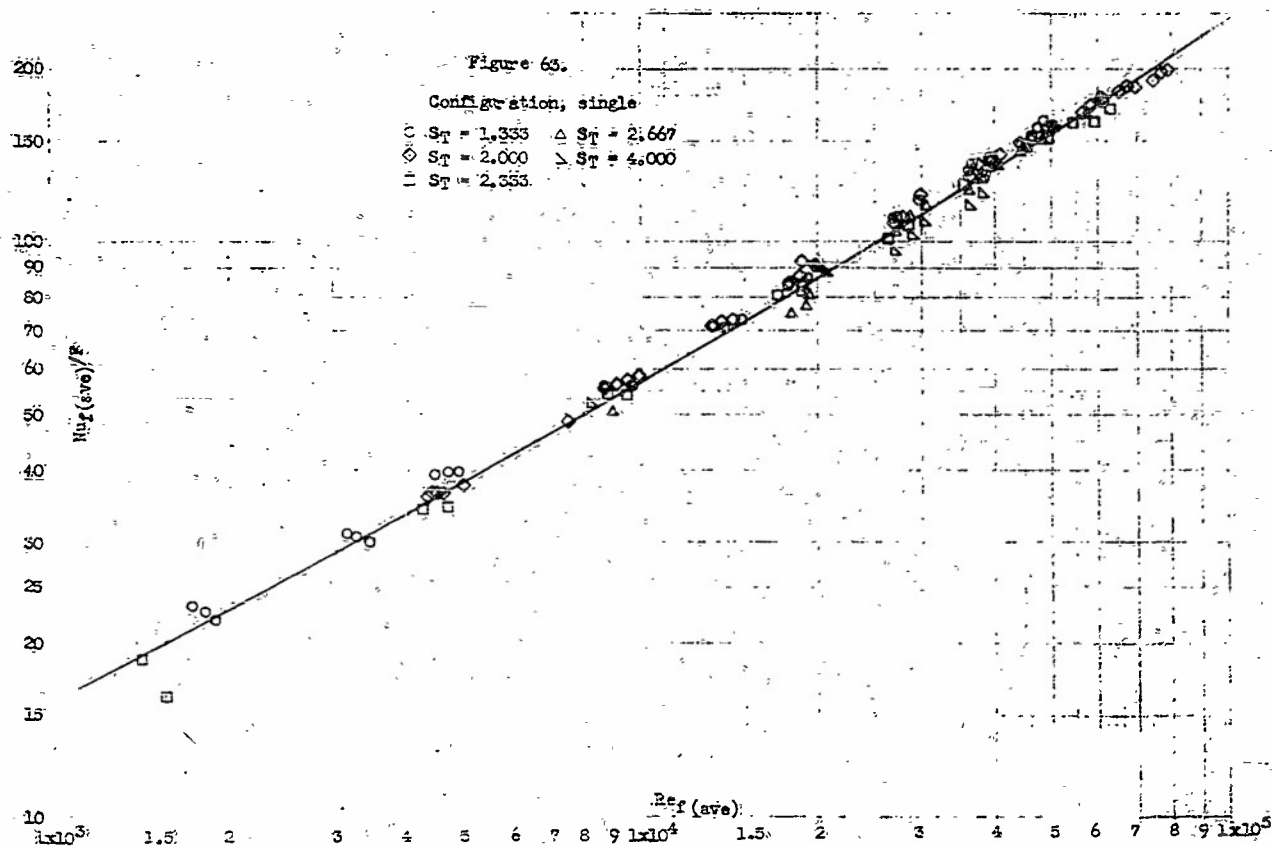
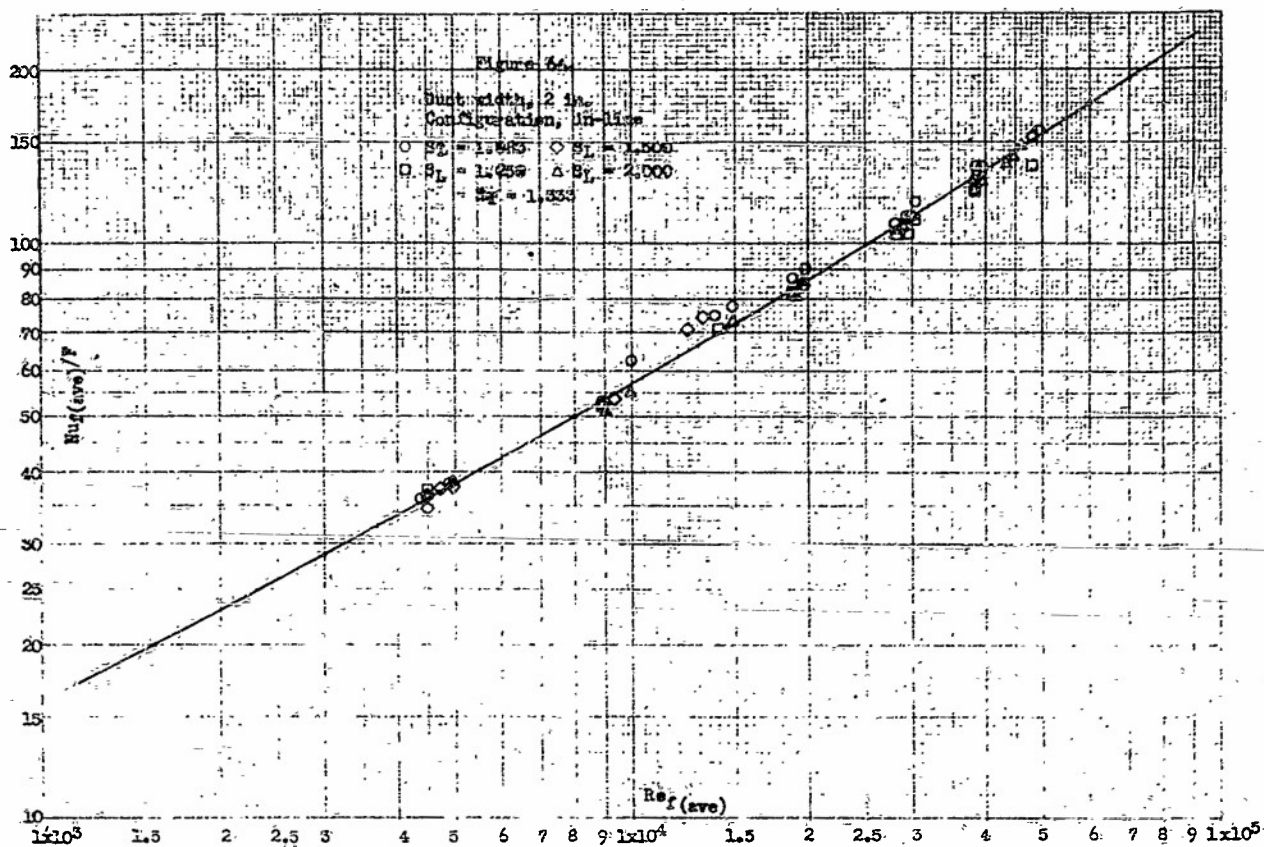
The configuration factor F has a different form for each type of cylinder arrangement. It is unity for a single cylinder in a free air stream. For all other configurations, it must become unity for infinite longitudinal and transverse pitches. This would describe a single cylinder in the free stream conditions.

The average film Nusselt number, $Nu_f(ave)$, for single cylinders in ducts of various widths are correlated by means of the factor

$$F_1 = (1 + \sqrt{d/w}) \quad (5)$$

so that a plot of $[Nu_f(ave)/(1 + \sqrt{d/w})]$ versus Re_f gives substantial agreement with the curve presented by McAdams. This is shown by the plot in Figure 63 which contains data for five duct widths.

For the correlation of the data obtained with in-line cylinders, the factor F_1 , obtained for a single cylinder, must be modified to take into account the finite longitudinal spacing of cylinders. The single cylinder may be considered as a special case of in-line cylinders for which the longitudinal pitch S_L is infinite. As previously defined, S_L is the longitudinal spacing in cylinder diameters. Thus, if the modification factor assumes the form $(1 + \phi)$, ϕ must be zero when S_L is infinite. It may be seen from Figures 55 and 56 that for in-line cylinders the Nusselt number-versus-Reynolds number lines are not parallel and do not possess the same curvature as that of the reference line shown in Figure 63. Consequently, the factor ϕ must be a function of the longitudinal pitch S_L , the ratio d/w , and of the Reynolds number. The ratio d/w may also be interpreted as the transverse pitch S_T of several rows of in-line cylinders, each row being in a duct of equal width. Thus, the data may be applied to banks of tubes by assuming the effect of duct walls to be negligible. The correlation factor obtained by numerical approximation based upon the experimental data is



$$\begin{aligned}
 F_2 &= (1 + \sqrt{d/w})(1 + \phi) \\
 &= (1 + \sqrt{1/S_T}) \left\{ 1 + \left[(1/S_L) - (0.872/S_L^2) \right] \times \right. \\
 &\quad \times \left. \left[1.81/S_T^2 - 1.46/S_T + 0.318 \right] \left[Re_f(0.526 - 0.354/S_T) \right] \right\} \quad (6)
 \end{aligned}$$

The agreement of experimental data, using the correlation factor F_1 with the reference line is shown in Figures 64, 65, and 66, respectively, for ducts of 2-, 3-, and 3.5-inch width, each with four longitudinal pitches. Agreement for the 2-inch wide duct as shown in Figure 64 is the best. The data for the 3.5-inch wide duct appear to deviate the most from the reference line particularly at the lower Reynolds number. Appreciable spread appears to exist with the correlated Nusselt number being on the average 10 to 30 per cent below the curve.

For the staggered configurations, the same type of the modification factor as for the in-line configuration is necessary. Here too, ϕ is required to become zero when S_L is infinite, to reduce to the factor for single cylinders. The form of correlation factor obtained in the same manner as for in-line cylinders is

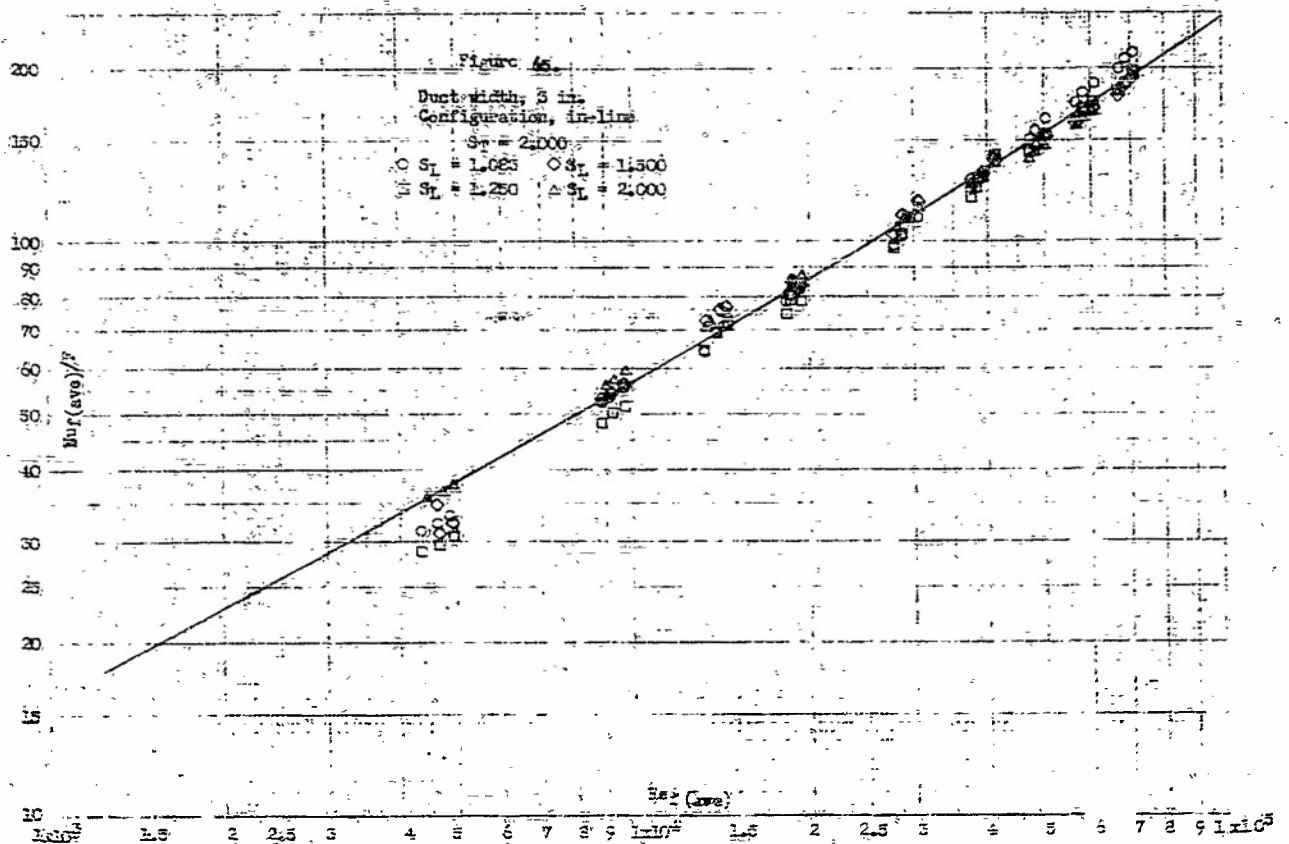
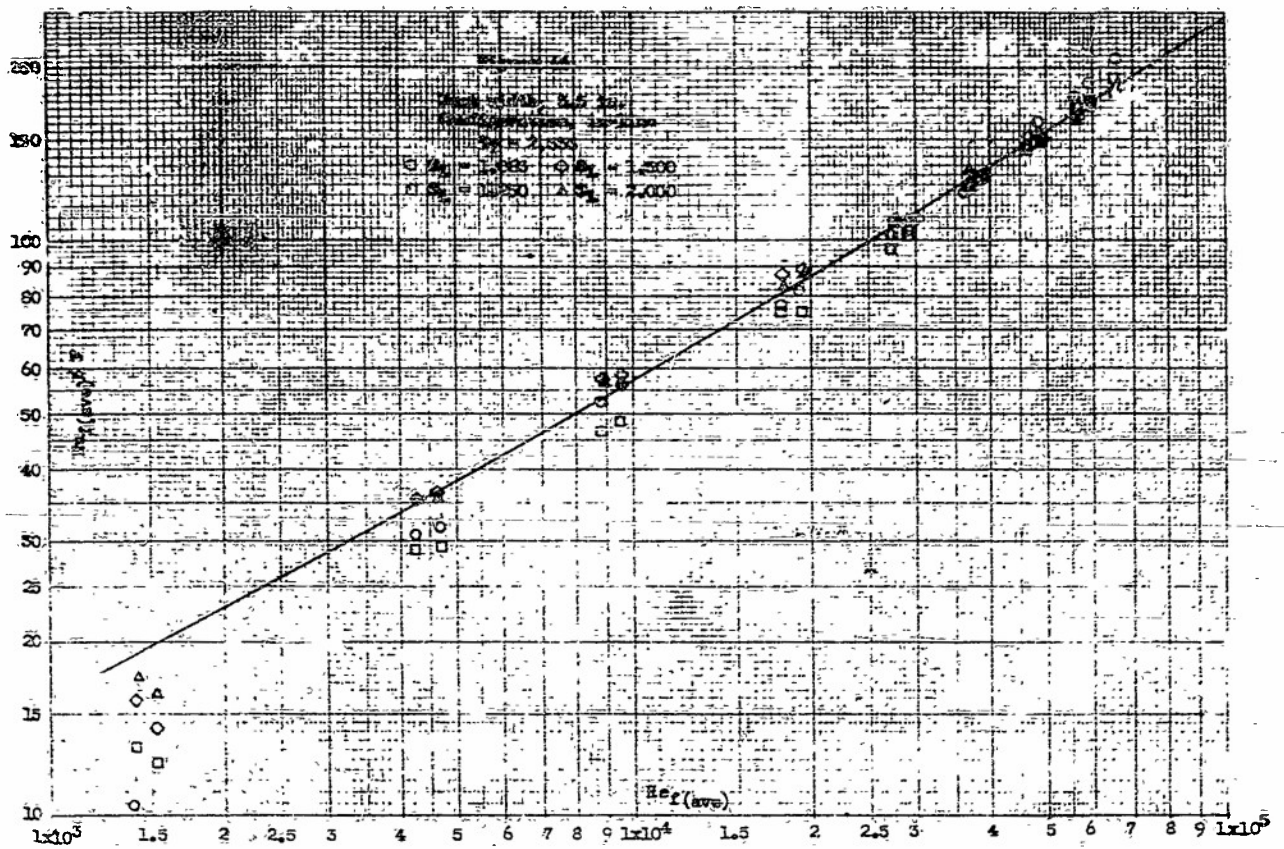
$$\begin{aligned}
 F_3 &= (1 + \sqrt{1/S_T}) \left\{ 1 + \left[(f_1/\sqrt{S_L}) - f_2/S_L \right] Re_f^{0.13} \right\} \quad (7) \\
 \text{where } f_1 &= [15.50/S_T^2 - 16.80/S_T + 4.15] \\
 \text{and } f_2 &= [14.15/S_T^2 - 15.53/S_T + 3.69]
 \end{aligned}$$

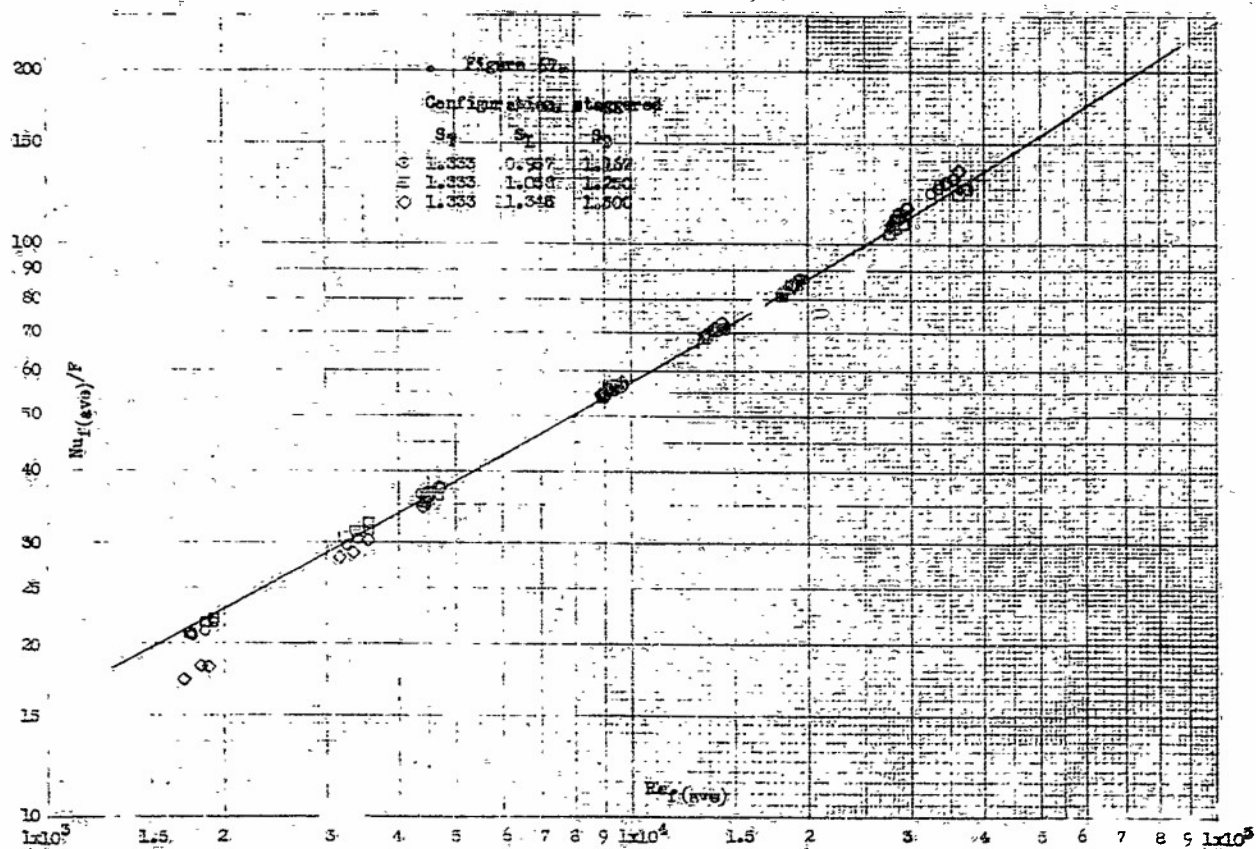
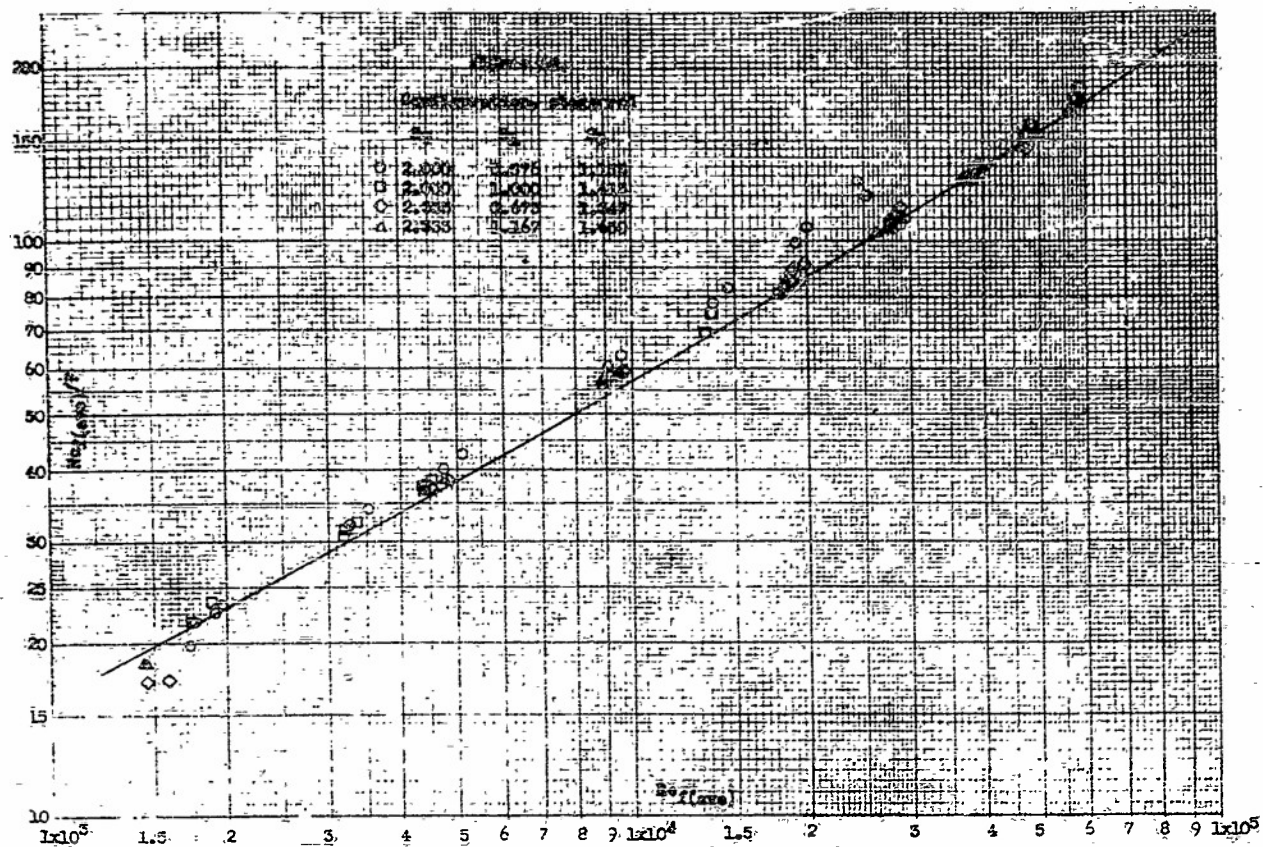
The accuracy of the correlation factor as applied to the experimental data is shown in Figures 67 and 68 plotted for seven cylinder arrangements in three ducts. The points shown in Figure 67 for the 2-inch wide duct are very close to the reference line except at the lower Reynolds numbers. The points in Figure 68 deviate somewhat more. Poor correlation at low Reynolds numbers, as shown in several of the figures, may have been caused by inaccurate determination of the low heat flow rates obtained under these conditions. Low heat flow was the result of the limitation of the internal temperature to 500°F and of low heat transfer coefficients. The small temperature differentials across the Transite shell, thus encountered, could be measured to an accuracy of ±1°F which may have resulted in errors in point heat transfer coefficients of as high as 15 per cent.

The data for the double-row, staggered configuration were not correlated because they were not available in sufficient varieties of cylinder arrangement to permit accurate evaluation of all the variables affecting the heat transfer coefficient.

Static Pressure Drop Correlation

For the correlation of the pressure drop data, the effects of variation of fluid properties were disregarded. Thus, the resulting relationships were limited to the flow of air in the incompressible-flow region. Preliminary investigation of the variation of friction factor determined in the conventional manner indicated a predominant effect of cylinder configuration. Therefore, in the correlation subsequently chosen, the effect of Reynolds number was not isolated. Strictly speaking, this effect was neglected since





the assumed variation of pressure drop with air flow rate suggested, for any given configuration, an essentially constant friction factor.

Figures 69, 70, and 71 show the correlation plots for single, in-line, and staggered configuration, respectively. The corrected pressure drop is determined by the product of the measured pressure drop per cylinder and the ratio of air density at test condition to standard air density (0.0765 pound per cubic foot). The corrected pressure drop is plotted as a function of the mass flow velocity modified by a configuration factor ψ . The slope of the line in each figure corresponds, for the greater range of the modified mass flow velocity, to the dimensionally specified value of 2. This suggests a constant friction factor. However, in the lower range of mass flow velocities, some deviation may be observed which must partly be ascribed to an increase of friction factor with reduced velocity and the dependency of the friction factor on flow velocity at low Reynolds numbers.

The line shown in Figures 69, 70, and 71 to fit the test data has the equation

$$(\Delta p)/\rho = 0.0111 G^2/\psi \quad (8)$$

As shown in Figure 69, the determination of the constant is not based only on data obtained with a 1.5-inch diameter cylinder, as in the case of the heat transfer data. Additional points are shown corresponding to three different configurations obtained by the use of a 1-inch diameter cylinder in a 2-inch and in a 3.5-inch wide duct, and by the use of a 1.938-inch diameter cylinder in a 3.5-inch wide duct.

The value of the configuration factor ψ is affected by the type of configuration. For the single cylinder, it is

$$\psi_1 = (1 - 1/S_L)^{2.7} \quad (9)$$

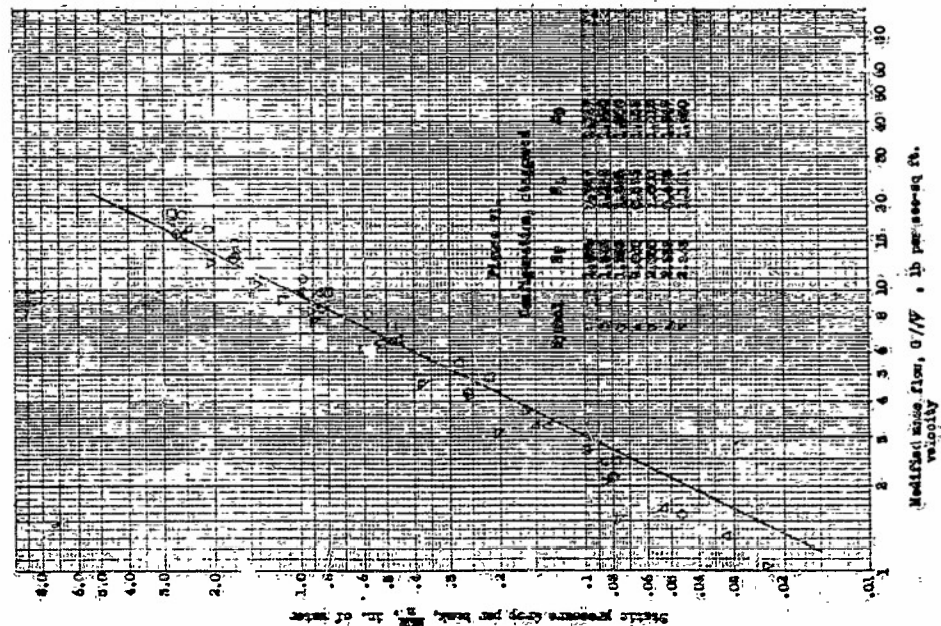
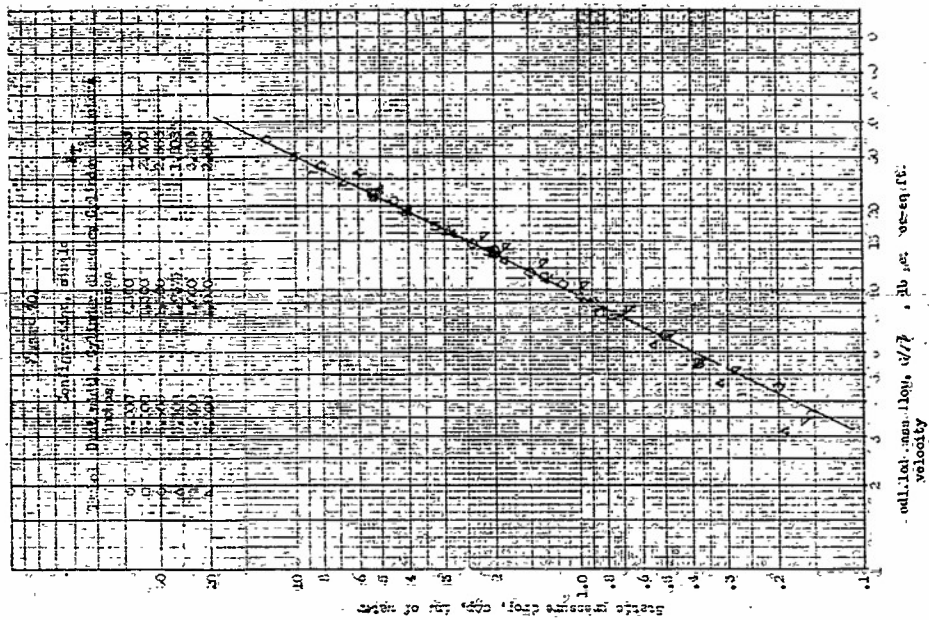
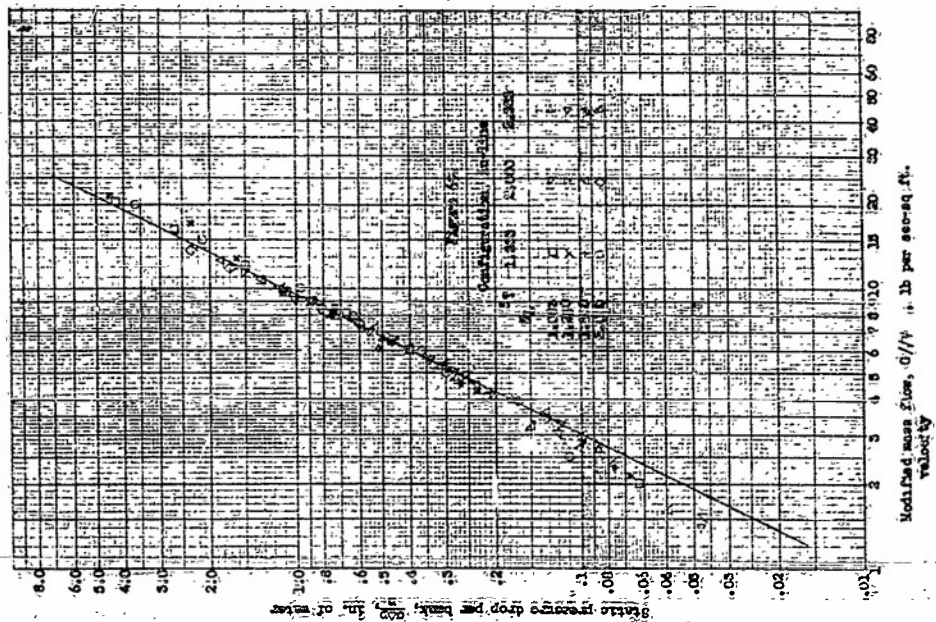
For cylinders in line, the expression for the single cylinder is further modified to the form

$$\psi_2 = \psi_1 (1 + 1/S_L)^{1.65} \quad (10)$$

Obviously, ψ_2 is equal to ψ_1 when the longitudinal spacing becomes infinite which would be equivalent to the single cylinder. Similarly, for cylinders staggered symmetrically relative to the axis of the duct, the expression for the single cylinder is modified to the form

$$\psi_3 = \psi_1 (1 + 1/S_L)^{(4.36 - 3.52/S_L)} \quad (11)$$

The modification factor for stagger, is only a function of longitudinal spacing and approaches unity as the spacing approaches infinity. However, the indicated dependency of the modification factor on longitudinal spacing alone may not be entirely accurate since appreciable scatter of the test points for the staggered configuration is observed in Figure 71. The modification factor is probably affected by the ratio of the maximum to the minimum flow area and should therefore, be also a function of



transverse pitch.

Like for the heat transfer data, correlation of the pressure drop data for staggered cylinders, in double rows was not completed because of insufficient data.

In general, the correlation as presented by equation (7) may lack validity because of the quality of the data on which it is based. In many instances, the location of the pressure taps relative to the configuration of the cylinders was such that, in all likelihood, incomplete recovery was measured, i.e., the flow velocity at the downstream tap was slightly greater than that at the upstream tap. The instrumentation for the measurement of pressure gradients did not permit very accurate determinations at low flow velocities because of insensitivity of the manometers.

The generalization of the pressure drop correlation to configurations of cylinders or tubes in multiple rows and banks may be somewhat inaccurate since the correlated data include the skin friction effect of the duct walls. The relative magnitude of the effect at high mass velocities may be insignificant in comparison with the pressure drop caused by the presence of the cylinders. However, at low velocity the tendency for increase of the friction factor may cause this effect to be of greater significance which would partly explain that, under these conditions, the test points lie above the correlated mean line.

VI. BIBLIOGRAPHY

1. Brown, A. I. and Marco, S. M., Introduction to Heat Transfer, Second Edition, McGraw-Hill, 1951.
2. Giedt, W. H., "Investigation of Variation of Point Unit Heat-Transfer Coefficient Around a Cylinder Normal to an Air Stream," Transactions, A.S.M.E., Vol. 71, p. 375, 1949.
3. Grimson, E. D., "Correlation and Utilization of New Data on Flow Resistance and Heat Transfer for Cross Flow of Gases Over Tube Banks," Transactions, A.S.M.E., Vol. 59, p. 583, 1937.
4. Hilpert, R., VDI-Forschungsheft, No. 355, 1932.
5. Hilpert, R., Forschung a. d. Geb. d. Ingenieurwes. Vol. 4, p. 245, 1933.
6. Hoge, E. C., "Experimental Investigation of Effects of Equipment Size on Convection Heat Transfer and Flow Resistance in Cross Flow of Gases Over Tube Banks," Transactions, A.S.M.E., Vol. 59, p. 573, 1937.
7. Knoblauch, O. and Reiher, H., "Waermeuebertragung," in W. Wien and F. Harms, Handbuch d. Experimentalphysik, Vol. 9, Part 1, p. 313, Leipzig, 1925.
8. Lohrisch, W., Forschungsarb. a. d. Geb. d. Ingenieurwes. No. 322, p. 46, 1929.
9. McAdams, W. H., Heat Transmission, McGraw-Hill, 1942.
10. Pierson, O. L., "Experimental Investigation of the Influence of Tube Arrangement on Convection Heat Transfer and Flow Resistance in Cross Flow of Gases Over Tube Banks," Transactions, A.S.M.E., Vol. 59, p. 563, 1937.
11. Schmidt, E. and Werner, K., "Heat Transfer Over the Circumference of a Heated Cylinder in Transverse Flow," NACA, T.M. 1050, Oct. 1943.
12. Thoma, H., Hochleistungskessel, Julius Springer, Berlin, 1921.
13. Winding, G. C. and Cheny, Jr., A. J., "Mass and Heat Transfer in Tube Banks," Industrial and Engineering Chemistry, Vol. 40, p. 1087, 1948.

APPENDICES

I. TEST APPARATUS AND INSTRUMENTATION

Description of Test Apparatus

The test set-up consisted primarily of a centrifugal fan, a thin-plate orifice meter with suitable piping, and steel or aluminum duct test sections in which the various cylinder arrangements were installed. A diagram of the test set-up is shown in Figure 1.

Air was supplied by a 20-inch diameter American Blower, Type F, fan with a rating of 600 cubic feet per minute at 3450 revolutions per minute. Air flow was measured by means of thin-plate orifices installed with flange taps, in a 6-inch diameter duct. The pressure differential across the orifice was measured with a ^{micromanometer} meter. Four orifices were required to cover the range of air flow. A 12-inch long, egg-crate straightening vane was installed at the blower discharge. Eight-mesh screens were installed at both ends of the round-to-rectangular transition piece at the end of the 6-inch duct and upstream of the test section. The air flow was regulated and the static pressure level in the test section was maintained constant by means of a bleed valve at the blower discharge, a throttling plate at the blower inlet, and a damper at the discharge of the test section.

All test ducts were rectangular in cross section and 4 inches high. The steel ducts were welded of hot rolled sheet steel and were 3, 4, and 6 inches wide. The inside surfaces were coated with aluminum foil to reduce heat loss from the test cylinder by radiation.

The 6-inch wide steel test duct was bolted directly to the round-to-rectangular transition piece, and the 4-inch and 3-inch wide ducts were connected to this transition piece with intermediate reducing sections. The 6-inch wide duct was 54 inches long with the test cylinder located 16 inches from the discharge end. The 4-inch and 3-inch wide steel ducts were 38 and 40 inches long, respectively, with the cylinder located in each 16 inches from the discharge end.

The aluminum ducts were made 2, 3, and 3-1/2 inches wide and were fabricated of 1/2-inch thick top and bottom plates and 3/16-inch thick side plates, bolted to the top and bottom plates. The joints were gasketed with heavy thread and sealed with Glyptol. All the inside surfaces were polished before assembly to reduce radiant heat loss from the test cylinder.

Each of the 3-1/2-inch and 3-inch wide aluminum ducts consisted of a 5-foot long inlet section and an 18-inch long interchangeable test

section. An exploded view of a typical test section is shown in the photograph of Figure 2. Details of the method of duct assembly, test cylinder installation, dummy cylinder locations, and static pressure tap adapters may also be seen. The test cylinder was located in the middle of the 18-inch test section proper.

The 2-inch wide aluminum inlet and test sections were made integral in a single 36-inch long section. The test cylinder was located 9 inches from the discharge end.

Instrumentation

All temperatures were measured by means of iron-constantan thermocouples and a Brown indicating potentiometer. Temperatures for determining the density in the calculation of the air flow were obtained from two thermocouples of 30-gauge wire placed in the upstream orifice run. Air temperatures in the test section were obtained from a single thermocouple probe of 30-gauge wire placed at the entrance to the inlet duct. Temperature measurements on the test cylinders were obtained from thermocouples imbedded in an internal reference surface and cemented to the outer surface of the test cylinder. The location and installation of these thermocouples is explained in the description of the test models in Appendix II.

All pressures were measured by means of manometers. Piezometer rings of four taps each were located one inch from the upstream and downstream orifice faces respectively. The upstream static pressure of the orifice and the static pressure in the test section were measured in inches of water with well-type Herrian manometers. The static pressure differential across the orifice was measured in inches of water on a micromanometer. Static pressure distributions along the aluminum test sections were obtained by means of 0.0135-inch diameter holes drilled along the horizontal center line of the test sections' side plates. Twenty taps were used in the 2-inch wide duct and 27 taps in the 3-inch and 3-1/2-inch wide ducts. The pressures were measured in inches of alcohol on a common-well type manometer board and were referred against the static pressure at the duct inlet. Variations of static pressure along the steel duct were not obtained.

Power was supplied to the heating coils of the test cylinders from a 110-volt a.c. source through a constant-voltage Sola transformer. The power input was adjusted by use of a variable auto transformer. The power input to the main heating coil was measured with a Weston precision wattmeter.

Nichrome-V wire. The outer surface of each coil was coated with several layers of Sauereisen cement, baked and ground smooth. The power leads were brought outside the model individually by means of eight separate binding posts which served also to align the heating coils and keep them in place. The heating coils were stacked inside the copper shell with a light press fit. A longitudinal slot 1/8-inch wide was cut on one side of the copper shell to allow for differences in thermal expansion between the copper and the Transite. Nine iron-constantan thermocouples were installed in the outer surface of the copper shell and evenly spaced over 180 degrees of the periphery, opposite the expansion slot.

This assembly was pressed with a light press fit into the laminated outer Transite shell of 3/32-inch thickness and 1.5-inch diameter. The surface thermocouples were installed by wrapping a prefabricated grid of 19 iron-constantan thermocouples, made of 0.004-inch wire, around the same 180 degrees of periphery as the inside thermocouples and by cementing the grid to the surface with Sauereisen cement. The thermocouple junctions were spaced so as to provide temperature measurements at 10-degree intervals.

The thermocouple grid was prefabricated by stringing the bare iron and constantan wires on a specially made jig to position the wires accurately. The constantan wires were positioned parallel and on 0.131-inch center line distance corresponding to 10-degree intervals on the cylinder surface and were clamped in place. Two iron wires were positioned normal to the constantan wires to provide a common positive lead. Each intersection of the iron and constantan wires was then spot-welded to form a junction to be located on a horizontal circumferential line around the test cylinder.

This grid was carefully positioned around the external surface of the assembled test cylinder and cemented in place by coating the entire surface with Sauereisen cement. After thorough drying and baking, the surface of the cylinder was ground to size to provide a smooth cylindrical surface. Inspection after grinding showed the thermocouple junctions and the lead wires to be practically at the surface.

The bottom plug and the top flange were positioned and sealed by means of wire ring gaskets and the entire assembly was clamped together securely with a spring-loaded assembly rod. Lead wires for the outer surface thermocouples were attached to the splice bolts in the outer shell and threaded through the top flange. All thermocouple lead wires were wrapped around the terminals on the top of the flange and the lead wire holes were sealed against leakage with Sauereisen cement. The terminals were insulated with powdered magnesia and glass cloth ribbon. The screw terminals in the top flange provided for quick and easy extension of the thermocouple and power leads and permitted complete removal of the cylinder from the test duct for modification or reworking.

The top flange and the graduated ring were indexed so that they could be accurately positioned with respect to the thermocouples on the surface of the outer shell. Both pieces were doweled to the body of the cylinder to maintain the correct reference position. The zero-graduation was set opposite the vernier-zero so that the first surface thermocouple

would face directly upstream and would indicate conditions at the stagnation point.

Unheated Cylinders

In tests of multiple cylinder arrangements, test cylinder B was used with other unheated cylinders. The unheated cylinders were made from 1.5-inch diameter aluminum bar stock and polished to reduce radiant heat loss from the test cylinder.

To produce in-line configurations, an unheated dummy cylinder was installed upstream and another downstream, in the same plane as the heated cylinder, as shown in Figure 4. The dummy cylinders were located as shown in Figure 72 and could be adjusted for variation of longitudinal spacings and clamped in place.

The same method of installation as for in-line cylinders was used for the two dummy cylinders in the center plane of symmetrically staggered configurations. In addition, to simulate true staggered configurations as shown in Figure 4, four half-cylinders were fastened in the side plates of the duct at predetermined locations, in the manner shown in the left half of Figure 73. Unused locating holes were plugged by means of gasketed inserts held in place by a back plate.

The double-row staggered configurations were also produced with the aid of dummy cylinders, as shown in Figure 4. Two cylinders were located upstream and two cylinders were located downstream in predetermined locations. The manner in which these dummy cylinders were located and fastened is shown in the right half of Figure 73.

Two unheated test cylinders of 1.00- and 1.938-inch diameter, respectively, were constructed for obtaining additional pressure drop data of single configurations. Having a top flange plate fitting the locations of the hold-down screws for the test cylinder, they were mounted in the same manner as the heated test cylinder B.

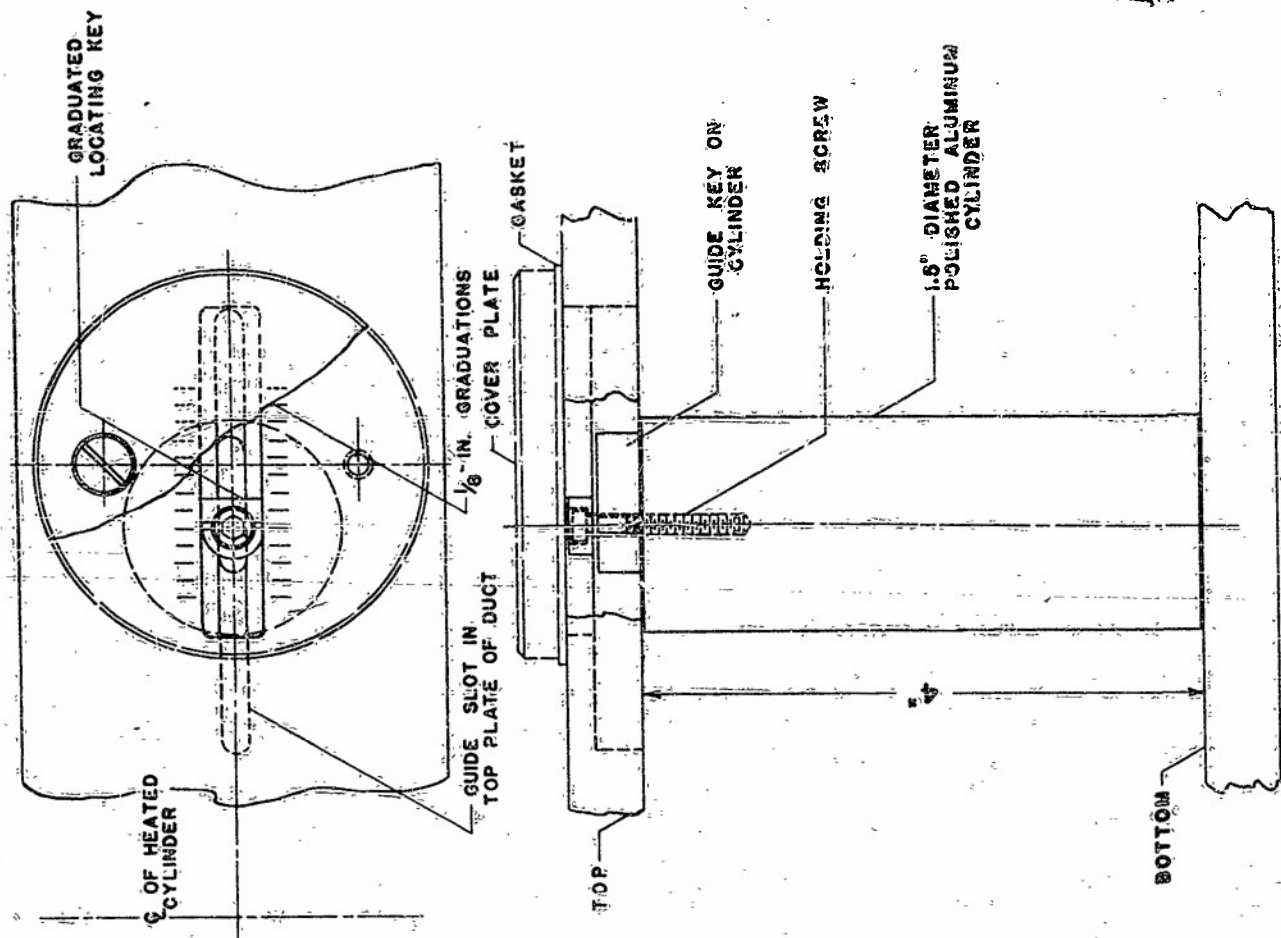


FIGURE 72. SKETCH SHOWING METHOD OF LOCATING AND HOLDING DUMMY CYLINDERS FOR IN-LINE AND STAGGER CONFIGURATIONS

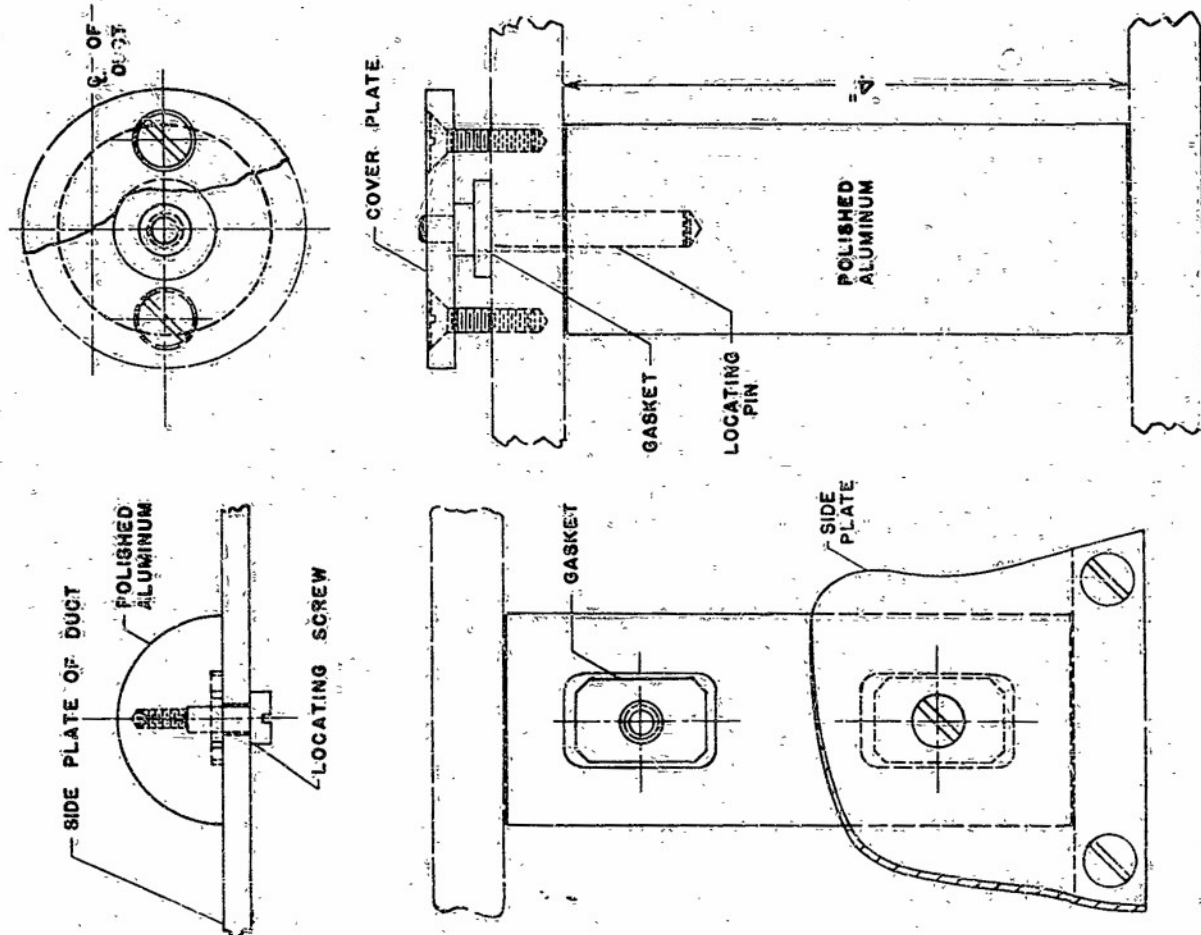


FIGURE 73. SKETCH SHOWING METHOD OF HOLDING DUMMY HALF-CYLINDERS FOR STAGGERED CONFIGURATION AND WHOLE CYLINDERS FOR DOUBLE-ROW STAGGERED CONFIGURATION

III. TEST PROCEDURE

This description of the test procedure refers specifically to that used with cylinder B. The procedure for cylinder A was similar, except for details of locating and indexing the test cylinder.

The guide ring to position test cylinder B in the tunnel was located on and fastened to each test duct by means of four hold-down screws. The test cylinder was inserted part-way into the duct from the top and the split top fairing ring was fastened in place. The top flange was then seated in the guide ring and the zero position on the graduated ring lined up with a scribe mark on the vernier support. The vernier support had been previously located so that the scribed line coincided with the guide ring center line which was perpendicular to the duct's longitudinal center line. The vernier-zero was set in line with the zero of the graduated ring. Thus, with the cylinder in this position, the two surface thermocouples which were diametrically opposite one another were exactly lined up with the duct's longitudinal center line and hence with the flow direction. The top flange of the test cylinder was securely bolted to the duct top plate and the position of the cylinder was visually inspected from the downstream end of the duct. The duct assembly and cylinder installation were checked for leaks before any test runs were started.

The blower was turned on and the desired air flow and the static pressure level in the duct were set by adjusting the bleed valve, the inlet throttling plate, and the discharge damper. The power supply to the heating coils was turned on and the input adjusted to the desired value by means of the variable auto transformer. Preliminary temperature readings were taken at 5-minute intervals until the same temperature readings were noted in at least two successive readings. Temperatures were then considered to be stable and all pressure and temperature data were recorded. During initial starts, at least one-half hour was required to reach thermal stability. Subsequent power or air flow changes required 10- to 15-minute stabilization periods.

After all data had been recorded for this cylinder position, nominally referred to as the zero-degree position, the hold-down screws were loosened, the model was rotated 5 degrees counter-clockwise, and the hold-down screws were re-tightened. After allowing the temperature to stabilize, while maintaining constant air flow and power input, the same data were recorded as before. Then either air flow or power input was changed to the next desired value and the same procedure repeated except that the cylinder was rotated 5 degrees clockwise after the data for the first position were recorded. Thus, only two model positions were required to obtain temperature readings at 5-degree intervals over 180 degrees of the periphery of the cylinder.

Except for spot-checking, the reproducibility of temperature profiles on the opposite side of the cylinder was not questioned, this procedure was used on all configurations in which the flow pattern was symmetrical about the duct center-line. In the staggered, double-row configurations additional positions of the test cylinder with 180 and 135 degrees of counter-clockwise rotation were required to obtain the non-symmetrical temperature

distributions.

Power input was arbitrarily limited so that the temperature at the internal surface of the external Transite shell did not exceed approximately 100°F. Air flow was limited by blower capacity and static pressure level in the test duct which was maintained at approximately 15 inches of water pressure above ambient conditions.

No changes in the overall pressure drop and in the pressure gradients in the duct were observed with variations of the power input to the test cylinder. Therefore, the multiple-tube manometer indicating the pressure variation along the duct wall was read only once for each air flow rate and configuration. The readings were taken after an appreciable equilibrium period. The upstream duct pressure was applied to the common well which was so positioned that the range of graduations of the manometer board was best utilized.

IV. CALIBRATION OF TEST CYLINDERS

Cylinder A

The eight pairs of thermocouples, located on radial lines 45 degrees apart on the internal and external surface of the Transite shell, did not give equal temperature drop measurements when operated in the same position relative to the air flow, while air velocity and power input were held constant. Therefore, all measurements were made with the same pair of thermocouples rotated to assume a required number of positions relative to the air flow direction to determine the thermal conductivity of the Transite shell as a function of temperature, necessary for computation of point heat transfer rates. The external and internal temperature profiles taken with the same pair of thermocouples for a large number of test runs were integrated graphically to determine, for each run, an average temperature difference and an average temperature of the Transite. The power inputs were correlated for end losses. The net power input for each test run was divided by the average temperature difference and appropriate constants to determine a thermal conductivity for the average temperature determined from the temperature distribution data. The resulting conductivity curve fitted the test data within ± 2 per cent. The calibration data so obtained were used for the calculation of point heat flow rates, based on measured temperature differentials and assumed purely radial heat flow.

Cylinder B

Preliminary calibration tests of cylinder B indicated that, under constant flow conditions and with a constant internal temperature, the surface temperature indicated by the 19 thermocouples, operated in the same peripheral position, were not equal. It was determined that the inequalities of temperature differentials so indicated were not due to thermocouple error but were caused by variations in the radial thermal conductance of the external Transite shell. This was ascribed to the inhomogeneity of the Transite and the probable existence of a small air gap of variable thickness between the copper shell and the internal surface of the Transite. Calculations showed that the conductance could be decreased by as much as 20 per cent by an air gap of 0.001-inch thickness. In addition, indication of the existence of an air gap was furnished by a change of the relative magnitudes of the variable temperature differentials measured by different thermocouples with changes in the temperature of the copper shell. This could be explained in part by the change of thermal conductivity of air with temperature and in part by the probable expansion and contraction of the copper shell with temperature, the latter causing a dimensional variation of the air gap.

In view of the above findings, it was necessary to perform an extensive calibration of the test cylinder. It was also established that an apparent increase of thermal conductance occurred at low air velocities when the calculations were based on the heat input to the two central heating elements. This was interpreted to indicate a percentage increase of end losses at low velocities. In the 2-inch test duct, constant thermal conductance was obtained at velocities greater than 60 feet per

second. Therefore, the calibrations were performed at this high velocity and the conductances so determined were used for the analysis of heat transfer at all velocities selected for investigation.

The procedure used in the calibration was to rotate the test cylinder one complete revolution in steps of 10 degrees for four power inputs and constant air velocity. Thus, a complete surface temperature profile was obtained, as determined by each thermocouple for the same power input and a corresponding internal temperature. These temperature profiles were similar but, when individually averaged over the entire circumference, indicated different values of temperature differentials between the copper shell and the outer surface of the cylinder. Since the smallest average differential was determined by thermocouple (6), indicating the greatest radial conductance, this thermocouple was taken as the reference.

Fixed flow conditions and power input defined the average convective heat transfer coefficient. This criterion and the assumption of purely radial heat flow served as a basis for correlating the conductances at all locations with the conductance at the location of thermocouple (6). For any thermocouple (x), the relationship

$$K_x (t_i - t_s)_x = h (t_s - t_b)_x \quad (12)$$

was assumed to be valid. The symbols were defined as follows:

- h average convective heat transfer coefficient
- t_s average surface temperature of the test cylinder
- t_i temperature of internal copper shell of the test cylinder
- t_b air temperature
- K_x thermal conductance between copper shell and outer surface of the test cylinder at location of thermocouple (x)

Therefore, the relative thermal conductance of any location (x) with reference to the location of thermocouple (6) was defined by

$$Y_x = \frac{K_x}{K_b} = \frac{K_x}{K_{ref}} = \frac{(t_i - t_s)_b}{(t_s - t_b)_b} \times \frac{(t_s - t_b)_x}{(t_i - t_s)_x} \quad (13)$$

The temperature differences in the above equation were the average values as determined from the calibration runs. The value of Y_x for any specific thermocouple locations were found to vary with internal copper shell temperature.

The absolute value of K_{ref} as a function of average Transite temperature was determined from single test runs at different power input at velocities of 60 feet per second or greater. The distribution of temperature differentials was determined by operating the test cylinder in two positions, with an angular displacement of 5 degrees. The distribution of heat flux was assumed to be determined at any peripheral

location by

$$q_x = K_{ref} Y_x (t_i - t_s)_x \quad (14)$$

Then, the average heat flux through the test length of the Transite shell, equal to the length of the two center heating elements for n thermocouple locations was

$$q_{ave} = (1/n) \sum_1^n q_x = (K_{ref}/n) \sum_1^n Y_x (t_i - t_s)_x \quad (15)$$

Also, the average heat flux was to be equal to the power input per unit surface area E/A . Therefore, the solution for the reference conductance K_{ref} at various power inputs and correspondingly different Transite temperatures was obtained by

$$K_{ref} = \frac{n(E/A)}{\sum_1^n Y_x (t_i - t_s)_x} \quad (16)$$

V. METHODS OF CALCULATION

The test data consist of measurements of the following quantities:

1. The inlet air temperature upstream of the metering section.
2. The static pressure upstream of the metering section.
3. Manometer reading of the pressure drop across the orifice.
4. Barometric pressure.
5. The inlet air temperature of the test section.
6. The inside surface or copper shell temperature of the test cylinder.
7. The outside surface temperatures of the test cylinder.
8. The manometer readings indicating static pressures at various locations along the wall of the test section.

In calculating the peripheral distribution of point unit heat transfer coefficients, the assumption of purely radial heat flow through the Transite shell is made because of the low thermal conductivity of the material. The small temperature gradients in the tangential direction, as compared to the temperature gradients in the radial direction, permit little tangential heat flow.

Investigation of the error resulting from the assumption of purely radial heat flow for large peripheral temperature gradients obtained in the tests indicates maximum local errors in the calculation of the radial heat flux, as outlined below, not in excess of 5 per cent. However, for most point heat transfer coefficients, the error resulting from this approximation is considerably smaller. For locations where the tangent to the surface temperature distribution curve has zero slope, the calculation error is nil.

The point heat transfer coefficient is defined as the rate of heat transfer per unit area and unit temperature difference in Btu per (hour-°F-square foot) which is equivalent to the convective heat flux per degree temperature difference, or

$$h = (q_{\text{conv}})/(t_s - t_p) \quad (17)$$

The convective heat flux is equal to the radial heat flux through the Transite shell less the radiant heat flux from the surface, or

$$q_{\text{conv}} = q_x - q_{\text{rad}} \quad (18)$$

Based on the assumption of purely radial heat flow, the total local heat flux q_x is expressed by equation (14) which is

$$q_x = K_{ref} \frac{Y}{x} (t_i - t_s) \quad (14)$$

where K_{ref} is evaluated at the mean of t_i and t_s as explained on page 88 of the description of test model calibration.

The point radiant heat loss q_{rad} is calculated by

$$q_{rad} = \sigma \epsilon F_e F_A (T_s^4 - T_b^4) \quad (19)$$

where $\sigma = 0.173 \times 10^{-8}$. The constants F_e and F_A for the configuration with aluminum duct walls and a cylinder surface of white cement are estimated as intermediate values between cases 2 and 7 of reference (1) to be 0.1 and 1, respectively. This estimate is considered to be conservative. However, numerical computations show that the amount of radiant heat flux is only a small fraction of the total heat flux. Therefore, any inaccurate evaluation of the constants in equation (17) would result in an insignificant error in the heat transfer coefficient. The film Nusselt number is calculated as defined by (hd/k_f) where k_f is the thermal conductivity of air, based on the mean of local surface temperature and the inlet air temperature.

For the purposes of data presentation and correlation, the bulk Reynolds number (dG/μ) is calculated. The rate of air flow in pounds per second is calculated according to standard procedure by use of data items (1) to (4) and a calibration curve for the orifice. The corresponding mass velocity G in pounds per second-square foot is determined by dividing the gross cross-sectional area of the test duct into the air flow rate. The bulk viscosity of air is evaluated at the inlet air temperature of the test section, data item (5), and the 1.5-inch test cylinder diameter is used for the characteristic dimension d , in feet.

Data plots for a typical surface temperature variation, the inlet air temperature, and the inside shell temperature are shown in Figure 74 for Run A-147 in a 2-inch wide duct with three in-line cylinders of $S_L = 1.250$. The mass velocity G is calculated from the mass flow and the duct gross cross-sectional area as 1.632 pounds per second-square foot. The calculated values of point film Nusselt number are plotted in Figure 75. The procedure of obtaining the Nusselt number variation is illustrated by the following calculations for $\alpha = 10^\circ$ with the surface temperature measured by thermocouple (2).

$$t_i = 410^\circ\text{F}$$

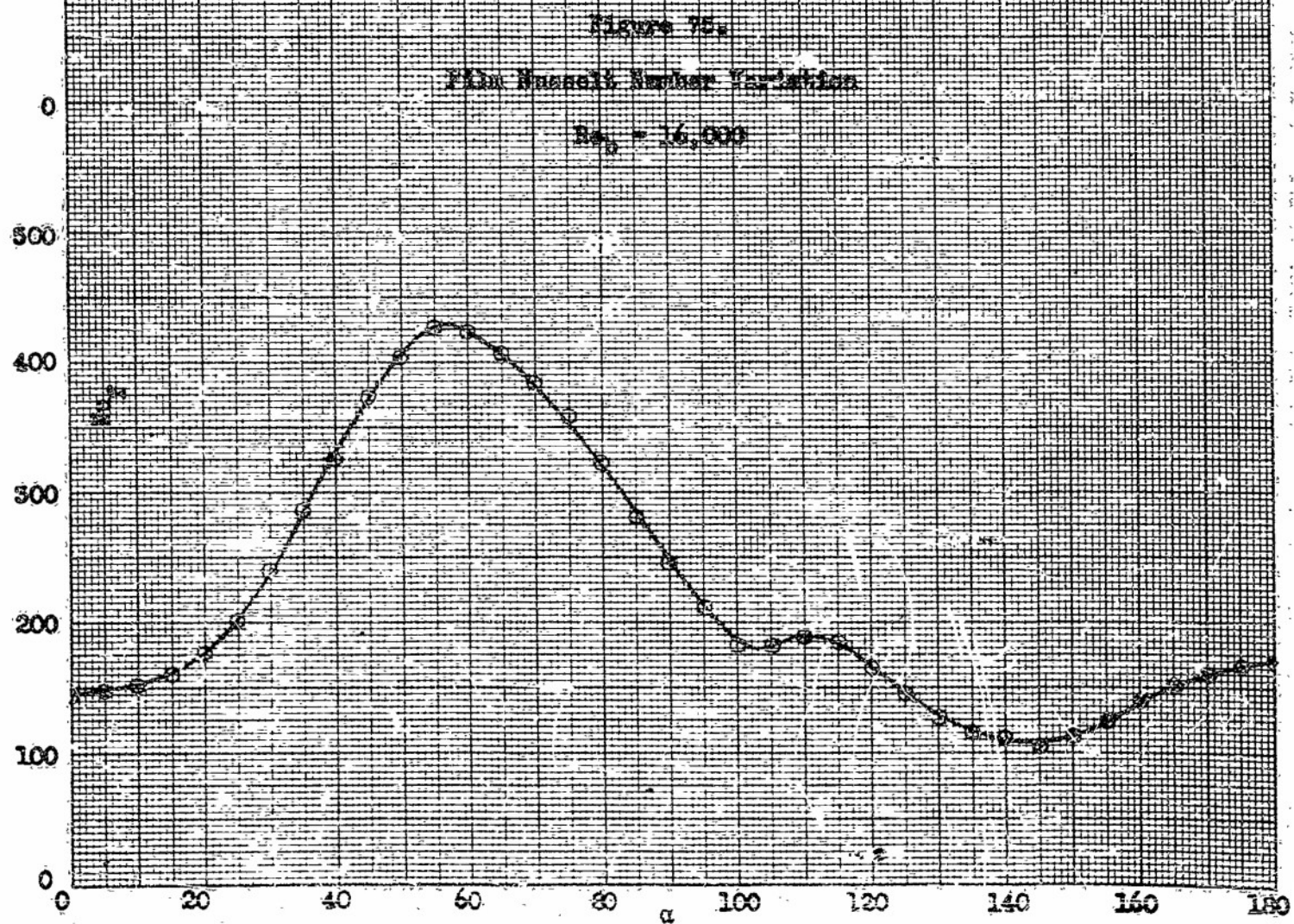
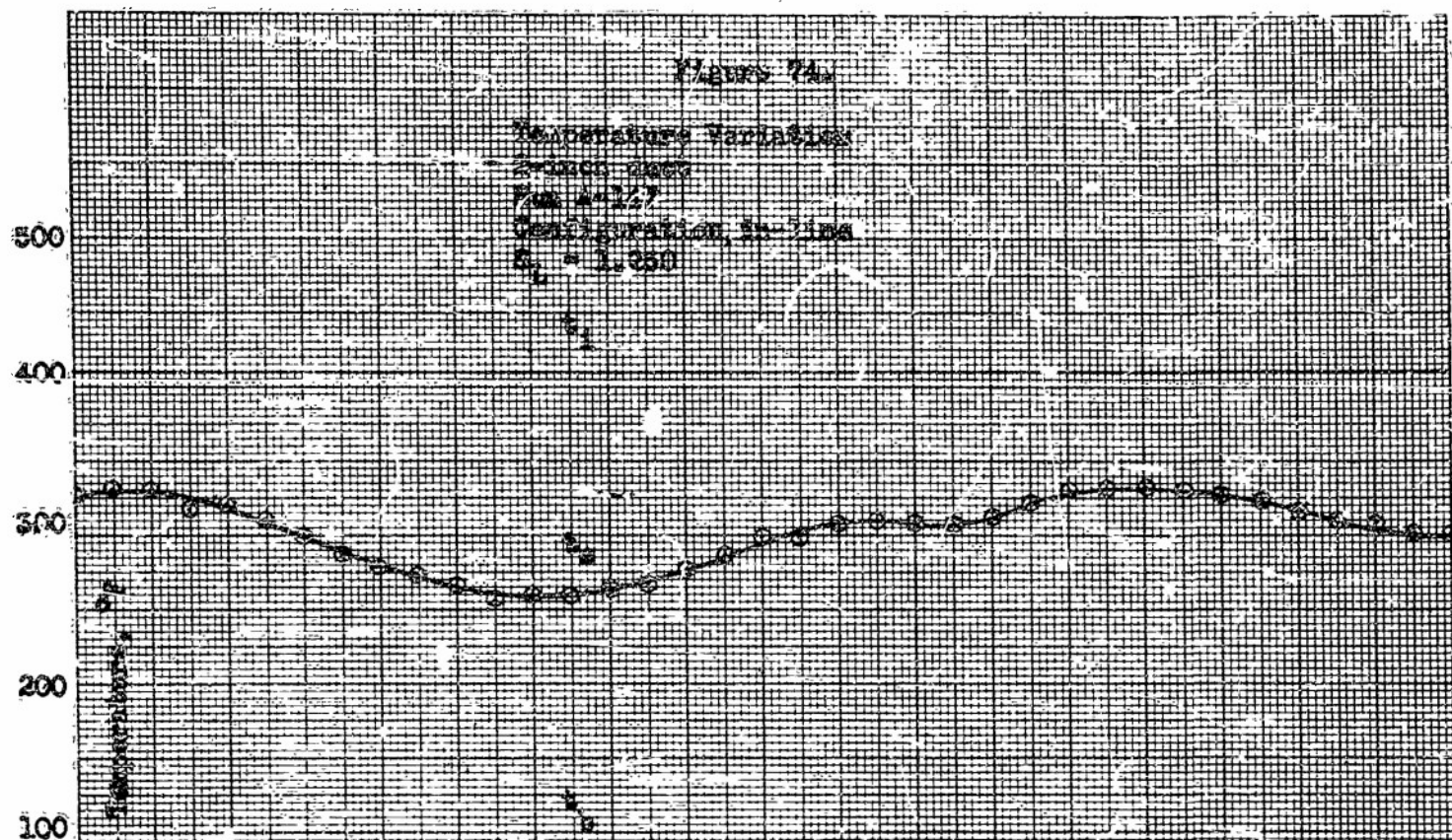
$$t_s = 328^\circ\text{F}$$

$$t_b = 91^\circ\text{F}$$

(1) Calculation of Total Heat Flux

Local average Transite temperature, $t_{tr} = (t_s + t_i)/2$

$$t_{tr} = (410 + 328)/2 = 369^\circ\text{F}$$



Reference conductance of Transite at $t_{tr} = 369^{\circ}\text{F}$,

$$K_{ref} = 68.5 \text{ Btu per (hr-sq ft-}^{\circ}\text{F)}$$

Relative conductance for location of thermocouple (2), at $t_i = 410^{\circ}\text{F}$

$$Y_2 = 0.941$$

Hence, from equation (14) for the location of thermocouple (2),

$$\begin{aligned} q_2 &= K_{ref} Y_2 (t_i - t_g)_2 \\ &= 68.5 \times 0.941 (410 - 328) \\ &= 5290 \text{ Btu per (hr-sq ft)} \end{aligned} \quad (14)$$

(2) Calculation of Radiant and Convective Heat Flux

From equation (19),

$$\begin{aligned} q_{rad} &= 0.0173 \times 10^{-8} [T_s^4 - T_b^4] \\ &= 0.0173 \times 10^{-8} [(460 + 328)^4 - (460 + 91)^4] \\ &= 51 \text{ Btu per (hr-sq ft)} \end{aligned} \quad (19)$$

Equation (17) then gives

$$\begin{aligned} q_{conv} &= q_x - q_{rad} \\ &= q_2 - q_{rad} \\ &= 5290 - 51 = 5239 \text{ Btu per (hr-sq ft)} \end{aligned} \quad (18)$$

(3) Calculation of Heat Transfer Coefficient and Local Film Nusselt Number

The heat transfer coefficient is calculated by equation (17)

$$\begin{aligned} h &= q_{conv} / (t_s - t_b) \\ &= 5239 / (328 - 91) = 22.1 \text{ Btu per (hr-sq ft-}^{\circ}\text{F)} \end{aligned} \quad (17)$$

To calculate the film Nusselt number $(hd/k_f)_2$, where d is the diameter of the test cylinder, the thermal conductivity of air k_f is determined at the local film temperature.

$$t_f = (t_s + t_b)/2$$

$$= (328 + 91)/2 = 209.5^\circ\text{F}$$

For $t_f = 209.5^\circ\text{F}$,

$$k_f = 0.0184 \text{ Btu per (hr-sq ft-}^\circ\text{F per ft)}$$

The local film Nusselt number is therefore

$$Nu_f = hd/k_f = 22.1(1.5/12)(1/0.0184) = 150$$

(4) Calculation of Bulk Reynolds Number

The bulk Reynolds number is calculated directly from

$$Re_b = dG/\mu_b$$

where μ_b is the viscosity at bulk air temperature, equal to the inlet air temperature

For $t_b = 91^\circ\text{F}$

$$\mu_b = 12.75 \times 10^{-6} \text{ lb per (ft-sec)}$$

Hence,

$$Re_b = (1.632 \times 1.5/12)(1/12.75)10^6 = 16,000$$

(5) Calculation of Modified Nusselt Number

The local film Nusselt numbers calculated as above for half of the periphery are plotted in Figure 75. The Nusselt number profile is correlated with other profiles obtained at the same bulk Reynolds number but different total heat flows by the modified Nusselt numbers $Nu_F \Phi_\mu$ to allow for different surface temperatures at the same locations. Thus, for $\alpha = 10^\circ$ and at $t_f = 209.5^\circ\text{F}$

$$\mu_f = 14.67 \times 10^{-6} \text{ lb per (ft-sec)}$$

the local modified Nusselt number is therefore

$$Nu_F \Phi_\mu = Nu_f \left(\frac{\mu_f}{\mu_b} \right)^{0.62}$$

$$= 150 \left(\frac{14.67 \times 10^{-6}}{12.75 \times 10^{-6}} \right)^{0.62}$$

$$= 164$$

The local modified Nusselt numbers for other locations are similarly calculated and plotted for presentation as shown by curve E in Figure 9.

(6) Calculation of Average Film Nusselt Number and Film Reynolds Number

The average film Nusselt number is obtained by calculating the weighted mean of the local film Nusselt numbers shown in Figure 75. The average film Nusselt number $Nu_f(\text{ave})$ for this run is determined to be 225.6. The average film Nusselt number is correlated against average film Reynolds number. The latter is determined by

$$Re_f(\text{ave}) = Re_b \frac{\mu_b}{\mu_f(\text{ave})}$$

where $\mu_f(\text{ave})$ should be the average of the air viscosities determined at local film temperatures. However, for simplicity of computations, $\mu_f(\text{ave})$ is the viscosity value determined at the average of the local film temperatures over the entire periphery. From Figure 74, the average of the surface temperatures is calculated to be $t_s(\text{ave}) = 300.4^\circ\text{F}$. For constant bulk air temperature, the average of the local film temperature is therefore

$$(300.4 + 91)/2 = 196^\circ\text{F},$$

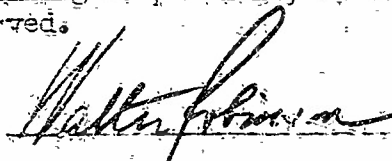
and the viscosity at this average film temperature is obtained as 14.40×10^{-6} lb per (ft-sec). Hence, the film Reynolds number is

$$Re_f = 16,000 \frac{12.76 \times 10^{-6}}{14.40 \times 10^{-6}} = 14,150$$

The test point for this run can be identified in Figure 64 at the film Reynolds number of 14,150 by the square symbol.

NOTE: In submitting this report it is understood that all provisions of the contract between the Foundation and the Cooperator and pertaining to publicity of the subject matter will be rigidly observed.

Supervisor

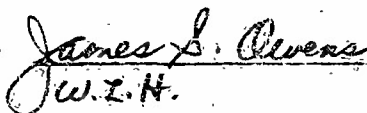


Date

9-28-51

FOR THE OHIO STATE UNIVERSITY RESEARCH FOUNDATION

Executive Director


J.W.I.H.

Date

2 October 1951

GOVERNMENT NOTICES

When Government drawings, specifications, or other data are used for any purpose other than in connection with a definitely related Government procurement operation, the United States Government thereby incurs no responsibility nor any obligation, whatsoever; and the fact that the Government may have furnished, or in any way supplied the said drawings, specifications, or other data, is not to be regarded by implication or otherwise as in any manner licensing the holder or any other person or corporation, or conveying any rights or permission to manufacture, use, or sell any patented invention that may in any way be related thereto.

The information furnished herewith is made available for study upon the understanding that the Government's proprietary interests in and relating thereto shall not be impaired. It is desired that the Office of the Judge Advocate, Air Materiel Command, Wright-Patterson AFB, Dayton, Ohio, be promptly notified of any apparent conflict between the Government's proprietary interests and those of others.